2014

Current limiting mechanism in MgB2 wire

Ashkan Motaman
University of Wollongong

UNIVERSITY OF WOLLONGONG

Institute for Superconducting and Electronic Materials

Current limiting mechanism in MgB_2 wire

Ashkan Motaman

This thesis is presented as part of the
requirement for the Award of the Degree of
Doctor of Philosophy of
the University of Wollongong

Aug 2014

Declaration

I, Ashkan Motaman, declare that this thesis, submitted in partial fulfillment of the requirements for the award of Doctor of Philosophy, in the Institute for Superconducting & Electronic Materials (ISEM), Faculty of Engineering, University of Wollongong, Australia, is wholly my own work unless otherwise referenced or acknowledged. This document has not been submitted for a qualification at any other academic institution.

Ashkan Motaman

Aug, 2014

Acknowledgment:

My last three and half years comprehensive research outcomes which has been executed at the laboratory of institute for superconducting and electronic materials, faculty of engineering - University of Wollongong, came together here to form this PhD thesis.

There is no end to appreciate and thanks the people who helped me out through this section of my life.

I would like to express my special appreciation and thanks to Professor Shi Xue Dou, you have been a tremendous mentor for me. I would like to thank you for encouraging my research and for allowing me to grow as a research scientist.

I would like to express my heartfelt gratitude to Ass. Prof. Jung Ho Kim, you have been a huge support to me on both research and my career and thanks indeed for your valuable advices and brilliant comments.

I am so grateful to Dr. Shahriar Hossain for his priceless supports on both technical and theoretical parts of my PhD project.

Thanks are also due to Dr. M Maeda, Dr. K. W. See, Dr.X. Xu, Dr. S. De Silva for their valuable support in measurement, technical and theoretical solutions.

Special thanks to Mr. R. Morgan, P. Hamersly and M. Davies for their expertise assistance in the instrumentation and experimental development.

Likewise, I wish to express my gratitude to the University of Wollongong's Research Centre for providing the scholarship and living allowances during the course of my study in the institute for superconducting and electronic

materials.

A special thanks to my family. Words cannot express how grateful I am to my mother, father, my brother, my sisters and my niece for all of the sacrifices that you've made on my behalf. Your prayer for me was what sustained me thus far. I would also like to thank all of my friends who supported me in writing, and incented me to strive towards my goal.

Published Articles:

- D. Patel, M.S.A. Hossain, A. Motaman, S. Barua, M. Shahabuddin, J. H. Kim, Cryogenics. 10.1016 (2014)
- H. Ağıl, Ö. Çiçek, E. Ertekin, A. Motaman, M. S. A. Hossain, S. X. Dou, A. Gencer, Journal of Superconductivity and Novel Magnetism, , Volume 26, Issue 5, pp 1525-1529, (2013)
- A. Motaman, S. Barua, D. Patel, M. Maeda, K. Cheong, J. H. Kim, S. X. Dou, M. S. A. Hossain, Journal of Superconductivity and Novel Magnetism, Volume 27, Issue 7, pp 1643-1645, (2014)
- M. Shahabuddin, N. S. Alzayed, S. Oh, S. Choi, M. Maeda, M. S. Shah, A. Motaman, M. S. A. Hossain, J. H. Kim, Solid State Communications, Volume 181, Pages 20–23, (2014)
- M.S. A. Hossain, A. Motaman, X. Xu, K. W. See, Ö. Çiçek, H. Ağıl, E. Ertekin, A. Gencer, K. Cheong, M. Maeda, S. Dou, Materials Letters, Volume 91, Pages 356–358, (2013)
- M. Maeda, M.S.A Hossain, A. Motaman, J.H. Kim, A. Kario, M. Rindfleisch, M. Tomsic & S.X. Dou, IEEE Transactions on Applied Superconductivity, 23 (3), 6200704-1-6200704-4, (2013).
- A. Motaman, M. S. A. Hossain, X. Xu, K. W. See, K. C. Chung & S. X. Dou, *Supercond. Sci. Technol.* 26 085013, (2013).
- M. S. A. Hossain, A. Motaman, S. Barua, D. Patel, M. Mustapic, J. H. Kim, M. Maeda, M. Rindfleisch, M. Tomsic, O. Cicek, T. Melisek, L. Kopera, A. Kario, B. Ringsdorf, B. Runtsch, A. Jung, S. X. Dou, W. Goldacker & P. Kovac, *Supercond. Sci. Technol.* 27 095016, (2014)

Abstract:

Since discovery of the MgB_2 as a superconductor; Lots of efforts have been taken by different researchers in worldwide to make this compound applicable for the electrical application.

Valuable superconducting properties of this compound such as but not limited to its high T_c, intrinsically "weak-link" free grain boundaries, rich multiple-band structure and its low fabrication cost, led to consideration of this compound by researcher as a strong substitute for nowadays commercial Nb-Ti superconductor which is more expensive than MgB_2.

The work presented in this thesis is focused on current limiting mechanisms in MgB_2 superconducting wires.

In the literature review chapter, we discussed on MgB_2 obstacles towards industrialization and electronic applications as well as undertaken protective measures to win over the existence obstacles. MgB_2 main obstacles in regards to electrical application lie on its rapid drop in critical current density (J_c) under applied magnetic field, and low upper critical field (H_{c2}), which exclude this compound from many industrial applications where a high J_c under high magnetic field is required.

A comprehensive study of the effects of structural imperfections in MgB_2 superconducting wire has been conducted in the chapter followed by literature review. As the sintering time and temperature change the MgB_2 structural imperfection therefore, sintering condition plays vital role in final superconducting properties of the MgB_2. Lower sintering temperature increases the MgB_2 structural imperfections due to increase in MgB_2 lattice disorder and leads to higher impurity scattering between the π and σ bands of

MgB_2, resulting in a larger upper critical field. From the other side, lower sintering temperature results in smaller MgB_2 grain size which improves the pinning forces, and thereby, enhances the critical current density. In spite of using the low sintering temperature, Voids and porosities still exist in the MgB_2 structure and suppress the critical current density.

After comprehensive study on the structure of stoichiometric compound of the MgB_2 wire, we continued our research on the MgB_2 wires treated with 10 wt.% malic acid ($C_4H_6O_5$), as this sample showed the best performance result so far among the other MgB_2 doped wires. State of art investigation has been executed on the pinning mechanism of the MgB_2 wires, treated with 10 wt.% malic acid ($C_4H_6O_5$), at different sintering temperatures. Our investigation revealed that flux pinning is dominated by point and correlated pinning at lower and higher magnetic fields, respectively, for the carbon-doped samples sintered at both 700 and 900°C. from the other side, the δl pinning is dominant at lower operating temperatures, and δT_c pinning starts to be dominant close to T_c, This means that spatial variation in the charge carrier mean free path is mainly responsible for the flux pinning mechanism in the malic doped MgB_2 wires sintered at 700 and 900°C.

We have also analyzed the pinning mechanism of the MgB_2 wire, 10% malic doped and un-doped, based on the percolation model. The critical current behavior measured from MgB_2 wires can be obviously explained by only four fitting parameters, the anisotropy parameter, the pinning force maximum, the upper critical field along the ab-plane, and the percolation threshold. Moreover, the temperature dependence of the upper critical field is further explained by the dirty-limit two-gap theory. With the carbon dopant, there was a clear decrease in the anisotropy parameter, resulting in an increased

high-field critical current density. In contrast, the pinning force maximum is found to be main factor affecting the low-field critical current density.

And finally in last chapter, we analyzed the correlation between the critical current density (J_c) and the n-value extracted from the electric field versus current density characteristic. The power-law relationship (m) between the J_c and the n-value, $n \propto J_c^m$, represents a critical index, which is strongly dependent on operating temperatures.

MgB_2 conductors still can have an impact in Magnetic Resonance Imaging (MRI) applications for the following reasons: (1) respectable properties for low to mid-field magnets operating at temperatures as high as 20 K; (2) wire manufacturing no more difficult than Nb-Ti wire manufacturing; (3) Mg and B are lower cost raw materials than Nb and Ti; (4) MgB_2 is 1/3 the density of Nb-Ti, so that the same kg of raw material will yield three times the piece length; (4) faster charging rate compared to Nb-Ti based magnet; and (5) the high critical temperature offers a larger thermal margin than the 9 K of Nb-Ti.

Contents

List of Figures

List of Tables

Index of abbreviations

Alternating current	AC
Boltzmann's constant	k
Carrier density	n_s
Coherence length	ξ
Critical current density	J_c
Critical transition temperature	T_c
Density of states	DOS
Energy gap	Δ
Field emission scanning electron microscope	FESEM
Flux pinning force	F
Full width at half maximum	FWHM
High resolution electron microscopy	HREM
High temperature superconductor	HTS
Hot isostatic pressing	HIP
Irreversibility field	H_{irr}
Lower critical field	H_{c1}
Low temperature superconductor	LTS
Penetration depth	λ
Phonon density of states	PDOS
Physical properties measurement system	PPMS
Powder-in-tube	PIT
Continues tube filling and forming	CTFF
Resistivity near Tc	ρ_0
Residual resistivity ratio	RRR
Scanning electron microscopy	SEM
Transmission electron microscopy	TEM
Upper critical field	H_{c2}
X-ray diffraction	XRD
X-ray photoemission spectroscopy	XPS

Chapter 1: INTRODUCTION

1.1 Superconductivity in a glance

Appearance of remarkable electromagnetic properties in certain materials when they are cooled to extremely low temperature is called superconductivity. To be more precise, superconducting materials show no resistance to the current flow below certain critical temperature (T_c), field (H_c) and current density (J_c). Many different groups of material show superconducting properties when their temperature reached to absolute zero (-273°C).

Discovery of superconductivity backs to 1911, when H. Kamerling Onnes had access to liquefied helium, enabled him to reduce the material's temperature to lowest possible level by having the liquefied helium at 0.9 K. His investigation on physical properties of different metallic materials at low temperature ended up with strange physical phenomenon in mercury when its resistivity dropped to zero at 4.2 K, called superconducting state [1]. Later, in 1913, Nobel Prize was given to him because of his valuable discovery.

Another great discovery in superconducting materials happened in 1933 by German researchers, Walther Meissner and Robert Ochsenfeld. They explored that superconducting materials repulse the magnet field in superconducting state which is known now as the Meissner effect [2]. The Meissner effect is so strong which can create enough forces to levitate the magnet over the superconductive material in superconducting state.

Figure. 1.1 shows the history of superconductor development with time.

After discovery of superconductivity, many materials have been examined by

researcher to see if they fall into this group. In 1986, the Ba-La-Cu-O system[3] shows superconductivity by having T_c higher than 35 K followed by, Tl-Ba-Cu-O with T_c of 125 K [4] and later on, Hg-Ba-Ca-Cu-O was shown to be superconducting at 134 K [5]. Up to now, the record for the highest superconducting temperature is still held by the Hg-based superconductor which was found in 1993.

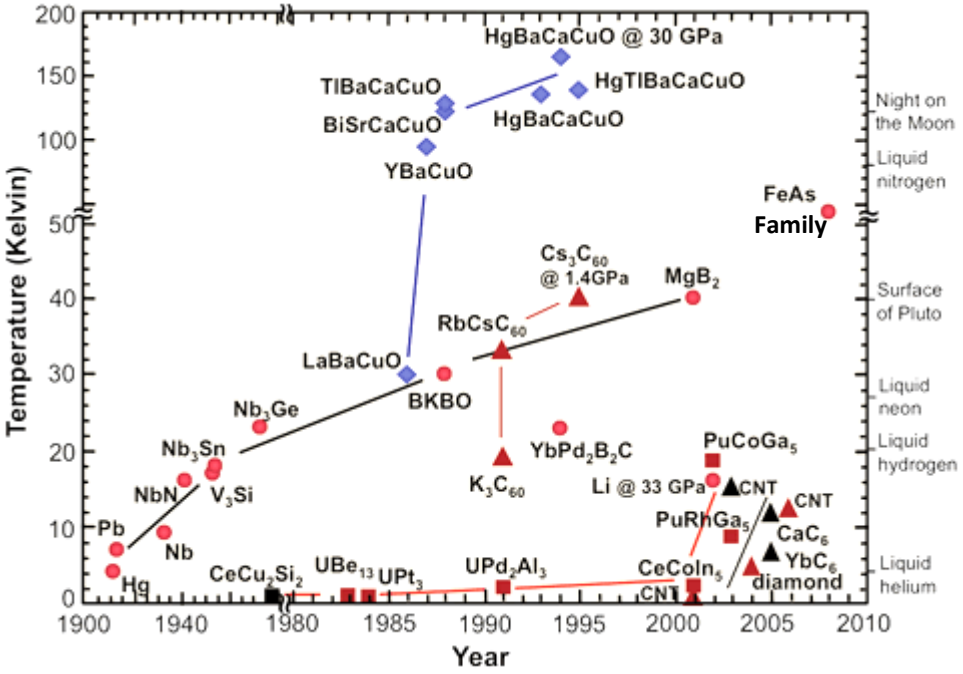

Fig 1.1: Superconductivity discovery over the time

A simple binary compound of Mg and boron, MgB_2, was discovered as a promising superconductor by Nagamtsu and his group in 2001. This simple binary compound showed highest T_c, 39 K, among other elemental or binary alloyed superconductors [6]. Due to spectacular properties of MgB_2, Many works have been taking so far to overcome existence obstacles and substitute this compound with expensive NbTi and Nb_3Sn wires in high magnetic field applications like MRI [7].

First iron based superconductor, lanthanum oxygen fluorine iron arsenide

(LaO1-xFxFeAs), was discovered in 2008 with T_c of 26 K [8]. Further study on this iron based superconductor revealed higher T_c around 52 K by replacing lanthanum with other elements such as samarium and neodymium [9, 10]. New compound, ($BaFe_{1.9}$ $Pt_{0.1}As_2$) with T_c around 23 K, in the family of FeAs-based superconducting materials was discovered year after [11]. Later in this year, high pressure technique was used for synthesis of $BaFe_2As_2$, resulted in higher T_c around 35 K [12].

American physicists John Bardeen, Leon Cooper, and John Schrieffer (the BCS theory) presented the first superconductivity theory. They won the Nobel Prize in 1972. According to the theory, the electrical transport in superconductors is due to the pairing of electrons (Cooper pairs) with opposite moment and spins instead of single electrons. The coherent travelling of electron pairs leads to resistance-less current flow through a superconducting material [13].

Josephson Effect predicted that electrical current would flow between two superconducting materials - even when they are separated by a non-superconductor or insulator [13]. This tunneling phenomenon was later confirmed and led him to win the Nobel Prize in Physics in 1973.

Superconducting materials applications are related to but not limited to: energy production storage, its distribution, in sensor materials, and high field magnets. Magnetic-levitation is one of the applications where transport vehicles such as trains can be made to "float" on strong superconducting magnets. A landmark for the commercial use of MAGLEV technology occurred in 1990 when it gained the status of a nationally-funded project in Japan.

In MRI, by impinging a strong superconductor-derived magnetic field into the

body as a non-invasive method, hydrogen atoms that exist in the body's water and fat molecules are forced to accept energy from the magnetic field. They then release this energy at a frequency that can be detected and displayed graphically by a computer. Through these data doctors are capable of predicting the illnesses faultlessly.

Today's MRI machines are made using niobium-alloy wires, which is quite expensive and requires liquid helium refrigeration to maintain superconducting properties, which also costly in maintaining. If the performance of MgB_2 can be improved, it can use to replace the expensive niobium-alloy wires, which reduces the cost of the equipment and higher T_c of MgB_2 is beneficial in reducing the cost for maintaining refrigeration. However, critical current density of pristine MgB_2 drops rapidly in the high magnetic field due to the weak pinning centers and low upper critical field.

Extensive researches have been performed to enhance the usability of MgB_2 including chemical doping, irradiation, thermo-mechanical processing techniques however chemical doping is known to be the simplest way to improve superconducting properties of it. Rapid developments in processing of MgB_2 in single crystals bulk samples, tapes, wires and thin films promise for the realization of practical applications in the near future.

The main objective of this research is to improve the superconducting performance of MgB_2 by means of chemical doping, to replace expensive superconducting materials and to understand the physics behind that as to ensure its benefits for large scale production.

1.2 Fundamental parameters in superconductivity

The critical temperature, *Tc*, the critical field, H_{c2}, and the critical current density, J_c, are three important parameters often used to characterize the performance of a superconductor. Special materials which show almost zero resistance to the electrical current flow and ideal magnetism below a certain temperature are called superconductors. This temperature is called the superconducting transition temperature or critical temperature (T_c). This temperature is the cross section between superconductivity and normal state which means, the resistivity back again above this temperature. As shown in Figure1.2, with increasing temperature above T_c, the resistivity regained again, and the material return to the normal state.

The critical temperature inherently depends on material's properties although impurities can vary this temperature a bit. In case of having pure and physically perfect materials, happening of sharp transition from normal state to superconducting state represents the pure material while a broadened transition belongs to less perfect crystal structure [13]. It has been earlier mentioned that Phenomena of showing perfect diamagnetism by a superconductor when it is in its superconducting state is known as Meissner effect.

The maximum current that can pass through superconductor in the superconducting state is known as the critical current [13, 14]. When this is expressed in terms of current per unit area, it is called the critical current density, J_c.

Above this value, the superconductivity is destroyed and the material turns back to the normal state.

Many intrinsic and extrinsic parameters can affect the critical current density which will be discussed further in the Chapter 2.

In case of applying magnet field, the superconducting state can be destroyed if

the applied field goes over the resistance of the superconductor. This threshold value is known as the critical magnet field and depends on the temperature by following a parabolic law (see eq. 1.1).

$$H_c = H_0 \left[1 - \left(\frac{t}{T_c}\right)^2\right] \quad (1.1)$$

Where, H_0 - critical field at absolute zero

Tc - transition temperature

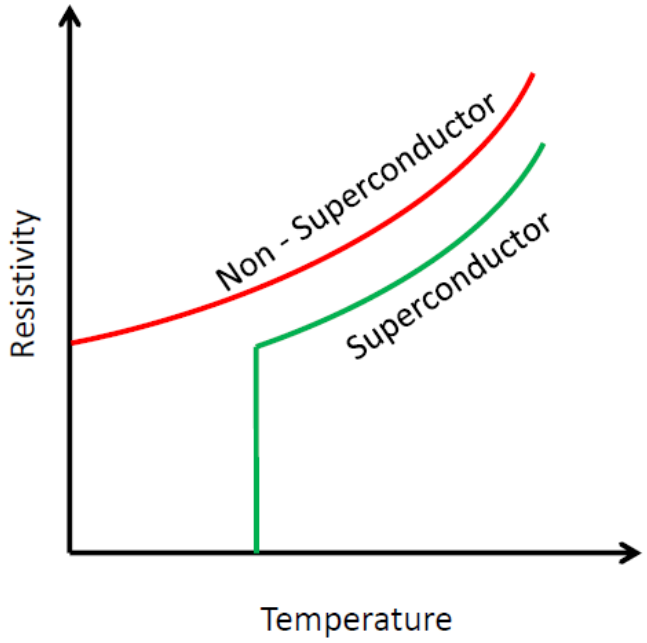

Fig 1.2: Temperature dependency in superconductor and normal material

The state of the superconducting material is determined by these three important parameters, i.e, J_c, T_c, and H_c, and therefore, they are called the critical parameters of the superconductor [14]. Relationship between critical parameters of a superconductor is elaborated in Figure 1.3.

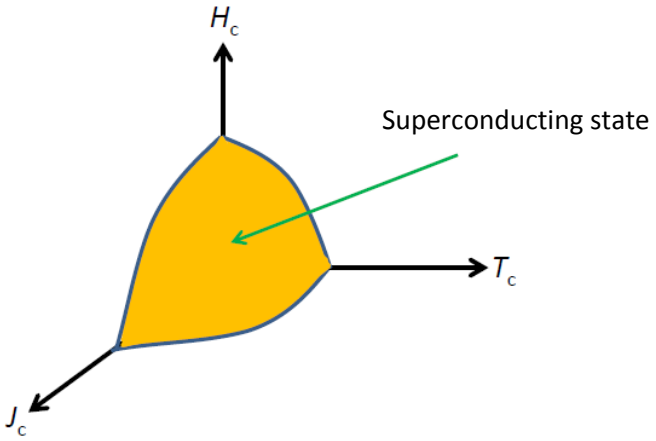

Fig 1.3: Relationship between three important superconducting parameters which determines the superconducting state [14]

Review on Meissner effect reveals that no magnet flux density exists in interior of superconducting material at superconducting state. Shield current creation is the result of superconductor due to exposition against the magnet field to cancel the applied magnet field [2, 13, 14]. So here the difference comes between a superconductor and a perfect conductor in expulsion of all magnetic fields by superconductor in superconducting state.

Two different responses of superconductors to the applied magnet field classified them into two different types as type I and type II.

Normally superconductors made of pure elements exhibit type I behavior while alloys generally shows type II properties [13, 14].

By exposing / placing a type I superconductor in a weak external magnet field, the field penetrates into the superconductor for only a short distance which is called the London penetration depth (λ_L), over which it decays to zero, according to Equation (1.2) given below [13, 14]:

$$B(x) = B(0)e^{\left(\frac{-x}{\lambda_L}\right)} \quad (1.2)$$

Where, B(0) - the flux density of the applied fields at the surface

x - the distance from the surface

however, the discrepancy was observed between the experimentally penetration depth, λ, and the London penetration depth, λ which was corrected by using the coherence length, ξ, and mean free path, l, according to the Eq. (1.3) [15]. The coherence length, ξ, is regarded as the distance between the surface and where the sample reaches the density of superconducting electrons which is of the order of 10^{-4}cm for a pure superconductor [13]. Here, ξ is treated as analogous to l and dependent on the purity of the material.

$$\frac{1}{\xi} = \frac{1}{\xi_0} + \frac{1}{l} \qquad (1.3)$$

Where, ξ_0 is the coherence length for a perfectly pure superconductor.

Reduction in coherence length increases by enhancing the impurity content [13, 16]. Thus the coherence length of an impure material is given by $\kappa = \lambda / \xi$, where κ is the Ginzburg-Laudau (GL) parameter.

Existence of impurities in superconductors leads to a higher normal state resistivity due to scattering of electrons which results in shortening of coherence length and higher K value [13].

Based on the BSC theory, existence of a gap in superconductors between the ground state and the quasi-particle state was seen with the width equal to 1.76 $K_b T_c$ where K_b is referred to Boltzmann's constant (see Figure 1.4). However all energy states are filled up to the fermi energy level for normal metals at absolute zero temperature [13]. BSC theory main concept is focusing on introduction of the so called cooper pairs which are responsible for the charge carriers in superconducting material. Tenancy of these cooper pairs is in a way to poses lowest energy level due to intensive electrons interaction near the Fermi energy level. Thermal agitation which is provided by rising the

temperature above absolute zero leads to de-pairing of these cooper pairs to decrease the energy gap Therefore, it will be zero at T_c.

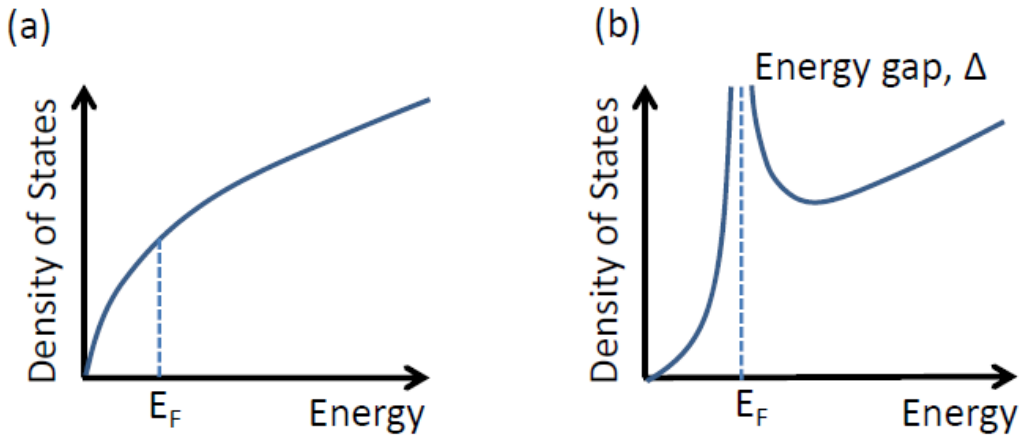

Fig 1.4: Density of states versus energy for metal in normal state (a) and in superconducting state (b) [16]

Abrikosov's investigation revealed the exact value of the GL parameter, K, which is used for classification of superconductor types when $\kappa < 1/\sqrt{2}$, the superconductor falls into type I, while if $\kappa > 1/\sqrt{2}$ the superconductor falls into type II [16].

Magnetic field penetration in type II superconductors showed same trend as in type I, up to the first critical field H_{c1}. But type II superconductor goes to the new mixed state (or Shubnikov state) by increasing the applied filed above the H_{c1}. Physical investigation revealed penetration of the magnetic field into the interior of superconductor in the form of the thin filament called magnetic vortices. Each of these magnetic vortices carries one magnetic flux quantum ($\Phi_0 = 2.067 \times 10^{-15}$ Tm^2) [14]. More vortices penetrate into the structure by further increasing of magnetic field above H_{c1}. But it needs to be noted that presence of magnetic vortices without movement under the applied field in the structure, as long as they are fixed, has no effect on the current flow. Normal cores surrounded by supper-current vortex form the flux lines which decay

over a distance of λ (T) for bulk samples. The diameter of the vortices is of the order of the superconductor coherence length, ξ, i.e. typically nanometers (coherence length of MgB_2 ≈ ξab(0) = 3.7–12.8 nm, ξ c(0) = 1.6–5.0 nm) [17]. Superconductors lose their superconducting properties at the upper critical field and back to normal state as can been in Figure 1.5.

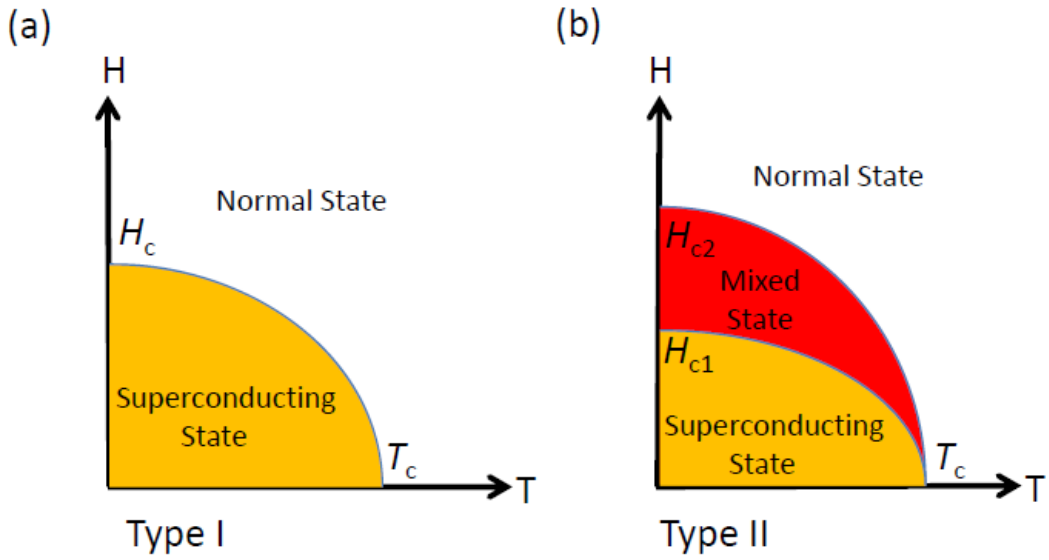

Fig 1.5: Diagram phase of type I (a) and type II (b) superconductors

As Figure 1.6 shows, flux lines tend to move under generated forces called Lorentz Force, when external current density, J, is applied to the type II superconductor in perpendicular direction of applied magnetic field. Obviously, generated Lorentz forces increase by increasing the applied magnetic field and can lead to vortices movement in the structure under enough force and result in resistivity in superconductor. Therefore, protective measures need to be taken for obstruction of the vortices movement in order to keep the material at the superconducting state. Pinning of the magnetic vortices can be effectively executed by structural defects such as dislocations, stacking faults, inclusions, impurities, and grain boundaries at atomic site

defects. It needs to be mentioned here that aforementioned defects act as effective pinning centers when their sizes match the vortices size. Therefore, the final performance of superconductor strongly depends on the type, density and extent of these defects which acting as pinning center for vortices in the superconductor structure [13].

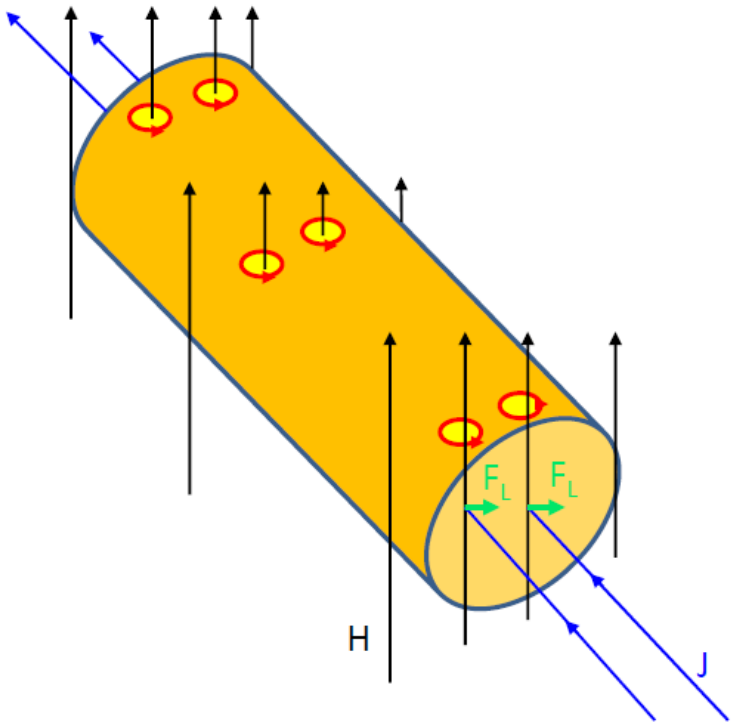

Fig 1.6: current transport in type II superconductor in mixed state [13]

Another important parameter in superconductors which determine the ultimate range of the magnet field for practical application is called H_{irr}. Above this field, which is known as de-pinning field as well, vortices start moving in the structure due to weak pinning and enhanced Lorentz force and result in low current density. Therefore H_{irr} value provides important information about the superconductor pinning properties, thus H_{irr} value close to H_{c2} value is a good indication of having strong pinning properties in the sample [13, 18].

1.3 Superconductor's application

Nowadays, superconducting materials are widely used in both commercial and industrial application such as but not limited to: energy production, storage, distribution, in sensor materials, and in high field magnets. The low-temperature superconductors (LTS), particularly NbTi (T_c of 9 K) and Nb3Sn (T_c of 18 K) are currently used in magnetic resonance imaging (MRI), nuclear magnetic resonance (NMR), and magnets for plasma fusion devices [7]. Outstanding properties of Nb - 47wt.%Ti alloy such as economically fabrication and manufacturing process, nano structure and its ductility have made this material suitable for high critical current application.

Nb_3Sn is one of the other promises superconducting material which now it's based-strand is fabricated in km length by possession of high critical current density [7].

Among the high-temperature superconductors (HTS), particularly bismuth strontium calcium copper oxide (BSCCO) (Bi-2223, T_c of 110 K, and Bi-2212, T_c of 85 K) and $YBa_2Cu_3O_{7-x}$ (YBCO, T_c of 92 K) are currently used for electric power applications and purposes [4, 7]. Electric generators made from superconducting wire are another fabulous invention compared to conventional generators wound with copper wire as their efficiency improved a lot. In fact, their efficiency is above 99%, and their size is about half that of conventional generators.

Recently use of superconductors in power generation application leads to tremendous improvement in relevant performances. Superconductor-based transformers and fault limiters are examples of superconducting materials in power generation application. In March 1997, The Swiss-Swedish Company

ABB was pioneer to connect a superconducting transformer to a utility power network followed by recent development of a 6.4 MVA fault current limiter - the most powerful in the world [19].

The most important application of superconductors in the electronic industry get engaged with ultra-high performance filters where the near zero resistance of the superconducting wire is vital and plays a great role. In another word, this is an ability of superconducting material to pass desired frequencies and block undesirable frequencies in high-congestion radio frequency applications such as cellular telephone systems. In military also there are widespread applications of superconducting materials. Use of HTSC superconducting quantum interference devices (SQUIDS) by the U.S. Navy for mines and submarines detection is an example of superconducting material application in military purposes. .in addition to those applications, Uses of superconductors in X-ray detectors and ultra-fast light detectors can be considered as emerging technologies [19].

Magnetic-levitation (MAGLEV) which is an interesting property and happened in presence of superconducting magnet results in flotation of transportation vehicle. Therefore friction eliminates between the train and track. In 1990, the nationally funded project in japan leads to the first commercial use of MAGLEV technology [19].

1.4 MgB_2 - Application in superconductivity

MgB_2 properties such as but not limited to high critical temperature, intrinsically “weak-link” free grain boundaries, rich multiple-band structure, and low fabrication cost resulted in a promising superconductor for high

magnetic field applications at temperatures near 20 K. The applications of MgB_2 are strongly dependent on the development of the cryo-cooler materials and systems. The cryogenic refrigeration systems and liquids which are required for operating at temperatures near 20 K are much less complex and more energy saving compared to those operate at temperatures of near 4 K. as an example, today's MRI machines are made using niobium-alloy wires, which are quite expensive and furthermore, they require liquid helium refrigeration to maintain their superconducting properties, which is also costly in an ongoing way. Therefore, improving the performance of MgB_2 can be the scientific and commercial solution for replacement of the expensive niobium-alloy wires and reduce the cost of the equipment. From other side, the higher T_c of MgB_2 is also beneficial by reducing the cost of maintaining the cryogenic materials. Many industry practical coils and magnets have been demonstrated by Hyper Tech Research (HTR) in the US, Columbus Superconductors in Italy, and Hitachi Ltd in Japan. First open MgB_2 MRI system consisting of 12 pancake shaped MgB_2 coils, each of them wounded of 1.8 km of MgB_2 wire, has been demonstrated by Columbus Superconductors and ASG Superconductors.

The MRI reached a central magnetic field of 1.0 T at an operating temperature of 16 K, produced cryogen-free open MRI systems. Application of MgB_2 is not limited to MRI magnets, and now is being used for FCL devices. This device which is being used in power transmission and distribution system provides a beneficial advantage by coping with continual increase in fault current levels which happens during upgrading existing power system and normally used to result in enormous cost.

MgB_2 outstanding properties in points of low manufacturing costs, the ability to form into long length wires and high critical current capacity under

economic cryogenic operational temperature resulted in use of this compound in the FCL applications. The performance of MgB_2 at high magnetic field applications is still under investigation, however, based on the preliminary laboratory achievements; it seems that, MgB_2 will be a strong competitor for Nb-based superconductors at high magnetic field applications in near future [7].

Having quick look to MgB_2 properties reveal that besides having a high *Tc*, the simple crystal structure, large coherence length, high critical field, transparency of grain boundaries to current flow, and low production - fabrication cost are all fascinating features for this binary compound to be used in both large-scale applications and electronic devices. Especially, from the economic- commercial point of view several times cheaper starting material, Mg and B, than Nb based superconductor attracted extraordinary attention from scientist to make it applicable for industrial usage.

But the major obstacle for MgB_2 at high magnet field lies on rapid drop of its critical current density due to weak pinning and low upper critical field. Many different processing techniques such as but not limited to chemical doping, irradiation, and thermo-mechanical processing have been examined on MgB_2 with the aim to improve its superconducting properties [20-31]. Among those techniques, Chemical doping is known to be the simplest and quickest way for improving the superconducting properties of MgB_2 and among the many investigated dopants , carbon dopants are at the forefront, due to their capability for improving the drawbacks of MgB_2, particularly in terms of enhancing the performance of *Jc* at high fields as well as enhancing the H_{c2} [18, 20-22, 24, 25, 32-38]. Rapid developments in the fabrication processing resulted in formation of MgB_2 in the forms of single crystals, bulk samples, tapes, wires, and thin films and hold promise for the realization of practical applications of

this compound in the near future.

1.5 Aim and outline of the thesis

The outline of the thesis is as follows;

Chapter 1: Comprehensive review on the history, fundamentals of the superconductivity, applications and the potential of MgB_2 for industrial superconducting applications.

Chapter 2: Full review on the superconducting properties of the MgB_2 as well as the fabrication processes

Chapter 3: Microstructural and crystallographic investigation on MgB_2 wire and correlation between the structural imperfection and critical current density.

Chapter 4: Detailed study of the pinning mechanism of MgB_2 wires treated with malic acid and their relationship with structural defects

Chapter 5: Investigation on the percolated nature of the MgB_2 current transport and correlation with the critical current density in terms of pinning mechanisms

Chapter 6: Introducing the power low relationship between the critical current density, micro structure and the n-value in MgB_2 superconducting wire

1.6 References

[1] H. K. Onnes, Comm. Phys. Lab. Univ. Liden, 122b (1911) pp.124.

[2] A. M. Forrest, European Journal of Physics, 4 (1983) 117.

[3] J. G. Bendorz, K. A. Muller, Zeitschrift fur Physik B Condensed matter, 64 (1986) 189.

[4] M. K.Wu, J. R. Ashburn, C. J. Torng, P. H. Hor, R. L. Meng, L. Gao, D. J. Huang, Y. Q. Wang, C. W. Chu, Physical Review Letters, 58 (1987) 908.

[5] A. Schilling, M. Cantoni, J. D. Guo, H. R. Ott, Nature 363 (1993) 56.

[6] J. Nagamatsu, N. Nakagawa, T. Muranaka, Y. Zenitani, J. Akimitsu, Nature, 410 (2001) 63.

[7] K. Vinod, R. G. A. Kumar, U. Syamaprasad, Superconductor Science and Technology, 20 (2007).

[8] H. Takahashi, K. Igawa, K. Arii, Y. Kamihara, M. Hirano, H. Hosono, Nature, 453 (2008) 376.

[9] Z. Wei, H.O. Li, W. Hong, Z. Lv, H. Wu, X. Guo, K. Ruan, Journal of Superconductivity and Novel Magnetism, 21 (2008) 213.

[10] R. Zhi-An, Y. Jie, L. Wei, Y. Wei, S. Xiao-Li, L. Zheng-Cai, C. Guang-Can, D. Xiao-Li, S. Li-Ling, Z. Fang, Z. Zhong-Xian, EPL (Europhysics Letters), 82 (2008) 57002.

[11] S. R. Saha, T. Drye, K. Kirshenbaum, N. P. Butch, P. Y. Zavalij, P. Johnpierre, Journal of Physics: Condensed Matter, 22 (2010) 072204.

[12] F. Ishikawa, N. Eguchi, M. Kodama, K. Fujimaki, M. Einaga, A. Ohmura, A. Nakayama, A. Mitsuda, Y. Yamada, Physical Review B, 79 (2009) 172506.

[13] A. C. Rose-Innes, E.H. Rhoderick, Introduction to Superconductivity, Second edition ed., Elsevier Science Ltd, Oxford OX5 1GB, England, 1969.

[14] W. Buckel, R. Kleiner, Superconductivity: Fundamentals and Applications, Second ed., WILEY-VCG Verlag GmbH & Co. KGaA, Weinheim, 2004.

[15] A. B. Pippard, Proceedings of the Royal Society of London. Series A. Mathematical and Physical Sciences, 216 (1953) 547.

[16] O.V. Shcherbakova, A.V. Pan, S.X. Dou, Manesium diboride supercoductors Development and Properties, First ed., VDM Verlag Dr. Muller Aktiengesellschaft & Co. KG and licensors, Germany, 2009.

[17] C. Buzea, T. Yamashita, Superconductor Science and Technology, 14 (2001) R115.

[18] E. W. Collings, M D Sumption, M Bhatia, M.A. Susner, S.D. Bohnenstiehl, Superconductor Science and Technology, 21 (2008) 103001.

[19] http://www.superconductors.org,

[20] J. H. Kim, S. Oh, Y. U. Heo, S. Hata, H. Kumakura, A. Matsumoto, M. Mitsuhara, S. Choi, Y. Shimada, M. Maeda, J. L. MacManus-Driscoll, S. X. Dou, NPG Asia Mater, 4 (2012) e3.

[21] Z. X. Shi, M. A. Susner, M. D. Sumption, E. W. Collings, X. Peng, M. Rindfleisch, M. J. Tomsic, Superconductor Science and Technology, 24 (2011) 065015.

[22] J. H. Kim, S. Oh, H. Kumakura, A. Matsumoto, Y. U. Heo, K. S. Song, Y. M. Kang, M. Maeda, M. Rindfleisch, M. Tomsic, S. Choi, S. X. Dou, Advanced Materials, 23 (2011) 4942.

[23] A. Kario, R. Nast, W. Häßler, C. Rodig, C. Mickel, W. Goldacker, B. Holzapfel, L. Schultz, Superconductor Science and Technology, 24 (2011) 075011.

[24] X. Zhang, D. Wang, Z. Gao, L. Wang, Y. Qi, Z. Zhang, Y. Ma, S. Awaji, G. Nishijima, K. Watanabe, E. Mossang, X. Chaud., Superconductor Science

and Technology, 23 (2010) 025024.

[25] X. Xu, S. X.Dou, X. L. Wang, J. H. Kim, M. Choucair, W. K. Yeoh, R. K. Zheng, S. P. Ringer, Superconductor Science and Technology, 23 (2010) 085003.

[26] J. H. Lee, S. Y. Shin, C. J. Kim, H. W. Park, Journal of Alloys and Compounds, 476 (2009) 919.

[27] R. C. L. J. V. Marzik, M. R. Nickles, D. K. Finnemore,J. Yue, M. Tomsic, M. Rindfleisch, M. D. Sumption, in: IEEE/CSC & ESAS European Superconductivity News Forum (ESNF), 2009.

[28] M Putti, R Vaglio, J. M. Rowell., Superconductor Science and Technology, 21 (2008) 043001.

[29] A. Wisniewski, R. Puzniak, J. Judek, C. Krutzler, M. Eisterer, H. W. Weber, J. Jun, S.M. Kazakov, J. Karpinski, Superconductor Science and Technology, 20 (2007) 256.

[30] A .Talapatra, S. K. Bandyopadhyay, P. Sen, A. Banerjee, R. Rawat., Superconductor Science and Technology, 20 (2007) 1193.

[31] B. J. Senkowicz, A. Polyanskii, R. J. Mungall, Y. Zhu, J. E. Giencke, P. M. Voyles, C. B. Eom, E. E. Hellstrom, D.C. Larbalestier, Superconductor Science and Technology, 20 (2007) 650.

[32] N. Varghese, K. Vinod, M. K. Chattopadhyay, S. B. Roy, U. Syamaprasad, Journal of Applied Physics, 107 (2010) 013907.

[33] O. V. Shcherbakova, A. V. Pan, S. X. Dou, R. Nigam, D. Wexler, Journal of Applied Physics, 107 (2010) 09E147.

[34] Z. Ma, Y. Liu, Q. Zhao, Z. Dong, L. Yu, Superconductor Science and Technology, 22 (2009) 085015.

[35] M. S. A. Hossain, C. Senatore, R. Fl¨ukiger, M. A. Rindfleisch, M .J.

Tomsic, J. H. Kim, S. X. Dou, Superconductor Science and Technology, 22 (2009) 095004.

[36] X. L. Wang, S. Soltanian, M. James, M. J. Qin, J. Horvat, Q. W. Yao, H. K. Liu, S. X. Dou, Physica C: Superconductivity, 408 (2004) 63.

[37] W. K. Yeoh, S. X. Dou, Physica C: Superconductivity, 456 (2007) 170.

[38] S. X. Dou, O. Shcherbakova, W. K. Yeoh, J. H. Kim, S. Soltanian, X. L. Wang, C. Senatore, R. Flukiger, M. Dhalle, O. Husnjak, E. Babic, Physical Review Letters, 98 (2007) 097002.

Chapter 2: MAGNESIUM DIBORIDE (MgB_2) LITERATURE REVIEW

2.1 Introduction

The discovery of superconductivity in MgB_2 emerged with its high critical temperature around 39 K which is the highest among other inter metallic superconductors has attracted great interest around the world [1]. Although high temperature superconductors are available but practical applications of MgB_2 rises up significantly due to its cheap fabrication cost, lower anisotropy, larger coherence lengths, and transparency of the grain boundaries to current flow, which makes it a significant applicant among other superconductors specially cuprates. Furthermore, a higher operating temperature and a higher device speed than the present electronics based on Nb are other promises of this binary compound, MgB_2 [2]. also, as earlier mentioned, the ease of fabrication in different forms such as bulk, wire, tape and thin film, is another fascinating feature of MgB_2 that supports its potential as the emerging superconductor for the next generation of superconductor's applications.

However enhancing the critical current density of MgB_2 is the only way to make this compound really viable. Although MgB_2 has emerged as a good candidate for many of the superconducting applications, but still more protective measures is needed to further enhance its superconducting properties to be suit with other application as well.

2.2 Crystal structure and two gap conductivity

The MgB_2 unit cell structure consists of a simple hexagonal AlB_2-type structure (space group P6/mmm), which is common among borides. Figure 2.1

shows The MgB_2 crystal structure [2].

In MgB_2 structure, hexagonal close-packed layers of magnesium separate graphite-type boron layers. The lattice parameters of MgB_2 are, a = 3.086 Å (equal to the in-plane Mg-Mg distance), and c = 3.524 Å (the distance between Mg- layers) which sit in the middle of the values of lattice parameters for the other AlB_2-type compounds. The magnesium atoms are located at the center of hexagons formed by boron atoms while donating their electrons to the boron planes which leads to fully ionization of Mg in the MgB_2 compound. It needs to be noted that the donated electrons to the system, however, are not localized on the anions and are spread over the whole MgB_2 lattice [3]. Similar to graphite, because of hexagonal structure, MgB_2 exhibits a strong anisotropy in the B-B lengths due to the significant longer distance between the boron planes than in-plane the B-B distance [4-6]. No structural transition reported so far for MgB_2 down to 2 K or under high pressure of 40 GPa [2].

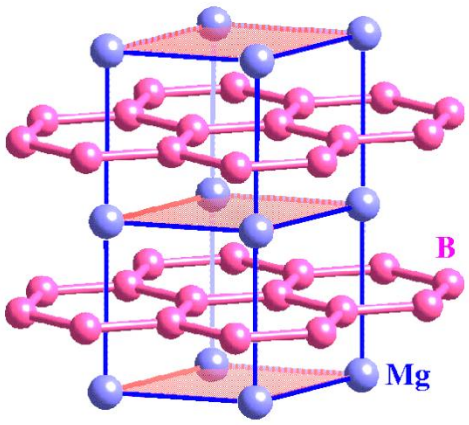

Fig 2.1: MgB_2 crystal structure

MgB_2 is the first among other binary compounds to fall onto the special group of multi-gap superconductors which was introduced 50 years ago. Many different experiments including heat capacity, Raman scattering, point

contacts, and optical and magnetic properties of polycrystalline samples or single crystals have been executed on MgB_2 structure to prove the multi gap nature of this compound [7-14].

The overlapping of the sp^2 boron orbitals create four bonds consisting of two σ-bonds within the neighboring atoms in the plane, while the remaining p orbitals extend above and below the plane and create other two π- bonds in MgB_2. One π-bond is conduction type, and the other one is valence type. The two other bonds are dimensional σ-bonds formed by the covalent p_{xy} boron orbitals and both σ-bonds are hole type [4, 5].

These four bonds create four discrete electron energy levels at the Fermi surface. Figure 2.2 shows The Fermi surface of MgB_2. Here, Γ, L, M, A are sites in Brillouin zone.in case of positioning of σ and π bands in Fermi surface, The σ-bands form two hole-like coaxial cylinders along the Γ- A line in MgB_2 structure while the π- bands form two tubular networks, one hole like near K and M, and an electron-like tubular network near H and L [3]. The asymmetry of the charge distribution in the σ-bonding with note to the presence of in-plane boron atoms provides strong coupling between the σ-bonding state and the in-plane vibration of boron atoms, which is mainly responsible for the superconductivity in MgB_2 [5, 15]. Existence electrons at these different Fermi levels form pairs with different bonding energies. Each π-bond and σ-bond has particular energy gaps at the Fermi surface. The average values of the gap are 6.8 meV and 1.8 meV for σ-bonds and for π–bonds respectively.

Experimental studies using several techniques, such as tunneling spectroscopy, point contact tunneling, specific heat capacity and etc, confirmed the existence of the two-gap superconductivity in MgB_2 [9, 10, 16-21].

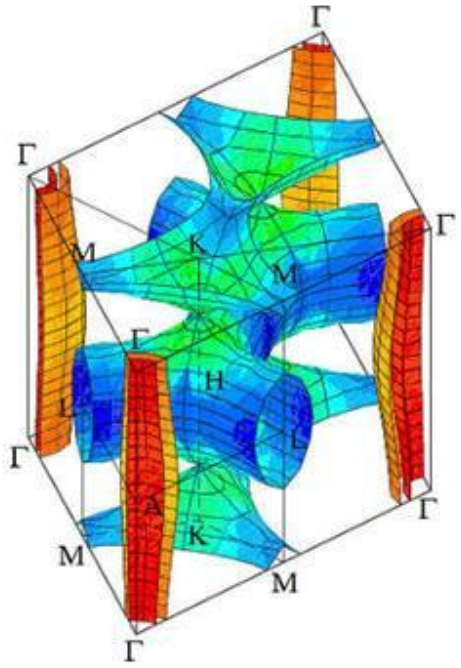

Fig 2.2: MgB_2 Fermi surface with Brillouin zone symmetry directions [4]

2.3 Fabrication methods

So far, MgB_2 has been fabricated successfully in various forms of bulk, thin films, powders, wires and tapes, as well as single crystals. Synthesis of the MgB_2 can be easily done by a simple chemical reaction route between B with Mg vapor, generally at temperatures above 650 ºC (which is the melting point of Mg). Figure 2.3 shows the binary diagram for Mg and B.

It has to be mentioned that the labels Solid, Liquid, and Gas in above diagram represent the Mg-rich solid, liquid, and gas phases, respectively [22]. From the MgB_2 equilibrium phase diagram, it is noted that the liquid phase of MgB_2 exists at the temperature range between 650 ºC-1000 ºC at 1 atm, which provide us a big sintering temperature range for MgB_2.

2.3.1 MgB_2 bulk

Two major processes called in-situ and ex-situ are used in fabrication of MgB_2. In the in-situ method, MgB_2 starting materials, B and Mg, are mixed and formed into the desired shape of pellet, wire or tape which is followed by a suitable heat-treatment under inert atmosphere (usually Ar) [23] while In the ex-situ method, already reacted powder of B and mg is used to form the sample into the desired shape [5, 24, 25].

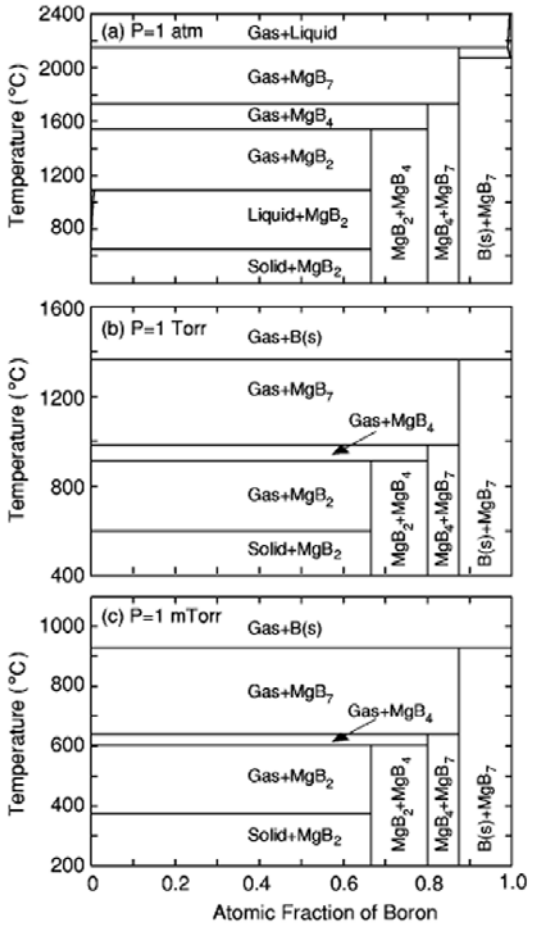

Fig 2.3: Binary phase diagram for Mg and B [23]

Higher density of final fabricated sample in ex-situ method is the main advantage of this method over the in-situ one; however, the main drawback of this is the poor grain connectivity due to already formed MgB_2 powder [6, 26, 27]. In addition to the poor grain connectivity which is earlier mentioned, the

commercially reacted powder normally shows a broad range of particle size distribution and leads to difficulties in controlling process parameters. Although use of milling devices, like Planetary ball milling, SPEX as well as fast milling processes, help in crushing the precursor powder and leads to fine grains of MgB_2 and more evenly distributes the MgO inclusions, which both have positive effects on improving the connectivity between the grains and flux pinning, and hence the critical current density [28-30]. But still the in-situ method leads to better results for MgB_2, such as better connectivity, relative ease in introducing doping, and better control over the stoichiometry. However, the biggest existing obstacle is the low density of the final product, which results in dissipation of the current flowing through the product [31]. Size and purity of starting material in in-situ prepared MgB_2 play an important role in grain connectivity [23, 28, 32]. The presence of MgO is inevitable in MgB_2 since the surface of Mg is easily oxidized in air and resulted oxide, MgO, is introduced to the system through the precursors. From the other side, boron usually contains B_2O_3 in small amounts. Therefore formation of MgO occurs faster than MgB_2 formation due to existence oxygen introduced in the system by precursor oxides and lower Gibbs free energy level for its formation than MgB_2 formation [33]. This greatly affects the inter-grain connectivity, and thereby also the critical current density [34]. According to Liao et al. [35], however, the presence of small amount of nano-size MgO is beneficial in increasing the effective flux pinning, and hence improving *Jc*.

Several techniques have been examined and introduced by many groups for increasing the density of MgB_2 based on applying high pressure and high temperature [36-38]. The in- situ product's density has been enhanced by applying hot iso-static pressing (HIP) and high pressure synthesis [31, 36, 39-42]. Flukiger et

al. [43] reported on a cold high pressure densification method which greatly enhanced the *Jc* due to improved density coming from better connectivity between the grains.

Mechanical alloying (MA) is another way to improve the superconducting properties of MgB_2. The high energy milling of starting materials results in fine grain structure of the end product which finally leads to enhanced superconducting properties. Mechanically alloyed samples show finer grains about 1000 times smaller than HIP samples and samples sintered at high pressure [30, 44-47]. The observed enhancement in H_{irr} and high *Jc* manifest improved flux pinning of MA samples. The reason behind lies on the smaller grains and the enhanced number of grain boundaries result in more pinning centers against vortices movements. Adding carbon as a dopant to the MgB_2 starting materials and using the high energy mechanical milling leads to huge enhancement of the critical current density and the upper critical field [44, 48].

Diffusion method is another way of fabrication high dense MgB_2, where Mg diffuses into the formed bulk or wire sample of B during synthesis process. The process is rather simple; however, a long sintering time is needed to obtain better properties. This long sintering, on the other hand, gives the advantage of better crystallinity. Compare to the in-situ process, the boron pellet that is buried in the Mg source in the diffusion method offers highly dense product. Less formation of MgO due to the low MgO diffusivity is another advantage of this technique. Therefore, this process offers a highly denser product with better *Jc* performance resulted from less voids formation in the final MgB_2 structure [49, 50].

2.3.2 MgB_2 tapes and wires

There is limited room for bulk samples in practical applications, while long-length conductors in the form of tapes and wires play critical role in practical application. Wires and tapes normally are fabricated based on the powder- in-tube (PIT) process and continuous tube forming and filling (CTFF). PIT process involves in filling metallic tubes with powder, followed by swaging, drawing and rolling the filled tubes into wires and tapes, as shown in Figure 2.4 [51]. Unlike the low *Tc* superconductors, NbTi and Nb_3Sn superconductors, weak links does not significantly affect the MgB_2 superconducting properties and still shows high transport critical current densities for tape and wire samples [43, 52-54]. The difference between in-situ and ex-situ PIT process stands in powder preparation. In in-situ method, a mixture of Mg and B powders is used to fill the metallic tubes followed by subsequent deformation and heat treatment [26, 55] while in The ex-situ PIT technique, already reacted MgB_2 powder is used directly for filling of the metallic tubes followed by the same deformation. Heat treatment at 600-1000 °C is usually applied to the cold-worked tape or wire to obtain superconductivity properties [2, 56].

Although the ex-situ fabrication process is cheaper and simpler due to no need for mixing the starting material powders but still the in-situ process has more advantage in case of improving the performance of *Jc* by many different methods such as chemical doping [27, 57].

The sintering temperature range for MgB_2 has been already mentioned, 600 to 1000 ° c, and many metals can react with Mg+B powders in in-situ and with MgB_2 powder in ex-situ method at this temperature range therefore, due to the effect of the sheath material on MgB_2 superconducting properties, selection of the sheath material for the fabrication of MgB_2 wires and tapes plays a crucial role in the final performance. Generally, normal metal cladding provides

parallel electrical conduction, acts as the thermal stabilization and protects the MgB_2 core against the mechanical deformations. To summarize the above talk, the MgB_2 sheath material must be selected in a way to preserve MgB_2 superconductivity and poses enough hardness and ductility to undergo much mechanical deformation to form the final product.

So far, the usual sheath materials which have been applied to MgB_2 core are stainless Steel (SS) [33, 51], iron [43, 57-63], Cu [56, 64, 65], Ag [65, 66], Ni [64, 67], and Cu–Ni [30,68-70]. Considering the commercialization of MgB_2 as well as its process condition, however, iron, so far has been found to be the best material for MgB_2 due to its ductility, low cost, and light weight, as well as its suitability for the fabrication process in large-scale of industrial production [71, 72].

In the CTFF process, which is another wire fabrication technique, powder is fed onto a strip of metal which this strip then being rolled to form a tube by continuously passing through different rolling rollers. In this technique, High purity of the long metallic strips, containing powders on it, are rolled continuously into a tube with an overlap-closed tube process and the powder being enclosed in the rolled sheath. In next step, the closed tube can be inserted into a seamless tube and deformed to the round wire [5, 68].

Another fabrication technique which is reactive liquid infiltration [73] has been used to fabricate both mono-filamentary and multi-filamentary wires several tens of meters in length. The process starts with inserting the cylindrical Mg rod into a steel clad thin niobium (Nb) tube and filling surrounding the Mg rod with fine boron powder. Sintering and heat treating of the MgB_2 compound inside the Nb tube result in a very compact, dense and finely grained MgB_2 in final fabricated product.

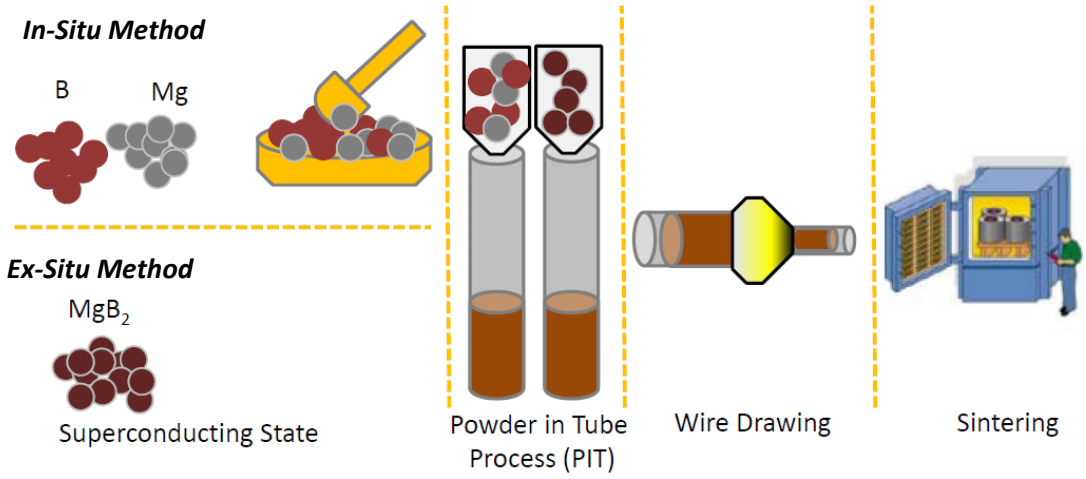

Fig 2.4: Powder in Tube (PIT) wire fabrication method for In-Situ and Ex-Situ methods [54]

Almost in a similar way, Togano et.al used the interface diffusion reaction method between a Fe-Mg alloy and a boron layer for fabrication of MgB_2 tape. In this method, Mg, in the Fe-Mg alloy, diffuses into the interface of the alloy and the boron layer during the heat treatment and leads to formation of a thin Mg rich layer. This rich Mg layer acts as a Mg source for formation of MgB_2 phase. Single crystals are currently fabricated by the solid–liquid reaction method using precursors of rich Mg, under high pressure in an Mg-B-N system and by the vapor transport method [75, 76].

Recently, Nishijima et al. [77], significantly improved the critical current density (nearly five times larger at 4.2 K at 5 T compared to the PIT process) and the transverse compressive stress tolerance of MgB_2 wires fabricated based on the internal Mg diffusion, IMD, technique [77]. The achieved improvement by this technique is attributed to better grain connectivity and more grain boundary pinning. This method can be considered as an improved version of the diffusion process, first reported by Giunichi and co-workers [73].

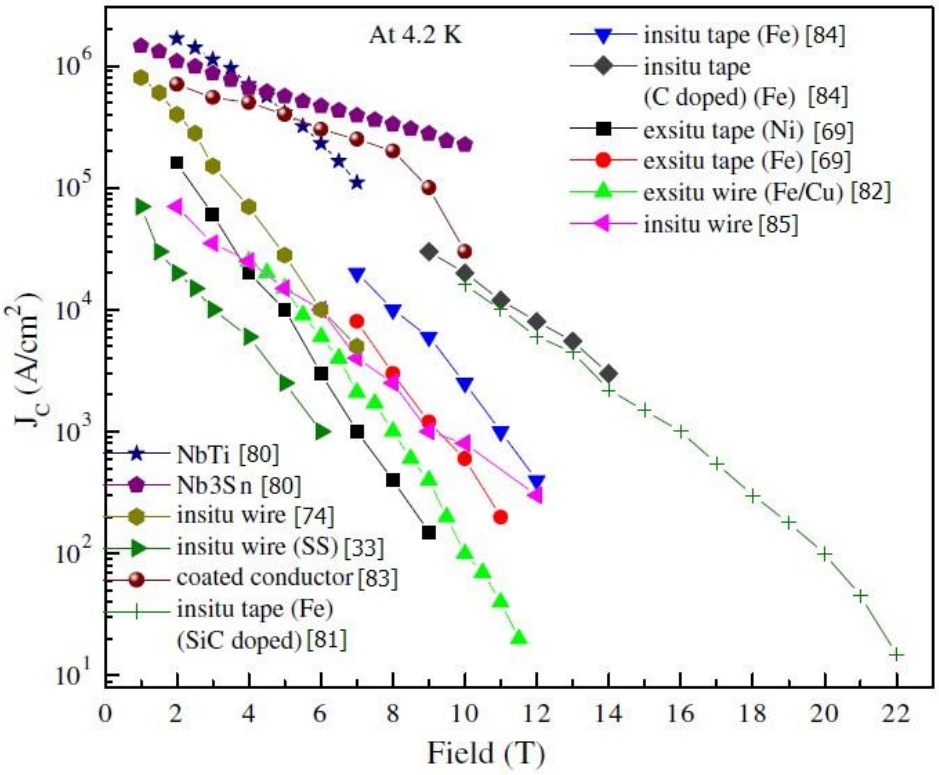

Fig 2.5: comparison between transport J_c of MgB_2 fabricated by different methods with other commercial superconductors (Data for the figure were taken from references given in the square brackets.) [80]

Although higher density and better connectivity are advantages of this method than the PIT process but from a practical point of view, this method is currently only suitable for making short samples due to hollow section in the middle of fabricated wire and brittle structure of the MgB_2. However; the feasibility of fabrication of long- length wires is under investigation. Figure. 2.5 shows a comparison of transport *Jc* in applied fields of MgB_2 conductors fabricated by different methods [2, 33, 54, 67, 73, 78-82].

2.4 Properties of MgB_2

The superconductor properties are defined by its critical temperature (T_c), the critical current (I_c) or critical current density (J_c), upper critical field (H_{c2}), and

the irreversibility field (H_{irr}). Superconductor's application purely depends on its superconducting properties and since one of the most important applications of superconductors is in the area of high current and high fields, therefore superconductors with higher J_c at higher applied magnetic field are preferred. Unfortunately the critical current density (J_c) of pristine MgB_2, however, drops rapidly by increasing the magnetic field, due to its poor pinning, low density and low upper critical field, H_{c2}. In order to get the benefit of the high T_c of MgB_2, the above- mentioned parameters need to be improved. So far the superconducting properties of MgB_2 have been already optimized by several techniques, such as chemical alloying, mechanical alloying, irradiation, and thermo-mechanical and magnetic shielding techniques.

2.4.1 Critical temperature

Critical temperature (*Tc*) is one of the most important parameter which limits the application temperature of a superconducting material. The *Tc* of MgB_2 is around 39 K (-234 ºC), which is the highest among the inter-metallic superconductors [1]. Crystal structure has a great impact on the value of *Tc*, hence, *Tc* get affected by variation in lattice parameters [83, 84]. Laboratory results revealed that some changes in the MgB_2 fabrication process, such as iso-static pressure [85-87] or neutron irradiation [88, 89], lead to changes in the MgB_2 lattice volume, which is responsible for reduced *Tc*. Furthermore, many studied performed on variation of stoichiometric compound and revealed that Mg deficiency could increase the MgB_2 lattice strain, which results in Tc deduction [90]. Another factor which reduces the MgB_2 T_c is attributed to its low crystallinity which results in higher disorder in the lattice

[91].

2.4.2 Critical current (I_C) / critical current density (*Jc*)

Critical current (Ic) or critical current density (*Jc*) is known as another important parameter in superconductors which determines the application of superconductor. Equation (2.1) provides The de-pairing current density (J_d) or the highest achievable current density in superconductors [92], which almost 15% of this current density can be achieved by optimization of flux pinning. Jd at 0 K and magnetic field > 1 T, is around 1.3 × 10^8 A/cm^2 in MgB_2, considering the parameters as λ = 80 nm and ξ = 12 nm [16].

$$J_d = \frac{\Phi_0}{3\sqrt{3\Pi\lambda^2\varepsilon_{\mu_0}}} \qquad (2.1)$$

Where Φ_0 is the superconducting flux quantum and μ_0 is the magnetic permeability.

This value is relevant for fields above 1 T, however, at zero-field, the value increases to 2 × 10^8 A/cm^2, since the π-band contribution increases in de-pairing current at low fields. However, it has to be considered that contribution of the π- band charge carriers in the de-pairing current is only 10% [6]. High inter-grain and intra-grain *Jc* in MgB_2 help this compound to show high transport current densities at low temperatures. The reported transport *Jc* in the wire/ tape geometry at 4.2 K is of the order of 10^6 A/cm^2 in self field and around 10^4 A/cm^2 at 8 T field [78].

Weak pinning in MgB_2 single crystal leads to low critical current density and rapid drop of *Jc* by increasing the magnetic field. Reported *Jc* of single crystal is nearly 10^5 A/cm^2 at low temperatures in self field [16, 93] while Thin films

show much higher critical current densities than single crystals, owing to their strong pinning at their grain boundaries. The highest *Jc* observed so far in tape is 3-4 × 10^7 A/cm^2 under self-field at low temperatures [16]. Fabricated Wires through the CTFF process showed values of *Jc* around 6 × 10^5 A/cm^2 at 4.2 K under self-field. The variation of J_c with magnetic fields becomes more gradual, however, allowing larger current density values at higher field: J_c at 5 T > 10^5 A/cm^2. By comparison between tapes and wires, it can be seen that tapes can achieve superior currents at relatively high magnetic fields than wires due to their geometrical shielding properties.

Many factors affect the MgB_2 critical current density including but not limited to grain boundaries, porosity of the sample, presence of impurities, purity, particle size distribution of precursor materials, and sintering conditions.

The grain boundaries act as weak links in superconductor and thereby reduce the inter-grain connectivity and results in limitation of J_c in high temperature superconductors (HTS) but the grain boundaries in MgB_2 are not only transparent to current flow, but also help to improve the J_c by grain boundary pinning [94]. Ball milling techniques are used to minimize the grain size which leads to more grain boundaries and finally results in higher *Jc* in MgB_2 [30].

Unfortunately the porous structure of MgB_2 is one of the obstacles which reduce the transport *Jc* [95]. Fabrication of dense MgB_2 structure in in-situ process is hard to be controlled due to the low packing density of the powder in the preparation and the evaporation of Mg during sintering process. Porosities in ex-situ process originates from the low packing density of the powder, however, the final high temperature heat treatment minimize the final porosity [51, 56, 61, 64, 71, 72, 96].

Starting powder purities and their particle size variation have strong direct

effect on the final product's grain size, grain connectivity, and superconducting properties. In has been reported by some authors that adding Mg extra than stoichiometric compound provides better mechanical, electrical, and superconducting properties by resulting in better grain connectivity, compared with the MgB_2 synthesized from stoichiometric starting elements [78, 97, 98].

The effect of the Mg on the critical current density has been studied in state off the art by Kumakura's group [99]. They improved the *Jc* of MgB_2 by using of MgH_2 as the Mg source. MgH_2 provides highly fresh and reactive Mg which favors the formation of high purity MgB_2.

Enhancement in the transport J_c value of MgB_2 tape by doping 10% SiC and use of nano-sized Mg powder has been reported by Yamada et al. Relevant values showed five times higher than those for tapes prepared with commercial Mg powder [100]. It needs to be noted that mixture of ultra-fine Mg with B powder by ball milling results in outstanding enhancement in MgB_2 *Jc* due to better grain connectivity [101, 102] but the nature of the boron precursor has the most influence on the superconducting properties of the MgB_2. Systematic studies on the effects of the boron source on the critical current density, resistivity, and phase formation have been executed by many different groups [103-106]. Two different structure of boron powder, crystalline and amorphous, resulted in two different J_c values which the samples made from crystalline boron powders show nearly an order of magnitude lower J_c compared to those made from amorphous precursors, which comes from different structure results in different reactivity rates. Zhang et al. [107] reported on significant enhancement of MgB_2 J_c made of crystalline boron by using ball-milling process. Enhancement came from higher reactivity due to smaller grain size

which results in in better connectivity and strong flux pinning. Effect of different crystalline boron purities on the superconducting properties of MgB_2 using 92% and 96% purity boron powders as precursors has been recently reported by X. Xu et al. [32]. Detailed study performed by the same group on the ball milling medium effect on the superconducting properties of MgB_2 [108]. Carbon content organic solvents improved the J_c of MgB_2 but Toluene has been identified as the most promising medium for ball milling among others such as ethanol and acetone. The most effective pinning centers are formed by grain boundaries in pure MgB_2 [27, 50, 109, 110]. The relationship between the crystallinity and the irreversibility field, and their effects on the critical current density has been systematically analyzed by Yamamoto et al. [111] systematically analyzed using the full width at half maximum (FWHM) values of peaks derived from powder X-ray diffraction. It needs to be noted that The FWHM of the (110) peak represents the in-plane disorder, while the FWHM of the (002) peak reflects the out-of-plane disorder. Low sintering condition as well as doping reduces crystallinity lead to apparently larger FWHM. Crystallinity degrades by disordering crystal lattice caused by various types of lattice defects or intra-granular precipitates [111]. Since the grain boundaries pinning force is controlled by the grain size and lattice strain therefore, both small crystal size and lattice distortion lead to improvement in grain boundary pinning forces.

2.4.3 Critical fields

MgB_2 is classified in type II superconductors characterized due to have two critical fields, called the upper critical field (H_{c2}) and the lower critical field

(H_{c1}). This is an intrinsic property defined by the B, T phase boundary between the superconducting and normal states of a type II superconductor. MgB_2 is an anisotropic material due to its inherent layered structure of boron planes which causes variation in the critical field values from the planes parallel to and perpendicular to the ab-plane, and these are denoted as $H_{c1(c2)} \| ab$, $H_{c1(c2)} \perp ab$. Anisotropy plays an important role in MgB_2 practical applications, since it strongly affects the pinning mechanism and critical currents [5]. the anisotropy ratio $\gamma = H_{c2} \| ab / H_{c2} \perp ab$ reported for textured bulk and partially oriented crystallites is between 1.1 and 1.7, while for c-axis-oriented films and single crystals is 1.2–2 and 1.7-2.7 respectively . Purity of the sample and parameters such as the penetration depth and the coherence length directly affect the value of the critical fields.

High purity single crystal samples have shown $Hc1 \| ab$ =250 mT, $Hc1 \perp ab$ = 120 mT at 5 K [112] and $H_{c2} \| ab$ =18 T, $H_{c2} \perp ab$ = 3.5 T at 0 K [112-114]. For polycrystalline materials the value for $Hc1$ at 0 K has varied from 150 to 480 Oe [19]. Pure polycrystalline MgB_2 shows rather low H_{c2} values (16 T at 0 K), however this can be greatly improved by chemical doping [69, 115-121]. MgB_2 critical field value can be improved by introducing the proper dopant into the structure results in structural disorder.

According to the equation (2.2), $Hc2$ is determined by ξ.

$$H_{c2} = \frac{\Phi_0}{2\Pi\mu_0\varepsilon^2} \qquad (2.2)$$

Where ξ is the coherence length, Φ_0 is the superconducting flux quantum, and μ_0 is the magnetic permeability [111]. According to equation (2.2), the H_{c2} of a superconducting material is inversely linked to its coherence length ξ,

therefore decrease in the coherence lengths results in the critical field enhancement [2, 6, 111]. Therefore, the impurity scattering increases the H_{c2} by resulting in a shorter mean free path, which causes a reduction in ξ. Increase in the MgB_2 structural disorder increases the electron scattering in the σ- and π-bands, which then accordingly affects the critical fields [6]. The coherence length values for polycrystalline MgB_2 along the ab- plane stands between 3.7 and 12.8 nm and along the c-axis they range between 1.6 and 5.0 nm. For single crystals they range along the ab-plane range between 8 and 12 nm and along the c-axis between 3 and 7 nm [5, 112]. Since MgB_2 has been classified in type two superconductors therefore the tuning of the intra-band to inter-band scattering ratio by selective dopant on both Mg and boron sites can improve the H_{c2} and reduce the anisotropy of the critical fields.

2.4.4 Irreversibility field

Knowledge of the irreversibility line comes as an important parameter in practical applications due to confinement of non-zero critical currents with the magnetic field below this line. The values of irreversibility fields at 0 K range between 6 and 12 T for MgB_2 bulk, films, wires, tapes, and powders. The H_{irr} of MgB_2 is ~0.5$Hc2$, in contrast to H_{irr} 0.8 H_{c2} for the low temperature superconductor (LTS) material [78]. Investigation of Yamamoto et al. [111] on structural disorder revealed strong relationship between the crystallinity and the H_{irr} of MgB_2.

They reported that grain boundary pinning is improved by increasing disorder in MgB_2 structure, which originated from the degradation of crystallinity, and hence improve the H_{irr} as well.

2.4.5 Flux pinning mechanisms

As mentioned above, increasing the applied filed above H_{c1} in a type II superconductor, generates a mixed state between superconductivity and normal state in a way that magnetic field additionally penetrates into the interior of superconductor in the form of thin filaments called vortices. The vortices movement in the structure results in resistivity, therefore, effective pinning of these vortices results in wider range of the superconductivity in type II superconductor material. Structural atomic defects such as inclusions, impurities, dislocations, and grain boundaries effectively pin vortices at atomic sites. These structural defects become the most effective pinning centers when their sizes roughly match the size of the vortices, i.e. the coherence length.

Practical performance of superconductors is greatly affected by the effectiveness of vortex pinning, and therefore, by the type, density, and extent of the defects, as well as by *Tc*, ξ and λ [5, 6, 93, 122]. As earlier mentioned, grain boundaries are considered to be the most dominant pinning centers [27, 50, 109, 123], while small MgO and $Mg(B,O)_2$ impurities in Δk- pinned grains also contribute to better pinning [24, 40].

Based on Dew-Hughes pinning mechanisms model, the normalized pinning force density can be expressed as in equation (2.3) [122].

$$F_P(b) = \frac{F_P}{F_{Pmax}} \propto b^p(1-b)^q \qquad (2.3)$$

Where the dimensionless parameters p and q depend on the specific characteristics of flux pinning in the superconductor, and b is the reduced field

(H/H_{c2} or H/H_{irr}).

Under this model, six different pinning mechanisms are defined, depending on the p and q values [5].

p = 0, q = 2	normal core pinning, volume
p = 1, q = 1	Δk-pinning, volume pins
p = 1/2, q =	normal core pinning, surface
p = 3/2, q =	Δk-pinning, surface pins
p = 1, q = 2	normal core pinning, point
p = 2, q = 1	Δk-pinning, point pins

This model although shows practicality to analyze the existence pinning mechanism in MgB_2 structure but unfortunately the p and q parameters obtained from the fitted results do not fall onto any of the above values.

Instead, another pinning mechanism based on the vortices and pinning centers which has been proposed by Qin et al. [124] has been used in this study. The δT_c pinning and δl pinning are two derived mechanisms involved in the core interaction. The spatial variation of the Ginzburg-Landau (GL) coefficient α associated with disorder in the T_c generates The δT_c pinning while the variation of the charge-carrier mean free path l near lattice defects generates the δl pinning. Solid vortex region analysis by this model defined different regions in terms of the single vortex, small-bundle, and thermal fluctuation regimes, depending on the applied magnetic field. The crossover field, B_{sb}, is defined as the field separating the single vortex regime from the regime where

the vortices form small bundles, below which the J_c is almost independent of the applied field.

The variation of B_{sb} with reduced temperature ($t = T/T_c$) for δT_c and δl pinning is given by equation (2.4) and (2.5), respectively:

$$B_{sb} = B_{sb}(0)\left[\frac{1-t^2}{1+t^2}\right]^{\frac{2}{3}} \quad (2.4)$$

$$B_{sb} = B_{sb}(0)\left[\frac{1-t^2}{1+t^2}\right]^{2} \quad (2.5)$$

This has been discussed in detail, with reference to the experimental data in Chapter 4 and Chapter 5.

2.4.6 Resistivity

Rowel et. al. analysis revealed a wide range reported resistivity values for MgB_2 so far. The reported resistivity values at room temperature vary from 20 μΩ cm up to 100 mΩ cm, covering all the sample types from bulk to thin films. Poor connectivity coming from the reduction of effective cross-sectional area of the sample results in high resistivities seen in many samples. Although the un-packed active cross section area results in a reduction in *Jc*, however, is not the only cause to explain the resistivity behavior of MgB_2. The presence of insulating precipitates in grain or in grain boundaries, the presence of porosity and the substitution of atoms, such as, carbon for boron, are some of the other factors affecting the resistivity of MgB_2.

The normal state resistivity in metals is controlled by contribution of two

important factors which the first one is the temperature dependent residual resistivity, ρ_0, originating from electron scattering at defects and second one is the phonon-mediated contribution, ρph, which increases with temperature [16].

$$\rho_T = \rho_0 + \rho_{ph}(T) \quad (2.6)$$

However, the final resistivity is given by the equation (2.7) for the two-band conductors, considering the two band conductivity.

$$\frac{1}{\rho(T)} = \frac{1}{\rho(\sigma(T))} + \frac{1}{\rho(\pi(T))} \quad (2.7)$$

Electron scattering at both σ- and π-bands strongly affect the resistivity at low temperatures; however, electron scattering at the π- band dominates the resistivity value at room temperature. The mean free path of the charge carriers in both bands is reduced by introducing of defects into the structure.. The temperature dependence of the resistivity in MgB_2 follows a power law relationship according to Equation (2.8), which is expected for metals according to the Bloch–Gruneisen behavior.

$$\rho(T) = \rho(0) + aT^n \quad (2.8)$$

Where, ρ0 is the residual resistivity, a is a parameter, and n is the power law dependence of the resistivity, which indicates the disorder of the material [126]. This model has been used to analyze resistivity in this study.

In addition, based on Sidorenko et al. model, the resistivity value near the superconducting transition point has been extracted to analyze the dependence of the flux-flow activation energy, U_0 [127], which is used to interpret the flux creep or flux flow mechanism in MgB_2, based on the thermal activation of flux line motion over the energy barrier U_0 of the pinning centers.

In this model, the thermally activated flux flow is expressed by the equation (2.9).

$$\rho(T,B) = \rho(0)exp\left[\frac{-U_0}{K_B T}\right] \quad (2.9)$$

here, U_0 is the flux-flow activation energy, which can be obtained from the slope of the linear part of the Arrhenius plot, ρ0 is a field independent pre-exponential factor, and k_B is Boltzmann's constant. This has been discussed in detail, with reference to the experimental data in Chapter 5 and Chapter 6.

2.5 Effects of doping on the superconductivity of MgB_2

So far many techniques such as, chemical doping, ball milling, thermo-mechanical processing and proton irradiation improved the critical current density of MgB_2. But however, chemical doping is considered as an especially easy and effective way to enhance the superconducting properties of MgB_2.

The dopant materials enter in the MgB_2 structure by two categories called substitution and addition effects. In the substitution mode, the dopant will be substituted into the B or the Mg crystal sites and result in impurity scattering of charge carriers yield changes in the electronic state, lattice distortions, and crystallinity. The addition effects, in contrast, will only act between the grains, producing a substantial effect on the grain growth and grain connectivity [119].

Although chemical doping improved many of MgB_2 superconducting properties but it affects the T_c adversely. Eisterer et al. [16] has explained four potential mechanisms that can reduce the T_c in reduction of the density of

states (DOS), reduction of the σ- gap anisotropy, hardening of the E_{2g} phonons, and intra-band scattering. Any changes in the lattice parameter changes the DOS and affects the T_c since also affect the E_{2g} phonon frequency [16, 86, 87, 90, 128, 129]. The highest *Tc* so far reported was 41.8 K for thin MgB_2 layers on boron crystals or for films grown on SiC [16].

So far, many dopants such as metal elements (Ti, Zr, Mo, Fe, Co, Ni, Cu, Ag, Al, Si, La and etc.), metal oxides (Al_2O_3, HoO_2,MgO, TiO_2, SiO_2, PrO_{11} and etc.), carbon and carbon inorganics (nano-C, C nanotubes, nano diamond, TiC, SiC, B_4C, Na_2CO_3 and etc.), nitrides, borides and silicides (Si_3N_4, ZrB_2,TiB_2, NbB_2, CaB_6, WSi_2, $ZrSi_2$ and etc.) and organic compounds (malic acid, maleic anhydride, paraffin, carbohydrate, toluene, ethanol, acetone, and tartaric acid) have been doped into MgB_2. The effects of doping those elements on the superconductivity of MgB_2 have been reported by many groups around the world [6]. Due to the large number of possible dopants, as can be seen from above paragraph, it is not possible to summarize the effects of each dopant on the superconductivity of MgB_2. Only the effects of some dopants, which showed considerable positive or highly negative impact on the superconductivity of MgB_2, will briefly be discussed here.

2.5.1 Effect of carbon (C) doping on the superconductivity of MgB_2

The metallic elements and metal oxides were introduced into the MgB_2 structure to generate the normal flux pinning centers, however, borides, nitrides, and C-containing dopants are more useful due to increasing H_{c2} while introducing pinning centers as well into the structure [6].

Proper doping can be resulted in following improvements:

- Enhancement of H_{c2} and H_{irr} due to more impurity scattering

- Wider distribution formation of point pinning centers.
- Generation of Localized lattice strains which is also in favors of flux pinning

So far carbon shows the most significant effect on improving the superconducting properties of MgB_2 Among the other dopants and therefore, abundant research work has been carried out so far to study this phenomenon. By using carbon as dopant, these elements will substitute into boron sites in MgB_2, and greatly impacts the carrier density due to having one more electron than boron. Therefore carbon donates more electron to the σ-band, hence modifying the superconducting properties such as J_c, H_{c2}, and H_{irr} [5, 6, 119]. But however the carbon doping showed vice versa effect on the transition temperature and reduced the T_c value due to the disorder originating from impurity/ defect formation within the MgB_2 grains [90, 91, 118, 119].

Calculation in MgB_2 band structure revealed that electron doping results in a reduction in the density of states (DOS) at the Fermi Level (E_F) [130]. The theoretical calculations show that the DOS at EF decreases due to the effects of carbon doping on boron sites [131]. The phonon spectra of carbon doped sample revealed a considerable peak shift of the E_{2g} mode towards higher energies compared to the un-doped MgB_2 [132, 133].

It needs to be mentioned that there is a difference between the nominal and actual C substitution levels. Depends on the fabrication process and technique as well as homogeneity of starting materials, the reported solubility of C in MgB_2 and its influence on the superconductivity vary considerably. In early studies on the carbon solubility, figures ranging from 1.25% to 30% were reported when elemental magnesium, boron, and carbon were used as

precursors, however as earlier mentioned, the actual carbon level is different from the nominal composition [134]. Carbon doping increases the MgB_2 anisotropy due to more lattice concentration and results insubstantial reduction in its *Tc*. Carbon doping greatly affect the a lattice parameter while has no or slight effect on c lattice parameter.

Avdeev et al. used a neutron diffraction method to estimate the carbon concentration level in doped MgB_2 with C [129]. Results revealed a linear relationship between the unit cell parameter a and the C content. Following formula estimates the level of C substitution, x, in the compound of Mg $(B_{1-x}C_x)_2$.

$$X = 7.5\Delta\left(\frac{c}{a}\right) \qquad (2.10)$$

Where Δ (c/a) is the change in c/a compared to the pure sample [129].

The real amount of substituted carbon in MgB_2 polycrystalline structure, known as actual C fraction, has been evaluated by S. Jemima et al.,[135] using the conventional solid–vapor reaction route and revealed that the actual composition is in disagreement with the nominal composition.

A large number of carbon sources have been studied as dopants Due to huge impact of C on superconducting properties of MgB_2. The common C source dopants used in MgB_2 are SiC [136-138], nano-carbon [54, 69], carbon nano tubes (CNTs) [117, 139], graphite [118], boron carbide (B_4C)[140-142], nano- diamond, hydrocarbons [121, 143-146], carbohydrates [147, 148], and graphene [149- 151] (which was rather recently revealed as an effective dopant).

Since SiC remarkably improved the superconducting properties of MgB_2, therefore many studies have been performed on the effects of the precursor

size, the sintering conditions, the optimum doping levels, and the different fabrication techniques for SiC-doped MgB_2 [63, 137, 152-156]. Finally a significant improvement happened in MgB_2 J_c by doping 10 wt% nano-SiC. 10 wt% SiC, MgB_2 bulk samples showed H_{irr} of 8 T and J_c of 10^5 A cm^{-2} under 3 T at 20 K, with a slight reduction in T_c [157]. It was also shown that substituted carbon with boron resulted in a large number of intra-granular dislocations and dispersed nano-size impurities, which significantly increases the pinning mechanism forces. Creation of more microscopic defects is the result of addition or substitution of carbon or SiC in MgB_2 structure. These microscopic defects act as electron scattering centers leading to an improvement in pinning forces [48]. Recently, Matsumoto et al. [158] reported very high values of $H_{c2}(0)$ exceeding 40 T for SiC-doped bulk MgB_2 sintered at 600 ºC.

Less sintering temperature is needed for considerable substitution of C in boron sites for nano carbon doped MgB_2 due to improved reactivity. Nano-C doped MgB_2 tapes show a better enhancement of the superconducting properties by sintering at 750 ˚C. Reported data showed J_c at 4.2 K for the 5 at% C-doped tape that reached 1.85×10^4 Acm^{-2} at 10 T and 2.8×10^3Acm-2 at 14 T, respectively [54].

It has been proved that use on CNT among the other various carbon precursors improve the mechanical and thermal properties of MgB_2 wires and it needs to be noted that the best performances in J_c was observed in the single wall carbon nano-tubes (SWCNT) doped samples sintered at 900˚C [119]. The inherent structure of CNT limited its usage due to formation of the entanglements and the agglomerates, which block the transport current. However ultra-sonication of mixed CNT with MgB_2 powder leads to a homogeneous mixture resulted in a significant improvement in J_c [139].

Huge enhancement in H_{c2}(t=o), from 16 to 32.5 T, with slight depression of T_c from 39.2 to 36.2 K for 3.8% of C doped MgB_2 was observed in samples prepared by CVD method [159].

B_4C also proved itself as one of the other successful C source material for MgB_2 by improving the superconducting properties due to the relatively low processing temperature and carbon substitution effects under high magnetic fields. A J_c value of 10^4 A cm^{-2}at 4.2 K and 9 T for MgB_2/Fe wires with 10 wt% B_4C powders was reported recently [140].

It needs to be noted that use of hydrocarbons and carbohydrates dopants for MgB_2 among the other C sources material resulted in a comparable J_c with those samples doped with nano-SiC and the reason behind lies down on lower decomposition temperature of hydrocarbons and carbohydrates, leading to highly fresh and reactive C which can be substituted with B at lower temperature than formation temperature of MgB_2.

Lower decomposition temperature results in more homogeneous mixture in the liquid state and finally smaller MgB_2 grain size due to lower sintering temperature which both improve the J_c of the final MgB_2 product.

2.5.2 Effect of other doping materials on the superconductivity of MgB_2

Effect of many other dopants than organic compound - C sources has been examined on MgB_2 superconducting properties. AL substation in Mg sites occurred by doping MgB_2 with Al and resulted in T_c degradation due to changes in carrier density and density of state at the Fermi surface [176, 177]. However Berenov et al. [178] reported on enhancement of MgB_2 J_c as well as its upper critical filed in self field at 20 K due to Al doping while slight

degradation in MgB_2 T_c was seen at low doping level.

Ti effects positively on the MgB_2 superconducting properties [179-182]. Zhao et al reported on formation of a TiB_2 nano-layer at the grain boundaries of MgB_2. This, TiB_2 nano-layered, formed of strongly coupled nanoparticles which significantly contribute in flux pinning mechanism to improve the MgB_2 J_c performance [181].

Chemical vapor deposition technique was used for uniform dispersion of Ti particles into the MgB_2 grain boundaries resulted in high J_c value.

No precipitation of TiB_2 particles was seen in this technique while existed in solid state reaction method.

Effects of Fe-nano scale particles dopant on MgB_2 superconducting properties was studied by Dou et al. [185]. Fe adversely affect the MgB_2 properties due to Fe and FeB formation at grain boundaries, acting as weak links and leads to J_c suppression.

In addition to above dopants, doping with small amounts of Si [176], Zr [179, 180], Ta [38], and Ag [186] resulted in J_c enhancement at low field application.

MgO as the main impurity phase is always present in the final formation of the main MgB_2 phase. The effect of this phase on final MgB_2 properties has been studied by several groups and will be discussed further in chapter 4. Iang et al. [187] reported on the J_c enhancement of the MgB_2 by doping with 2.5 Wt% nano-MgO due to better grain connectivity and cored density. Later on, Perner et al. [188] reported that doping MgB_2 with micro sizes MgO results in more effective flux pinning due to concentration of nano-MgO particles at grain boundaries. J_c Enhancement of the polycrystalline MgB_2 bulk sample doped with Bi-2212 was reported by Shen et al. [189]. Microstructural investigation revealed the presence of the decomposed Bi-2212 at the MgB_2 grain boundaries acting as

effective pinning centers.

Interestingly enough, Haruta et al. [190] reported on effective way to introduce pinning centers in MgB_2 structure by deposition of MgB_2 thin film in an O_2 atmosphere which out came J_c result was higher than un-doped thin film in both direction of applied field, perpendicular and parallel to c axis.

2.5.3 Summary of parameters of MgB_2

Summaries of literature review for MgB_2 superconducting properties can be found in below table for ease of referring in the thesis [2].

Table 2.1: List of superconducting parameters of MgB_2 [80]

Parameter	Values
Critical temperature	39 ~ 40 K
Lattice parameters	a = 0.3086 nm
	c = 0.3524 nm
Theoritical density	ρ = 2.55 gcm-3
Resistivity near Tc	ρ (40 K) = 0.4 ~ 16 μΩ cm
Resistivity ratio	RRR = ρ (300 K)/ ρ (40 K) = 1 ~ 27
Upper critical field	Hc2 // ab(0) = 14 ~ 39 T
	Hc2 // c(0) = 2 ~ 24 T
Lower critical field	Hc1(0) = 27 ~ 48 mT
Irreversibility field	Hirr = 6 ~ 35 T
Coherence length	ξab (0) = 3.7 ~ 12 nm
	ξc (0)= 1.6 ~ 3.6 nm
Penetration depth	λ(0) = 85 ~ 180 nm
Energy gap	Δ(0) = 1.8 ~7.5 meV

2.6 References

[1] J. Nagamatsu, N. Nakagawa, T. Muranaka, Y. Zenitani, J. Akimitsu, Nature, 410 (2001) 63.

[2] C. Buzea, T. Yamashita, Superconductor Science and Technology, 14 (2001) R115.

[3] J. Kortus, I. I. Mazin, K. D. Belashchenko, V. P. Antropov, L. L. Boyer, Physical Review Letters, 86 (2001) 4656.

[4] H. J. Choi, D. Roundy, H. Sun, M. L. Cohen, S. G. Louie, Nature, 418 (2002) 758.

[5] O. V. Shcherbakova, A. V. Pan, S. X. Dou, Manesium diboride supercoductors Development and Properties, First ed., VDM Verlag Dr. Muller Aktiengesellschaft & Co. KG and licensors, Germany, 2009.

[6] E. W. Collings, M D Sumption, M Bhatia, M.A. Susner, S.D. Bohnenstiehl, Superconductor Science and Technology, 21 (2008) 103001.

[7] F. Bouquet, Y. Wang, I. Sheikin, T. Plackowski, A. Junod, S. Lee, S. Tajima, Physical Review Letters, 89 (2002) 257001.

[8] F. Bouquet, R. A. Fisher, N. E. Phillips, D. G. Hinks, J. D. Jorgensen, Physical Review Letters, 87 (2001) 047001.

[9] F. Giubileo, D. Roditchev, W. Sacks, R. Lamy, D. X. Thanh, J. Klein, S. Miraglia, D. Fruchart, J. Marcus, P. Monod, Physical Review Letters, 87 (2001) 177008.

[10] P. Szabó, P. Samuely, J. Kaˇcmarˇcík, J. Klein, J. Marcus, D. Fruchart, S. Miraglia, C. Marcenat, A. G. M. Jansen., Physical Review Letters, 87 (2001) 137005.

[11] Y. Bugoslavsky, Y. Miyoshi, G. K. Perkins, A. V. Berenov, Z. Lockman, J. L. MacManus-Driscoll, L. F. Cohen, A. D. Caplin, H. Y. Zhai, M. P.

Paranthaman, H. M. Christen, M. Blamire, Superconductor Science and Technology, 15 (2002) 526.

[12] F. Manzano, A. Carrington, N. E. Hussey, S. Lee, A. Yamamoto, S. Tajima, Physical Review Letters, 88 (2002) 047002.

[13] X. K. Chen, M. J. Konstantinović, J. C. Irwin, D. D. Lawrie, J. P.Franck, Physical Review Letters, 87 (2001) 157002.

[14] J. J. Tu, G. L. Carr, V.Perebeinos, C. C. Homes, M. Strongin, P. B .Allen, W. N. Kang, Eun-Mi. Choi, Hyeong-Jin. Kim, S. I. Lee., Physical Review Letters, 87 (2001) 277001.

[15] T. Dahm, N. Schopohl, Physical Review Letters, 91 (2003) 017001.

[16] M. Eisterer, Superconductor Science and Technology, 20 (2007) R47.

[17] C. Wälti, E. Felder, C. Degen, G. Wigger, R. Monnier, B. Delley, H. R. Ott, Physical Review B, 64 (2001) 172515.

[18] G. Karapetrov, M. Iavarone, W. K. Kwok, G. W. Crabtree, D. G. Hinks, Physical Review Letters, 86 (2001) 4374.

[19] A. Sharoni, I. Felner, O. Millo, Physical Revie B 63 (2001) 220508.

[20] H. Schmidt, J.F. Zasadzinski, K.E. Gray, D.G. Hinks, Physical Review B, 63 (2001) 220504.

[21] F. Bouquet, Y. Wang, R. A. Fisher, D. G. Hinks, J. D. Jorgensen, A. Junod, N.E. Phillips, EPL (Europhysics Letters), 56 (2001) 856.

[22] Z. K. Liu, D.G. Schlom, Q. Li, X. X. Xi, Applied Physics Letters, 78 (2001) 3678.

[23] W. H¨aßler, B. Birajdar, W. Gruner, M. Herrmann, O. Perner, C. Rodig, M. Schubert, B. Holzapfel, O. Eibl, L. Schultz, Superconductor Science and Technology, 19 (2006) 512.

[24] P. Kováč, I. Hušek, T. Melišek, J. C. Grivel, W. Pachla, V. Štrbík, R.

Diduszko, J. Homeyer, N. H. Andersen., Superconductor Science and Technology, 17 (2004) L41.

[25] R. A. Ribeiro, S. L. Bud'ko, C. Petrovic, P. C. Canfield, Physica C: Superconductivity, 384 (2003) 227.

[26] B. A. Glowacki, M. Majoros, M. Vickers, J. E. Evetts, Y. Shi, I. McDougall, Superconductor Science and Technology, 14 (2001) 193.

[27] A. V. Pan, S. Zhou, H. K. Liu, S. X. Dou, Superconductor Science and Technology, 16 (2003) 639.

[28] J. Jiang, B J Senkowicz, D. C. Larbalestier, E. E. Hellstrom, Superconductor Science and Technology, 19 (2006) L33.

[29] A. Malagoli, V. Braccini, C. Bernini, G. Romano, M. Vignolo, M. Putti, C. Ferdeghini, Superconductor Science and Technology, 23 (2010) 025032.

[30] A. Kario, R. Nast, W. Häßler, C. Rodig, C. Mickel, W. Goldacker, B. Holzapfel, L. Schultz, Superconductor Science and Technology, 24 (2011) 075011.

[31] P. Kováč, T. Melišek, M. Dhallé, A.d. Ouden, I. Hušek, Superconductor Science and Technology, 18 (2005) 1374.

[32] X. Xun, M. J. Qin, K. Konstantinov, I. d. S. Dayse, W. K. Yeoh, J. H. Kim, S. X. Dou, Superconductor Science and Technology, 19 (2006) 466.

[33] W. Goldacker, S. I. Schlachter, B. Obst, M. Eisterer, Superconductor Science and Technology, 17 (2004) S490.

[34] R. F. Klie, J. C. Idrobo, N. D. Browning, K. A. Regan, N. S. Rogado, R. J. Cava, Applied Physics Letters, 79 (2001) 1837.

[35] X. Z. Liao, A. C. Serquis, Y. T. Zhu, J. Y. Huang, D. E. Peterson, F. M. Mueller, H. F. Xu, Applied Physics Letters, 80 (2002) 4398.

[36] A. Serquis, L. Civale, D. L. Hammon, X. Z. Liao, J. Y. Coulter, Y. T. Zhu,

M. Jaime, D. E. Peterson, F. M. Mueller, V. F. Nesterenko, Y. Gu, Applied Physics Letters, 82 (2003) 2847.

[37] T.A. Prikhna, W. Gawalek, Y. M. Savchuk, V. E. Moshchil, N. V. Sergienko, T. Habisreuther, M. Wendt, R. Hergt, C. Schmidt, J. Dellith, V.S. Melnikov, A. Assmann, D. Litzkendorf, P. A. Nagorny, Physica C: Superconductivity, 402 (2004) 223.

[38] T. A. Prikhna, W. Gawalek, A. B. Surzhenko, V. E. Moshchil, N. V. Sergienko, Y. M. Savchuk, V. S. Melnikov, P. A. Nagorny, T. Habisreuther, S. N. Dub, M. Wendt, D. Litzkendorf, J. Dellith, C. Schmidt, G. Krabbes, A. V. Vlasenko, Physica C: Superconductivity, 372–376, Part 3 (2002) 1543.

[39] T. Futatsumori, H. Ikeda, Physica C: Superconductivity, 469 (2009) 1229.

[40] A. Serquis, X. Z. Liao, Y. T. Zhu, J. Y. Coulter, J. Y. Huang, J. O. Willis, D. E. Peterson, F. M. Mueller, N. O. Moreno, J. D. Thompson, V. F. Nesterenko, S. S. Indrakanti, Journal of Applied Physics, 92 (2002) 351.

[41] T. C. Shields, K. Kawano, D. Holdom, J. S. Abell, Superconductor Science and Technology, 15 (2002) 202.

[42] A. Serquis, L. Civale, J. Y. Coulter, D. L. Hammon, X. Z. Liao, Y. T. Zhu, D. E. Peterson, F. M. Mueller, V. F. Nesterenko, S. S. Indrakanti, Superconductor Science and Technology, 17 (2004) L35.

[43] R. Flukiger, M. S. A. Hossain, C. Senatore, Superconductor Science and Technology, 22 (2009) 085002.

[44] M. Herrmann, W. H¨aßler, C. Mickel, W. Gruner, B. Holzapfel, L. Schultz, Superconductor Science and Technology, 20 (2007) 1108.

[45] Y. F. Wu, Y. F. Lu, G. Yan, J. S. Li, Y. Feng, H. P. Tang, S. K. Chen, H. L. Xu, C. S. Li, P. X. Zhang, Superconductor Science and Technology, 19

(2006) 1215.

[46] M. Herrmann, W. Häßler, O. Perner, C. Rodig, M. Schubert, B. Holzapfel, L. Schultz, Physica C: Superconductivity, 460 (2007) 593.

[47] B. J. Senkowicz, A. Polyanskii, R. J. Mungall, Y. Zhu, J. E. Giencke, P. M. Voyles, C. B. Eom, E. E. Hellstrom, D.C. Larbalestier, Superconductor Science and Technology, 20 (2007) 650.

[48] B. J. Senkowicz, J. E. Giencke, S. Patnaik, C. B. Eom, E. E. Hellstrom, D .C. Larbalestier, Applied Physics Letters, 86 (2005) 202502.

[49] P. C. Canfield, D. K. Finnemore, S. L. Bud'ko, J. E. Ostenson, G. Lapertot, C. E. Cunningham, C. Petrovic, Physical Review Letters, 86 (2001) 2423.

[50] S. Ueda, J. I. Shimoyama, I. Iwayama, A. Yamamoto, Y. Katsura, S. Horii, K. Kishio, Applied Physics Letters, 86 (2005) 222502.

[51] A. Serquis, L. Civale, D. L. Hammon, J. Y. Coulter, X. Z. Liao, Y. T. Zhu, D. E. Peterson, F. M. Mueller, Applied Physics Letters, 82 (2003) 1754.

[52] P. Kov´aˇc, I. Huˇsek, E. Dobroˇcka, T. Meliˇsek, W. Haessler, M. Herrmann, Superconductor Science and Technology, 21 (2008) 015004.

[53] J. Horvat, W. K. Yeoh, J. H. Kim, S. X. Dou, Superconductor Science and Technology, 21 (2008) 065003.

[54] Y. Ma, X. Zhang, G. Nishijima, K. Watanabe, S. Awaji, X. Bai, Applied Physics Letters, 88 (2006) 072502.

[55] S. Jin, H. Mavoori, C. Bower, R. B. van Dover, Nature, 411 (2001) 563.

[56] G. Grasso, A. Malagoli, C. Ferdeghini, S. Roncallo, V. Braccini, A. S. Siri, M. R. Cimberle, Applied Physics Letters, 79 (2001) 230.

[57] A. Matsumoto, H. Kumakura, H. Kitaguchi, H. Hatakeyama, Superconductor Science and Technology, 16 (2003) 926.

[58] S. K. Chen, K. S. Tan, B. A. Glowacki, W. K. Yeoh, S. Soltanian, J. Horvat,

S. X. Dou, Applied Physics Letters, 87 (2005) 182504.

[59] C. H. Jiang, T. Nakane, H. Hatakeyama, H. Kumakura, Physica C: Superconductivity, 422 (2005) 127.

[60] S. Hata, T. Yoshidome, H. Sosiati, Y. Tomokiyo, N. Kuwano, A. Matsumoto, H. Kitaguchi, H. Kumakura, Superconductor Science and Technology, 19 (2006) 161.

[61] O. Shcherbakova, S. X. Dou, S. Soltanian, D. Wexler, M. Bhatia, M. Sumption, E. W. Collings, Journal of Applied Physics 99 (2006) 08M510.

[62] X. Xu, J. H. Kim, S. X. Dou, S. Choi, J. H. Lee, H. W. Park, M. Rindfleish, M. Tomsic, Journal of Applied Physics, 105 (2009) 103913.

[63] H. Fujii, K. Togano, H. Kumakura, K. Ozawa, Superconductor Science and Technology, 20 (2007) 579.

[64] A. Polyanskii, V. Beilin, I. Felner, M. I .Tsindlekht, E. Yashchin, E. Dul'kin, E. Galstyan, M. Roth, B. Senkowicz, E. Hellstrom1, Superconductor Science and Technology, 17 (2004) 363.

[65] E. Martínez, L. A. Angurel, R. Navarro, Superconductor Science and Technology, 15 (2002) 1043.

[66] M. Majoros, B. A. Glowacki, M. E. Vickers, Superconductor Science and Technology, 15 (2002) 269.

[67] H. Suo, C. Beneduce, M. Dhalle, N. Musolino, J. Y. Genoud, R. Flukiger, Applied Physics Letters, 79 (2001) 3116.

[68] M. D. Sumption, M. Bhatia, S. X. Dou, M. Rindfliesch, M. Tomsic, L. Arda, M. Ozdemir, Y. Hascicek, E.W. Collings, Superconductor Science and Technology, 17 (2004) 1180.

[69] W. Häßler, M. Herrmann, C. Rodig, M. Schubert, K. Nenkov, B. Holzapfel, Superconductor Science and Technology, 21 (2008) 062001.

[70] M. A. Susner, T. W. Daniels, M. D. Sumption, M. A. Rindfleisch, C. J. Thong, E. W. Collings, Superconductor Science and Technology, 25 (2012) 065002.

[71] P. Kov´aˇc, I. Huˇsek, T. Meliˇsek, Superconductor Science and Technology, 15 (2002) 1340.

[72] P. Fabbricatore, M. Greco, R. Musenich, P. Kov´aˇc, I. Huˇsek, F. .G¨om¨ory, Superconductor Science and Technology, 16 (2003) 364.

[73] G. Giunchi, S. Ceresara, G. Ripamonti, A. Di Zenobio, S. Rossi, S .Chiarelli, M. Spadoni, R. Wesche, P.L. Bruzzone, Superconductor Science and Technology, 16 (2003) 285.

[74] K. Togano, T. Nakane, H. Fujii, H. Takeya, H. Kumakura, Superconductor Science and Technology, 19 (2006) L17.

[75] S. Y. Lee, J. H. Lee, J. H. Lee, J. S. Ryu, J. Lim, S. H. Moon, H. N. Lee, H. G. Kim, B. Oh, Applied Physics Letters, 79 (2001) 3299.

[76] A. I. Posazhennikova, T. Dahm, K. Maki, EPL (Europhysics Letters), 60 (2002) 134.

[77] G. Nishijima, S. J. Ye, A. Matsumoto, K. Togano, H. Kumakura, H. Kitaguchi, H. Oguro, Superconductor Science and Technology, 25 (2012) 054012.

[78] K. Vinod, R. G. A. Kumar, U. Syamaprasad, Superconductor Science and Technology, 20 (2007) R1.

[79] A. Matsumoto, H. Kumakura, H. Kitaguchi, H. Hatakeyama, Superconductor Science and Technology, 17 (2004) S319.

[80] W. Pachla, P. Kováč, I. Hušek, T. Melišek, M. Müler, V. Štrbík, A. Mazur, A. Presz., Superconductor Science and Technology, 18 (2005) 552.

[81] K. Komori, K. Kawagishi, Y. Takano, H. Fujii, S. Arisawa, H. Kumakura,

M. Fukutomi, K. Togano, Applied Physics Letters, 81 (2002) 1047-1049.

[82] M .D. Sumption, M. Bhatia, M. Rindfleisch, M. Tomsic, E. W. Collings, Applied Physics Letters, 86 (2005) 102501.

[83] T. Takenobu, T. Ito, D. Hieu Chi, K. Prassides, Y. Iwasa, Physical Review B, 64 (2001) 134513.

[84] S. Lee, T. Masui, A. Yamamoto, H. Uchiyama, S. Tajima, Physica C: Superconductivity, 397 (2003) 7.

[85] T. Schneider, D. Di Castro, Physical Review B, 72 (2005) 054501.

[86] S. Deemyad, T. Tomita, J. J. Hamlin, B. R. Beckett, J. S. Schilling, D. G. Hinks, J. D. Jorgensen, S. Lee, S. Tajima, Physica C: Superconductivity, 385 (2003) 105.

[87] S. L. Bud'ko, R. H. T. Wilke, M. Angst, P. C. Canfield, Physica C: Superconductivity, 420 (2005) 83.

[88] C. Tarantini, H. U. Aebersold, V. Braccini, G. Celentano, C. Ferdeghini, V. Ferrando, U. Gambardella, F. Gatti, E. Lehmann, P. Manfrinetti, D. Marr, A. Palenzona, I. Pallecchi, I. Sheikin, A. S. Siri, M. Putti, Physical Review B, 73 (2006) 134518.

[89] M. Putti, V. Braccini, C. Ferdeghini, F. Gatti, G. Grasso, P. Manfrinetti, D. Marre, A. Palenzona, I. Pallecchi, C. Tarantini, I. Sheikin, H. U. Aebersold, E. Lehmann, Applied Physics Letters, 86 (2005) 112503.

[90] A. Serquis, Y. T. Zhu, E. J. Peterson, J. Y. Coulter, D. E. Peterson, F. M. Mueller, Applied Physics Letters, 79 (2001) 4399.

[91] J. H. Kim, S. X. Dou, J. L. Wang, D. Q. Shi, X. Xu, M. S. A. Hossain, W.K. Yeoh, S. Choi, T. Kiyoshi, Superconductor Science and Technology, 20 (2007) 448.

[92] E. J. Nicol, J. P. Carbotte, Physical Review B, 72 (2005) 014520.

[93] Z. X. Shi, A. K. Pradhan, M. Tokunaga, K. Yamazaki, T. Tamegai, Y. Takano, K. Togano, H. Kito, H. Ihara, Physical Review B, 68 (2003) 104514.

[94] D. C. Larbalestier, L. D. Cooley, M. O. Rikel, A. A. Polyanskii, J. Jiang, S. Patnaik, X. Y. Cai, D. M. Feldmann, A. Gurevich, A. A. Squitieri, M. T. Naus, C. B. Eom, E. E. Hellstrom, R. J. Cava, K. A. Regan, N. Rogado, M. A. Hayward, T. He, J.S. Slusky, P. Khalifah, K. Inumaru, M. Haas, Nature, 410 (2001) 186.

[95] C. F. Liu, G. Yan, S. J. Du, W. Xi, Y. Feng, P. X. Zhang, X. Z. Wu, L. Zhou, Physica C: Superconductivity, 386 (2003) 603.

[96] K. Yamamoto, K. Osamura, S. Balamurugan, T. Nakamura, T. Hoshino, I. Muta, Superconductor Science and Technology, 16 (2003) 1052.

[97] R. Zeng, L. Lu, W. X. Li, J.L. Wang, D. Q. Shi, J. Horvat, S. X. Dou, M. Bhatia, M. Sumption, E. W. Collings, J. M. Yoo, M. Tomsic, M. Rindfleisch, Journal of Applied Physics, 103 (2008) 083911.

[98] R. Zeng, L. Lu, J. L. Wang, J. Horvat, W. X. Li, D. Q. Shi, S. X. Dou, M. Tomsic, M. Rindfleisch, Superconductor Science and Technology, 20 (2007) L43.

[99] H. Fujii, K. Togano, H. Kumakura, Superconductor Science and Technology, 15 (2002) 1571.

[100] H. Yamada, M. Hirakawa, H. Kumakura, A. Matsumoto, H. Kitaguchi, Applied Physics Letters, 84 (2004) 1728.

[101] C. Fischer, C. Rodig, W. Hassler, O. Perner, J. Eckert, K. Nenkov, G. Fuchs, H. Wendrock, B. Holzapfel, L. Schultz, Applied Physics Letters, 83 (2003) 1803.

[102] H. Fang, S. Padmanabhan, Y. X. Zhou, K. Salama, Applied Physics Letters,

82 (2003) 4113.

[103] R. A. Ribeiro, S. L. Bud'ko, C. Petrovic, P. C. Canfield, Physica C: Superconductivity, 385 (2003) 16.

[104] R. A. Ribeiro, S. L. Bud'ko, C. Petrovic, P. C. Canfield, Physica C: Superconductivity, 382 (2002) 194.

[105] Z. Sihai, A. V. Pan, J. Horvat, M. J. Qin, H. K. Liu, Superconductor Science and Technology, 17 (2004) S528.

[106] S. K. Chen, K. A. Yates, M. G. Blamire, J. L. MacManus-Driscoll, Superconductor Science and Technology, 18 (2005) 1473.

[107] Y. Zhang, X. Xu, Y. Zhao, J . H. Kim, C. Lu, S. H. Zhou, S. X. Dou, Superconductor Science and Technology, 21 (2008) 115004.

[108] X. Xu, J. H. Kim, W. K. Yeoh, Y. Zhang, S. X. Dou, Superconductor Science and Technology, 19 (2006) L47.

[109] X. Song, S. E. Babcock, D. C. L. C. B. Eom, R. J. C. K. A. Regan, S. L. Bud'Ko, P. C. Canfield, D. K. Finnemore, Superconductor Science and Technology, 15 (2002) 511.

[110] A. Yamamoto, J. Shimoyama, S. Ueda, Y. Katsura, I. Iwayama, S. Horii, K. Kishio, Physica C: Superconductivity, 445-448 (2006) 806.

[111] A. Yamamoto, J. Shimoyama, S. Ueda, Y. Katsura, I. Iwayama, S. Horii, K. Kishio, Applied Physics Letters, 86 (2005) 212502.

[112] L. Boeri, G. B. Bachelet, E. Cappelluti, L. Pietronero, Superconductor Science and Technology, 16 (2003) 176.

[113] G. K. Perkins, J .Moore, Y. Bugoslavsky, L. F. Cohen, J. Jun, S. M. Kazakov, J. Karpinski, A. D. Caplin, Superconductor Science and Technology, 15 (2002) 1156.

[114] L .Lyard1, P. Samuely, P. Szab´o, C. Marcenat, T. Klein, K .H. P. Kim, C.

U. Jung, H-S Lee, B. Kang, S. Choi, S I. Lee, L. Paulius, J. Marcus, S. Blanchard, A.G.M. Jansen, U. Welp, G. Karapetrov, W. K. Kwok, Superconductor Science and Technology, 16 (2003) 193.

[115] S. X. Dou, O. Shcherbakova, W. K. Yeoh, J. H. Kim, S. Soltanian, X. L. Wang, C. Senatore, R. Flukiger, M. Dhalle, O. Husnjak, E. Babic, Physical Review Letters, 98 (2007) 097002.

[116] M. S .A. Hossain, J. H. Kim, X. Xu, X. L.Wang, M. Rindfleisch, M.Tomic, M. D. Sumption, E. W.Collings, S.X. Dou, Superconductor Science and Technology, 20 (2007) L51.

[117] A. Serquis, G. Serrano, S. M. Moreno, L. Civale, B. Maiorov, F. Balakirev, M. Jaime, Superconductor Science and Technology, 20 (2007) L12.

[118] C. Shekhar, R. Giri, R. S. Tiwari, O. N. Srivastava, S. K. Malik, Journal of Applied Physics, 102 (2007) 093910.

[119] W. K. Yeoh, S. X. Dou, Physica C: Superconductivity, 456 (2007) 170.

[120] J. H. Kim, X. Xu, M. S. A. Hossain, D. Q. Shi, Y. Zhao, X. L. Wang, S. X. Dou, S. Choi, T. Kiyoshi, Applied Physics Letters, 92 (2008) 042506.

[121] A. Vajpayee, V. P. S. Awana, G. L. Bhalla, P. A. Bhobe, A.K. Nigam, H. Kishan, Superconductor Science and Technology, 22 (2009) 015016.

[122] D. Dew-Hughes, Low Temperature Physics, 27 (2001) 713.

[123] A. Yamamoto, J. I. Shimoyama, S. Ueda, S. Horii, K. Kishio, Physica C: Superconductivity, 445-448 (2006) 801.

[124] M. J. Qin, X. L. Wang, H. K. Liu, S. X. Dou, Physical Review B, 65 (2002) 132508.

[125] J. M. Rowell, Superconductor Science and Technology, 16 (2003) R17.

[126] I. M. Obaidat, B. A. Albiss, Crystal Research and Technology, 43 (2008) 83.

[127] A. Sidorenko, V. Zdravkov, V. Ryazanov, S. Horn, S. Klimm, R. Tidecks, A. Wixforth, T. Koch, T. Schimmel, Philosophical Magazine, 85 (2005) 1783.

[128] S. X. Dou, A. V. Pan, S. Zhou, M. Ionescu, X. L. Wang, J. Horvat, H. K. Liu, P. R. Munroe, Journal of Applied Physics, 94 (2003) 1850.

[129] M. Avdeev, J. D. Jorgensen, R. A. Ribeiro, S. L. Bud'ko, P. C. Canfield, Physica C: Superconductivity, 387 (2003) 301.

[130] J. Kortus, O. V. Dolgov, R. K. Kremer, A. A. Golubov, Physical Review Letters, 94 (2005) 027002.

[131] R. F. Klie, J. C. Zheng, Y. Zhu, A. J. Zambano, L. D. Cooley, Physical Review B, 73 (2006) 014513.

[132] W. X. Li, Y. Li, R. H. Chen, R. Zeng, M. Y. Zhu, H. M. Jin, S. X. Dou, Journal of Physics: Condensed Matter, 20 (2008) 255235.

[133] W. X. Li, Y. Li, R. H. Chen, R. Zeng, S. X. Dou, M. Y. Zhu, H. M. Jin, Physical Review B, 77 (2008) 094517.

[134] A. Bharathi, S. Jemima Balaselvi, S. Kalavathi, G. L. N. Reddy, V. Sankara Sastry, Y. Hariharan, T. S. Radhakrishnan, Physica C: Superconductivity, 370 (2002) 211.

[135] S. Jemima Balaselvi, N. Gayathri, A. Bharathi, V.S. Sastry, Y. Hariharan, Physica C: Superconductivity, 407 (2004) 31.

[136] Z. X. Shi, M. A. Susner, M. D. Sumption, E. W. Collings, X. Peng, M. Rindfleisch, M. J. Tomsic, Superconductor Science and Technology, 24 (2011) 065015.

[137] Z. Ma, Y. Liu, Q. Zhao, Z. Dong, L. Yu, Superconductor Science and Technology, 22 (2009) 085015.

[138] W. X. Li, R. Zeng, L. Lu, Y. Li, S. X. Dou, Journal of Applied Physics, 106

(2009) 093906.

[139] W. K.Yeoh, J. H. Kim, J. Horvat, S. X. Dou, P. Munroe, Superconductor Science and Technology, 19 (2006) L5.

[140] P. Lezza, C. Senatore, R. Fl¨ukiger, Superconductor Science and Technology, 19 (2006) 1030.

[141] A. Yamamoto, J. I Shimoyama, S. Ueda, S.H. I. Iwayama, K. Kishio, Superconductor Science and Technology, 18 (2005) 1323.

[142] J. Y. Lao, W. Z. Li, J. G. Wen, Z. F. Ren, Applied Physics Letters, 80 (2002) 500.

[143] J. H. Kim, S. Oh, Y.-U. Heo, S. Hata, H. Kumakura, A. Matsumoto, M. Mitsuhara, S. Choi, Y. Shimada, M. Maeda, J. L. MacManus-Driscoll, S.X. Dou, NPG Asia Mater, 4 (2012) e3.

[144] J. H. Kim, S. Oh, H. Kumakura, A. Matsumoto, Y. U. Heo, K. S. Song, Y. M. Kang, M. Maeda, M. Rindfleisch, M. Tomsic, S. Choi, S.X. Dou, Advanced Materials, 23 (2011) 4942.

[145] M. S. A. Hossain, C. Senatore, R. Fl¨ukiger, M. A. Rindfleisch, M .J. Tomsic, J. H. Kim, S. X. Dou, Superconductor Science and Technology, 22 (2009) 095004.

[146] Z. Gao, Y. Ma, X. Zhang, D. Wang, Z. Yu, H. Yang, H. Wen, E. Mossang, Journal of Applied Physics, 102 (2007) 013914.

[147] X. Zhang, D. Wang, Z. Gao, L. Wang, Y. Qi, Z. Zhang, Y. Ma, S. Awaji, G. Nishijima, K. Watanabe, E. Mossang, X. Chaud., Superconductor Science and Technology, 23 (2010) 025024.

[148] O. V. Shcherbakova, A. V. Pan, J. L. Wang, A. V. Shcherbakov, S. X. Dou, D. Wexler, E. Babi´, M. Jer˘cinovi´, O. Husnjak, Superconductor Science and Technology, 21 (2008) 015005.

[149] K. S. B. De Silva, S. Gambhir, X. L. Wang, X. Xu, W. X. Li, D. L. Officer, D. Wexler, G. G. Wallace, S. X. Dou, Journal of Materials Chemistry, 22 (2012) 13941.

[150] K. S. B. De Silva, X. Xu, W. X. Li, Y. Zhang, M. Rindfleisch, M. Tomsic, Applied Superconductivity, IEEE Transactions on, 21 (2011) 2686.

[151] X. Xu, S. X.Dou, X. L. Wang, J. H. Kim, M. Choucair, W. K. Yeoh, R.K. Zheng, S. P. Ringer, Superconductor Science and Technology, 23 (2010) 085003.

[152] R. Zeng, S. X. Dou, L. Lu, W.X. Li, J.H. Kim, P. Munroe, R. K. Zheng, S. P. Ringer, Applied Physics Letters, 94 (2009) 042510.

[153] S. C. Yan, G. Yan, Y. F. Lu, L. Zhou., Superconductor Science and Technology, 20 (2007) 549.

[154] A. Yamamoto, J. Shimoyama, I. Iwayama, Y. Katsura, S. Horii, K. Kishio, Physica C: Superconductivity, 463-465 (2007) 807-811.

[155] O. Shcherbakova, S. X. Dou, S. Soltanian, D. Wexler, M. Bhatia, M. Sumption, E. W. Collings, Journal of Applied Physics, 99 (2006) 08M510.

[156] W. Pachla, W. Pachla1, A. Morawski, P. Kov´aˇc, I. Huˇsek, A. Mazur, T. Lada, R. Diduszko, T. Meliˇsek, V. ˇStrb´ık, M. Kulczyk, Superconductor Science and Technology, 19 (2006) 1.

[157] S. X. Dou, S. Soltanian, J. Horvat, X. L. Wang, S. H. Zhou, M. Ionescu, H. K. Liu, P. Munroe, M. Tomsic, Applied Physics Letters, 81 (2002) 3419.

[158] A. Matsumoto, H. Kumakura, H. Kitaguchi, B.J. Senkowicz, M.C. Jewell, E. E. Hellstrom, Y. Zhu, P. M. Voyles, D. C. Larbalestier, Applied Physics Letters, 89 (2006) 132508.

[159] R. H. T. Wilke, S. L. Budko, P. C. Canfield, D. K. Finnemore, R. J. Suplinskas, S. T. Hannahs, Physical Review Letters, 92 (2004) 217003.

[160] H. Yamada, M. Hirakawa, H. Kumakura, H. Kitaguchi, Superconductor Science and Technology, 19 (2006) 175.

[161] J. H. Kim, S. Zhou, M. S. A. Hossain, A. V. Pan, S. X. Dou, Applied Physics Letters, 89 (2006) 142505.

[162] K. S. B. De Silva, X. Xu, S. Gambhir, X. L. Wang, W. X. Li, G. G. Wallace, S. X. Dou, Scripta Materialia, 65 (2011) 634.

[163] W. X. Li, X. Xu, Q. H. Chen, Y. Zhang, S. H. Zhou, R. Zeng, S. X. Dou, Acta Materialia, 59 (2011) 7268.

[164] S. Stankovich, D. A. Dikin, R. D. Piner, K. A. Kohlhaas, A. Kleinhammes, Y. Jia, Y. Wu, S. T. Nguyen, R. S. Ruoff, Carbon, 45 (2007) 1558.

[165] S. Gilje, S. Han, M. Wang, K. L. Wang, R. B. Kaner, Nano Letters, 7 (2007) 3394.

[166] M. J. McAllister, J. L. Li, D. H. Adamson, H. C. Schniepp, A. A. Abdala, J. Liu, M. Herrera-Alonso, D. L. Milius, R. Car, R. K. Prud'homme, I. A. Aksay, Chemistry of Materials, 19 (2007) 4396.

[167] M. J. Allen, V. C. Tung, R. B. Kaner, Chemical Reviews, 110 (2009) 132.

[168] A. K. Geim, K. S. Novoselov, Nat Mater, 6 (2007) 183.

[169] A. A. Balandin, S. Ghosh, W. Bao, I. Calizo, D. Teweldebrhan, F. Miao, C.N. Lau, Nano Letters, 8 (2008) 902.

[170] G. Eda, Y. Y. Lin, S. Miller, C. W. Chen, W. F. Su, M. Chhowalla, Applied Physics Letters, 92 (2008) 233305.

[171] I. K. Moon, J. Lee, R. S. Ruoff, H. Lee, Nat Commun, 1 (2010) 73.

[172] D. Li, M. B. Muller, S. Gilje, R. B. Kaner, G. G. Wallace, Nat Nano, 3 (2008) 101.

[173] W. Chen, L. Yan, P.R. Bangal, The Journal of Physical Chemistry C, 114 (2010) 19885.

[174] W. Chen, L. Yan, P.R. Bangal, Carbon, 48 (2010) 1146.

[175] C. Mattevi, G. Eda, S. Agnoli, S. Miller, K.A. Mkhoyan, O. Celik, D. Mastrogiovanni, G. Granozzi, E. Garfunkel, M. Chhowalla, Advanced Functional Materials, 19 (2009) 2577.

[176] M. R. Cimberle, M. Novak, P. Manfrinetti, A. Palenzona, Superconductor Science and Technology, 15 (2002) 43.

[177] P. Toulemonde, N. Musolino, R. Flükiger, Superconductor Science and Technology, 16 (2003) 231.

[178] A. Berenov, A. Serquis, X. Z. Liao, Y. T. Zhu, D.E. Peterson, Y. Bugoslavsky, K. A. Yates, M. G. Blamire, L. F. Cohen, J. L. MacManus-Driscoll, Superconductor Science and Technology, 17 (2004) 1093.

[179] D. Goto, T. Machi, Y. Zhao, N. Koshizuka, M. Murakami, S. Arai, Physica C: Superconductivity, 392–396, Part 1 (2003) 272.

[180] Y. Zhao, Y. Feng, D. X. Huang, T. Machi, C. H. Cheng, K. Nakao, N. Chikumoto, Y. Fudamoto, N. Koshizuka, M. Murakami, Physica C: Superconductivity, 378–381, Part 1 (2002) 122.

[181] Y. Zhao, D. X. Huang, Y. Feng, C. H. Cheng, T. Machi, N. Koshizuka, M. Murakami, Applied Physics Letters, 80 (2002) 1640.

[182] S. Haigh, P. Kovac, T. A. Prikhna, M. S. Ya, M.R. Kilburn, C. Salter, J. Hutchison, C. Grovenor, Superconductor Science and Technology, 18 (2005) 1190.

[183] N. E. Anderson Jr, W. E. Straszheim, S. L. Bud'ko, P. C. Canfield, D. K. Finnemore, R. J. Suplinskas, Physica C: Superconductivity, 390 (2003) 11.

[184] D. K. Finnemore, W. E. Straszheim, S. L. Bud'ko, P. C. Canfield, N. E. Anderson, R. J. Suplinskas, Physica C: Superconductivity, 385 (2003)

278.

[185] S. X. Dou, S. Soltanian, Y. Zhao, E. Getin, Z. Chen, O. Shcherbakova, J. Horvat, Superconductor Science and Technology, 18 (2005) 710.

[186] D. Kumar, S. J. Pennycook, J. Narayan, H. Wang, A. Tiwari, Superconductor Science and Technology, 16 (2003) 455.

[187] C. H. Jiang, H. Hatakeyama, H. Kumakura, Physica C: Superconductivity, 423 (2005) 45.

[188] O. Perner, W. Häßler, J. Eckert, C. Fischer, C. Mickel, G. Fuchs, B. Holzapfel, L. Schultz, Physica C: Superconductivity, 432 (2005) 15.

[189] T. M. Shen, G. Li, X. T. Zhu, C. H. Cheng, Y. Zhao, Superconductor Science and Technology, 18 (2005) L49.

[190] M. Haruta, T. Fujiyoshi, T. Sueyoshi, K. Miyahara, T. Doi, H. Kitaguchi, S. Awaji, K. Watanabe, Superconductor Science and Technology, 18 (2005) 1460.

Chapter 3: MICROSTRUCTURAL AND CRYSTALLOGRAPHIC IMPERFECTIONS OF MgB_2 SUPERCONDUCTING WIRE AND THEIR CORRELATION WITH THE CRITICAL CURRENT DENSITY

A comprehensive study of the effects of structural imperfections in MgB_2 superconducting wire has been conducted. As the sintering temperature becomes lower, the structural imperfections of the MgB_2 material are increased, as reflected by detailed X-ray refinement and the normal state resistivity. The crystalline imperfections, caused by lattice disorder, directly affect the impurity scattering between the π and σ bands of MgB_2, resulting in a larger upper critical field. In addition, low sintering temperature keeps the grain size small, which leads to a strong enhancement of pinning, and thereby, enhanced critical current density. Owing to both the impurity scattering and the grain boundary pinning, the critical current density, irreversibility field, and upper critical field are enhanced. Residual voids or porosities obviously remain in the MgB_2, however, even at low sintering temperature, and thus block current transport paths.

3.1: INTRODUCTION

The synthesis of MgB_2 material at low sintering temperature keeps the grain size small, which leads to a strong enhancement of pinning [1]. Nevertheless, 30-40% void content, resulting in severe degradation of critical current, is still hard to avoid in the in-situ process [2]. Such a drawback indicates that there is still room to further enhance the superconducting performance, especially the critical current. In early works of Flukiger [3] and Tanaka [4], it was shown that

core or packing density is strongly related to the critical current. It was further reported that the porosities or voids hindered grain connectivity, and are apparently argued to be the prime cause for reduced critical current. A direct way to eliminate the void formation, the internal Mg diffusion method [5-8], has been developed, and denser wires and bulks can be fabricated. Nevertheless, a central void area due to the Kirkendall effect of magnesium still remains one of disadvantages in terms of commercialization. According to the recent literature [9], the void fraction is significantly diminished by homogeneous carbon capping as an alternative method, approaching the theoretical limit of 30% voids, which exactly corresponds to the increase in the measured low field critical current density. It is to be noted, however, that the performance of such MgB_2 is still far below the de-pairing current density of MgB_2.

The major challenge is how to improve grain connectivity or how to remove voids to further raise the critical current without electrical dissipation. To achieve this, the structural or microscopic origin for the enhancement needs to be studied in depth [10-15]. MgB_2 is a two-band superconductor, and the superconducting properties can be greatly influenced in various ways that depend on this, for example, by microstructural imperfections[16-21], but there is no consensus as yet, mainly because of difficulties in obtaining atomic-scale transmission electron microscope (TEM) images. In this study, as an extension to studies on MgB_2 wire, the variation of various structural parameters and defects has been extensively evaluated and is discussed with the critical current performance. We clarify that the structural or microscopic mechanism arises from intrinsic defects and a resulting increase in the impurity scattering rate.

3.2: EXPERIMENTAL PROCEDURE

MgB_2 wire was fabricated by the in-situ power-in-tube process. Magnesium (Mg, 99.9%, 325 mesh) and boron (B, 99.8%, 1 μm) powders were used as starting materials with the composition of Mg: B = 1: 2. The mixed powders were put into an iron (Fe) tube with a length of 140 mm. The Fe tube had an outer diameter (O.D.) of 10 mm and an inner diameter (I.D.) of 8 mm. The composite was drawn down to an O.D. of 0.8 mm. The fabricated wires were then wrapped in Zr foil and sintered at 650 to 1000^{o}C for 30 min under high purity argon (Ar, 99.9%) gas. All samples were initially characterized by detailed X-ray diffraction analysis. The morphology and microstructure were characterized by field emission-scanning electron microscopy (SEM) and transmission electron microscopy (TEM). Transport measurements to determine resistivity (ρ) were carried out by the standard ac four-probe method. Transport critical current (J_c) was characterized by the standard four-probe method with the criterion of 1μVcm^{-1}. In the case of the irreversibility field (B_{irr}), two kinds of criteria were applied: 1) B_{irr} was defined at a J_c (or I_c) criterion of 100 Acm^{-2} (or 0.1 A), as obtained from a linear extrapolation of the field dependence of the critical current density (or critical current) and 2) B_{irr}(T) was defined as the field where the temperature dependent resistance at constant magnetic field, R(H_{irr}, T) = 0.1Rns, with Rns being the normal state resistance at 40 K.

3.3: RESULTS AND DISCUSSION

MgB_2 phase is known to start to form from 580^{o}C under Ar atmosphere [22]. Two exothermal peaks are commonly observed. The first peak around 450^{o}C

might be related to the MgO formation due to a reaction between Mg and B_2O_3. B_2O_3 is known to melt around this temperature. The second peak around 600°C is attributed to the MgB_2 formation. Based on this study, we thus sintered the MgB_2 wire at 650°C for 30 min as a reference, and the structural analysis of this MgB_2 wire was directly confirmed by high-energy synchrotron radiation (SR) powder diffraction using a large Debye-Scherrer camera equipped with an imaging plate as a highly sensitive X-ray detector, at an experimental hutch of SPring-8, Japan. The SR diffraction pattern is shown in Figure 3.1.

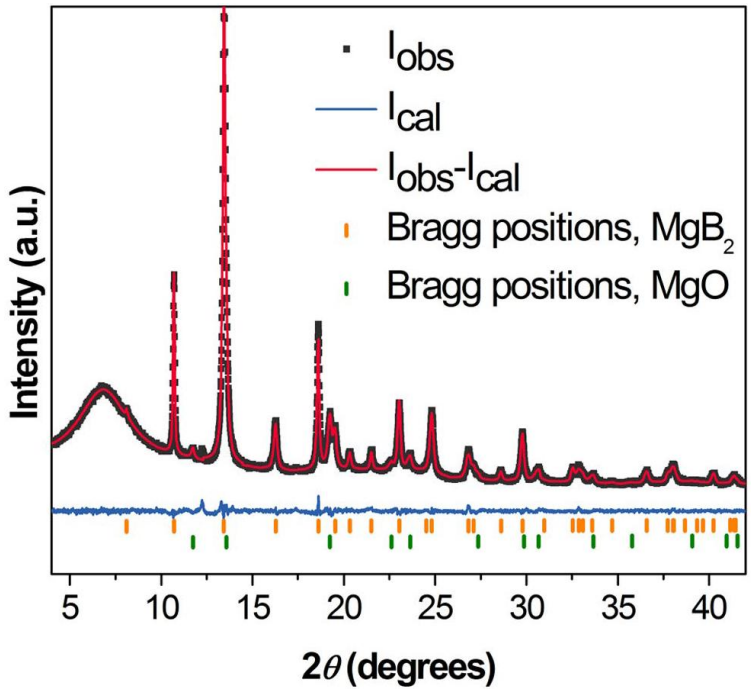

Fig 3.1: High-energy SR diffraction pattern of pure MgB_2 wire sintered at 650°C for 30 min. The markers indicate the Bragg peak positions for MgB_2 and MgO, respectively.

To obtain more information, the Rietveld refinement of the crystal structure was carefully carried out with the RIETAN-2000 program [23]. As shown in Table 3.1, the a- and c-axis lattice parameters were estimated to be 3.0832(2) Å and 3.5221(2) Å, respectively, which are consistent with the literature [24].

In general, the results of refinement can be assumed to be reliable when the

value of χ^2 (goodness of fit) is under 1.69 [25]. This means that our calculation is quite reasonable. Peak broadening, which is caused by smaller size crystallites or sub-grains, and micro-strain within the crystal lattice, was also analyzed using an asymmetric pseudo-Voigt function [26]. The calculated crystallite size was 44 nm, and lattice strain was 0.34%. This induced strain directly affects the impurity scattering between the π and σ bands of MgB_2 [27]. Interestingly, a large fraction of MgO (7 – 10% mass fraction) still existed in our samples. Spherical MgO particles 30-40 nm in size were obviously observed along the [011] beam orientation, and one of these is shown in Figure 3.2.

Table 3.1. Results of Reitveld refinement on the XRD data.

Crystal system	Hexagonal
Space group	P6/mmm
SR powder diffraction experiment	
Radiation source	Synchrotron
λ (Å)	0.499902 (2)
Δ 2θ(°)	0.01
Temperature (K)	300
Reliability factors and goodness of fit	
R_{wp} (%)	2.23
R_p (%)	1,74
R_B (%)	1.82
R_F (%)	0.9
χ^2	0.93
Lattice parameters and unit-cell volume	
a (Å)	3.0832 (2)
c (Å)	3.5221 (2)
V (Å^3)	28.997 (3)
Peak broadening parameters	
X	0.058 (1)
Y	0.262 (36)
Crystallite size (nm)	44 (1)

Lattice distortion (%)	0.34 (6)

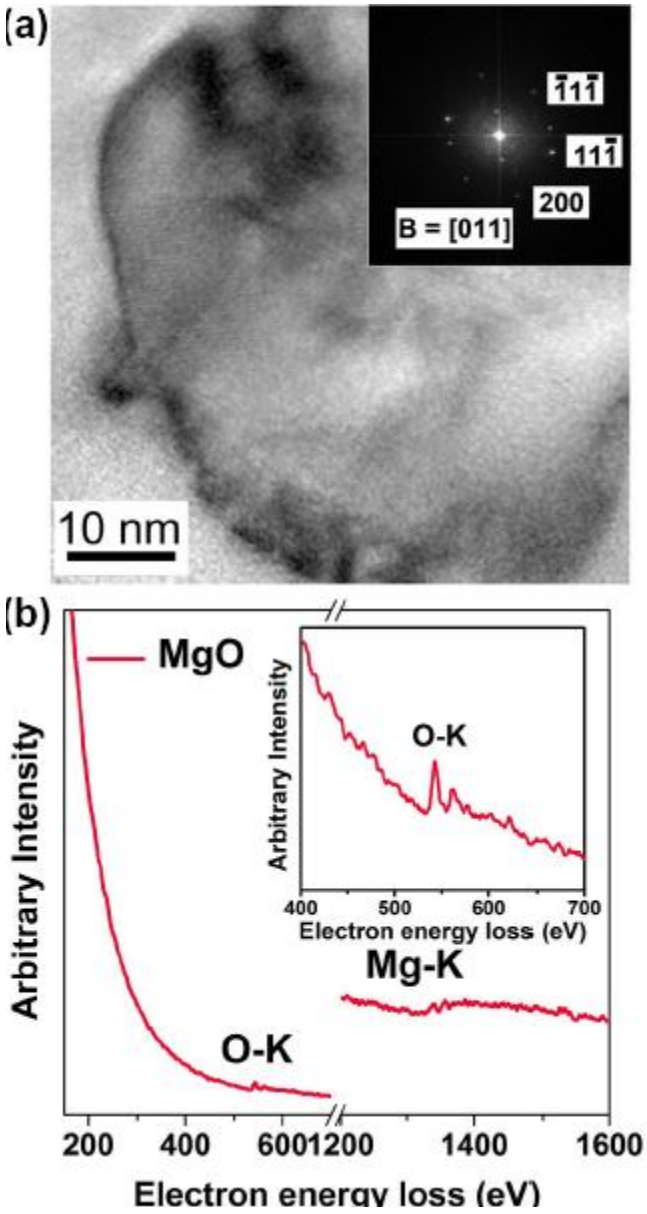

Fig 3.2: (a) Bright field-scanning transmission electron microscope (BF-STEM) image of an MgO particle in the MgB2 wire sintered at 650oC for 30 min, with inset showing the Fast Fourier transform (FFT) pattern, which coincides with MgO in the [011] beam orientation. (b) EELS spectrum of O-K and Mg-K edges, with the inset showing an enlargement of the O K edge.

The fast Fourier transform (FFT) pattern and electron energy loss spectrum (EELS) in Figure 3.2 are obviously confirmed. It is believed that the presence of nano-MgO precipitates in the MgB_2 polycrystalline grains is a common structural feature that has its origin in the magnesium powder. With regards to

role of the MgO particles, however, there is still controversy from the viewpoint of flux pinning. If the MgO particles have a homogeneous small size (< 10 nm) they would be helpful for enhancing the pinning [28]. In contrast, large-size MgO particles could act as an impurity phase, causing poor connectivity between grains [29,30].

In order to evaluate the effects of grain connectivity in depth, we sintered three wire samples at different sintering temperatures (650, 800, and 1000 ^{o}C) for a comparative study. The onset transition temperatures of the corresponding MgB_2 wires are estimated to be 37.5, 37.9, and 38.8 K, respectively, as shown in Figure 3.3.

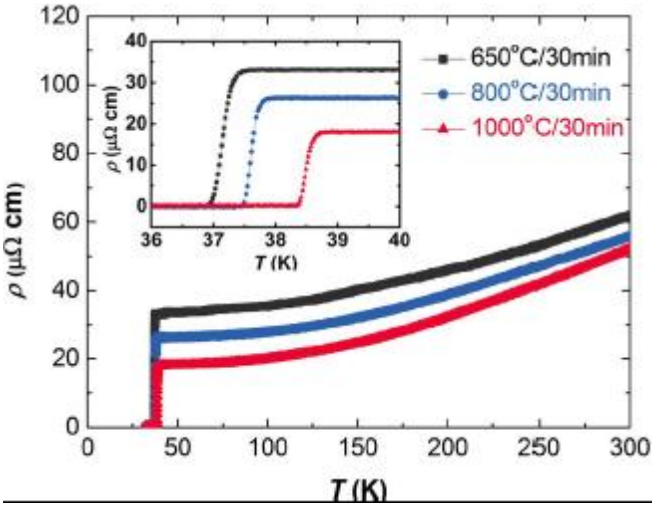

Fig 3.3: Temperature dependence of the resistivity (ρ) at 0 T for wires sintered at 650, 800, and 1000^{o}C. The inset shows an enlargement of the transition region.

With increasing sintering temperature, the critical transition temperature increased. The lower transition temperature observed in our sample sintered at 650^{o}C might be related to the strong impurity scattering between the π and σ bands of MgB_2, which is caused by crystalline imperfections, that is, a high degree of lattice disorder. The correlation between the lattice strain and the transition temperature was first reported by Serquis et al.[31] Lattice disorder

also can influence the resistivity and the critical current density [27]. It is generally argued that the residual resistivity, $\rho_{40}K$, is related to the intra-grain impurity scattering. Whereas the difference between the residual resistivity and the room temperature resistivity, $\Delta\rho = \rho_{300K} - \rho_{40K}$, is affected by inter-grain scattering [32]. In particular, the quantitative value of the residual resistivity seems to be closely correlated with the impurity scattering between the σ and π bands, resulting in the close correlation with the critical temperature. Importantly, the active cross-sectional area fraction (AF) [33] is usually defined as, $A_F = \Delta\rho_{ideal} / (\rho_{300\ K}-\rho_{40\ K})$, where $\rho_{40\ K}$ and $\rho_{300\ K}$ are the resistivity measured at 40 K and 300 K, respectively. $\Delta\rho_{ideal}$ is the resistivity difference between 40 K and 300 K for an ideal sample, and the value of 7.3 $\mu\Omega$ cm is typically used [34]. From the resistivity measurements, the A_F values were found to be 25.3, 24.7, and 21.4%, respectively, with increasing sintering temperature. It is to be noted that the grain connectivity represented by the A_F become poorer. This is because the amount of voids or porosities due to Mg evaporation increases with increasing sintering temperature. Clearly, the A_F of our wires fabricated by the powder-in-tube (PIT) process is still far below that for well-connected MgB_2 thin films [35]. From the viewpoint of the grain connectivity, a low temperature sintering process would be beneficial. Beside this, a low critical temperature is also known to be associated with grains that are kept small to improve the pinning or critical current density. Moreover, the broadening of the transition temperature was found to become larger with increasing external magnetic field up to 8.7 T, as shown in Figure 3.4.

In particular, the wire sintered at high temperature had a transition with a much longer tail at 8.7 T. This is probably due to thermally activated flux creep or flow [36]. From these viewpoints, wire sintered at low temperature will

be considered for further studies. The wire sintered at 650°C for 30 min under Ar is expected to exhibit the best critical current density.

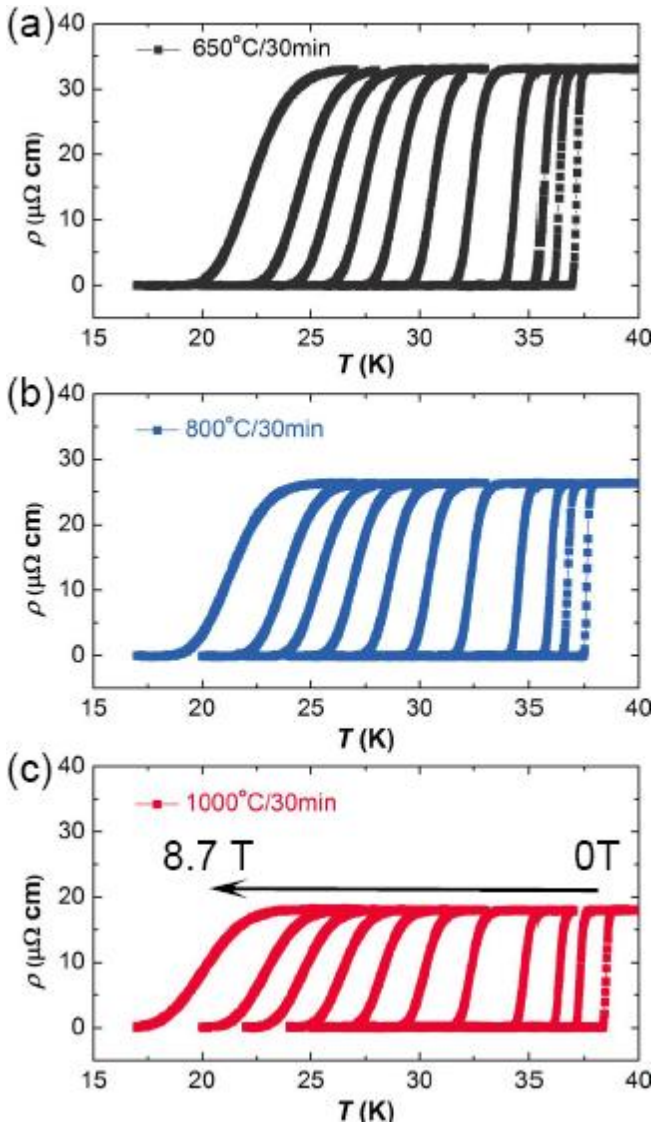

Fig 3.4: Resistivity versus temperature (ρ-T) measurements for wires sintered at (a) 650, (b) 800, and (c) 1000°C for 30 min at different applied magnetic field of 0, 0.25, 0.5, 1, 2, 3, 4, 5, 6, 7, and 8.7 T.

Critical current densities measured at different operating temperatures (4.2 K – 30 K) are shown in Figure 3.5(a). At 10 T and 4.2 K, the critical current density was estimated to be 3,000 A/cm^2, which is comparable to the values in previous reports [32]. In addition, the critical current density exceeds 10^5 A/cm^2 at 4 T and 4.2 K, and the corresponding value is more than 10^4 A/cm^2 at 20 K.

The field dependence of the critical current density or critical current (Figure 3.5(b)) can be numerically fitted by the following integral equation:[27, 37]

$$J_c = \int_0^{\infty} \left(\frac{P(J)-P(c)}{1-P(c)}\right)^{1.79} dJ \quad (3.1)$$

where p(J) is the fraction of grains with critical current density above J and Pc is the percolation threshold, the minimum fraction required for a superconducting current flow. The critical current of each grain is calculated with a grain boundary pinning model:

$$J_c = F_m . \frac{\left(1-\frac{B}{B_{c2}}\right)^2}{\sqrt{B_{c2}B}} \quad (3.2)$$

where F_m is the pinning force maximum.

The upper critical field, B_{c2}, has an angular dependence, which can be described by:

$$B_{c2}(\theta) = \frac{B_{c2}^{ab}}{\sqrt{\gamma^2 Cos^2(\theta)+Sin^2(\theta)}} \quad (3.3)$$

from the anisotropic Ginzburg-Landau theory. Here, only four fitting parameters, the upper critical field (B_{c2}), the anisotropy parameter (γ), the pinning force maximum (F_m), and the percolation threshold (Pc) are needed to describe the field dependence of the critical current for each temperature. We previously reported that for polycrystalline wire samples, the percolation threshold, Pc, is usually 0.26, and that value was used in this work as well [9,20,27]. The best fitting parameters are listed in Table 3.2, and the corresponding fitting curves are shown together in Figure 3.5(b).

For practical applications, the temperature dependence of the irreversibility

field (B_{irr}) for the MgB_2 is also of importance, as shown in Figure 3.6.

Two different kinds of criteria are applied to estimate B_{irr}. It can be observed that the estimated values from the resistivity are larger than from the critical current density. This is probably due to the differences between the ac and dc transport measurements. The general trend is similar, however, as a function of operating temperature. We also can estimate the irreversibility field from the Kramer plot, as shown in inset of Figure 3.6.

Table 3.2. Percolation model fitting parameters.

Temp. (K)	F_m (ATcm^{-2})	B_{c2} (T)	Gamma (γ)	P_c
4.2	3767123	24.7	4	0.26
10	2739726	17.4	3.1	0.26
15	1815068	12.4	2.4	0.26
20	1232877	9.45	2.33	0.26
25	582192	6.45	2.2	0.26
30	102740	4.05	2.1	0.26

According to the Kramer plots, the pinning force, $F_p = Ic^{1/2} \times B^{1/4}$, is expected to be a linear function of field. Long tails at the offset in the measured data were observed, however. This method for the determination of the irreversibility field might be underestimating it, in view of the actual upper critical field. Another interesting feature is the strong relationship between the upper critical field and the irreversibility field. The irreversibility field is commonly known to be enhanced by inducing structural defects, such as distortion and poor crystallinity [9]. In addition, an increase in the upper critical

field affects the irreversibility field. In our study, superior superconducting properties, especially the field dependence of the critical current density, can be governed by the larger upper critical field from imperfections in the crystalline structure, as well as the strong pinning from small grains. Therefore, structural imperfections are very crucial for superior critical current density. The structural imperfections are known to be induced by both carbon doping and the low temperature sintering process. It is very difficult, however, to reduce the voids.

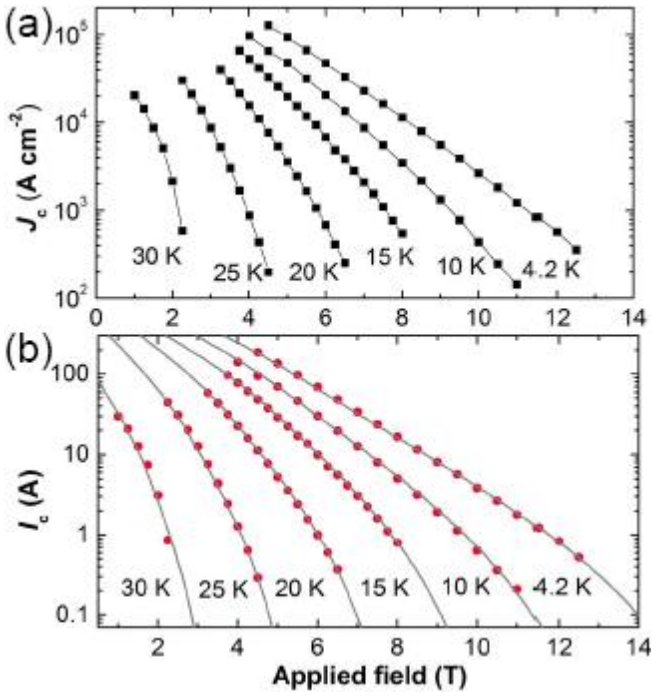

Fig 3.5: Field dependence of (a) the critical current density and (b) the critical current for wire sintered at 650°C for 30 min at different operating temperatures of 4.2, 10, 15, 20, 25, and 30 K. All fitting lines of Figure 3.5(b) are calculated using the percolation model.

Figure 3.7 shows SEM images of polished core surface for samples sintered at 650°C, 800°C, and 1000°C for 30 min. As can be seen in the images, porosities/voids remained the sample, regardless of sintering temperatures. Voids were present due to mainly Mg melting. This phenomenon occurs

because melted magnesium at around 650°C starts to diffuse into solid amorphous boron.

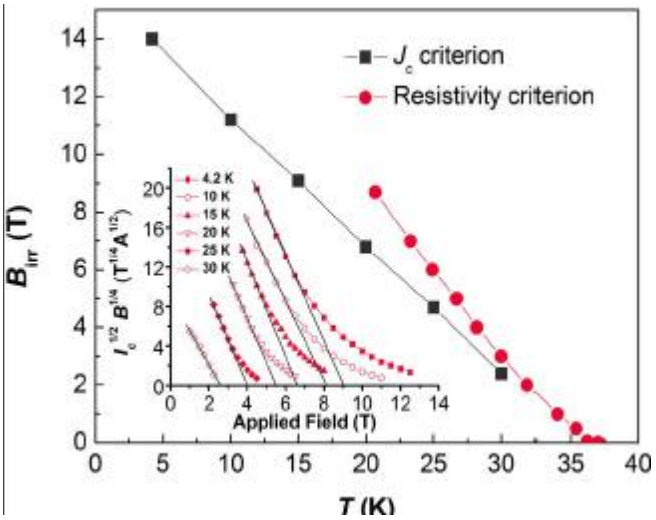

Fig 3.6: Temperature dependence of the irreversibility field (B_{irr}) of wire sintered at 650°C for 30 min. Inset shows the Kramer plots at different temperatures.

As a result, voids normally reduce the active superconducting area and the current transport paths. In order to obtain more clues, the microstructure near voids is further observed by scanning TEM (STEM) image and energy dispersive X-ray (EDX) spectroscopy elemental mapping, as can be seen in Figure 3.8.

Very interestingly, oxygen (O) surrounding voids are obviously found as a thin layer, indicating existence of MgO. Since voids were originally obtained from spaces of Mg powders. That is, residual Mg near by the voids would be oxidized to form MgO. It is noted that MgO particles segregated near voids severely degrade the connectivity between crystalline MgB_2 grains and shorten current transport paths. From this observation, it is expected that dense MgB_2 core, without voids or porosities, can bring superior critical current.

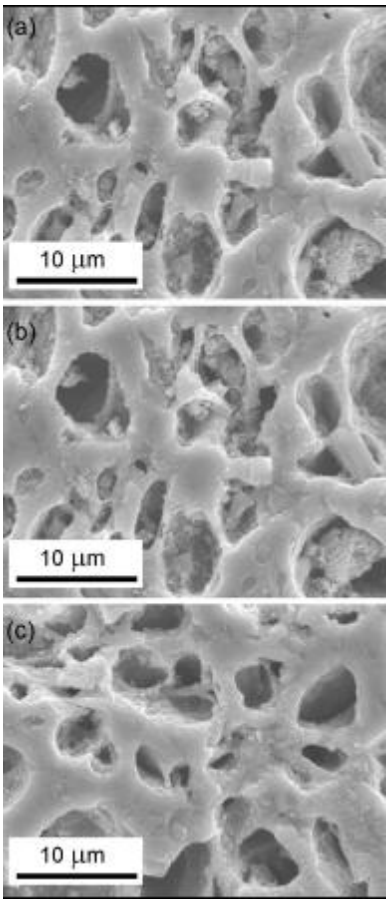

Fig 3.7: SEM images of polished core surface for samples sintered at 650°C, 800°C, and 1000°C.

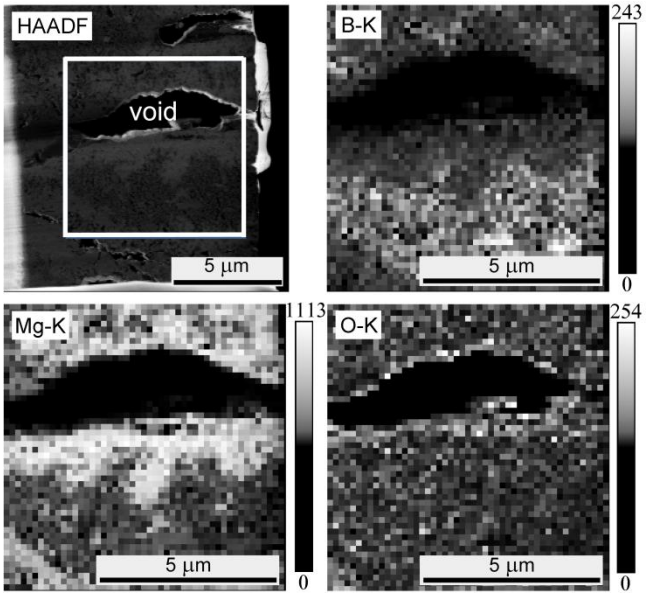

Fig 3.8: STEM image of the MgB_2 near void and EDX element maps from the selected area.

Moreover residual boron powders are still remained even after sintering process, as can be seen in Figure 3.9. For this, STEM image and EDX spectroscopy were again used. Coarse crystalline MgB_2 grains are found to be blocked by the residual boron powders, thereby degradation of the current transport paths as well. Therefore, we believe that the elimination of the voids and residual boron powders is very important to further improve the transport critical current of MgB_2 superconductor for practical applications.

As can be seen in Figure 3.10, a large fraction of MgO particles are randomly existed because MgO formation could easily take place before MgB_2 is formed. This indicates that the MgO formation yields deficient magnesium, resulting in residual boron powders (Figure 3.9). Thus reducing exposure to oxygen plays an important role in this MgB_2 system. Alternatively, excess magnesium, which can compensate the magnesium deficiency due to the MgO formation, would be effective way to reduce residual boron powders in the MgB_2 matrix.

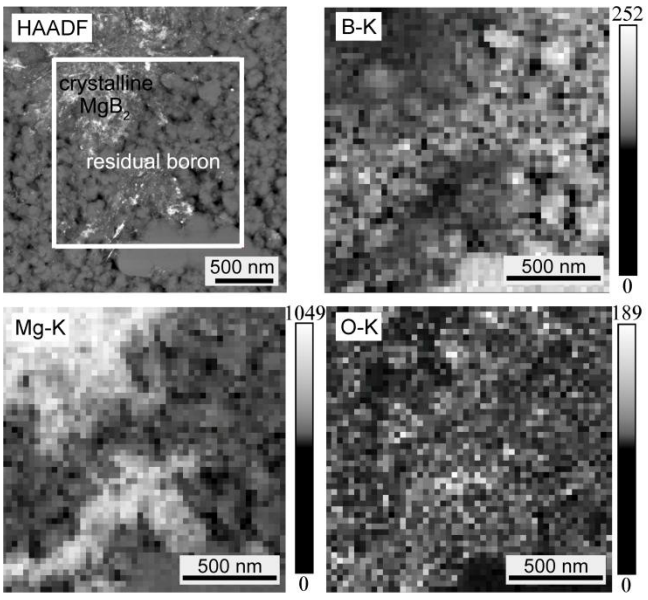

Fig 3.9: STEM image of the MgB_2 and residual boron and EDX element maps from the selected area.

3.4: CONCLUSIONS

In summary, detailed structural analysis has been conducted on MgB_2 superconducting wire sintered at various temperatures. It was found that the lower transition temperature due to low sintering temperature is related to higher impurity scattering between the π and σ bands of MgB_2 caused by high lattice disorder and crystalline imperfections. Strong impurity scattering causes a larger upper critical field, and thereby, increases the critical current density.

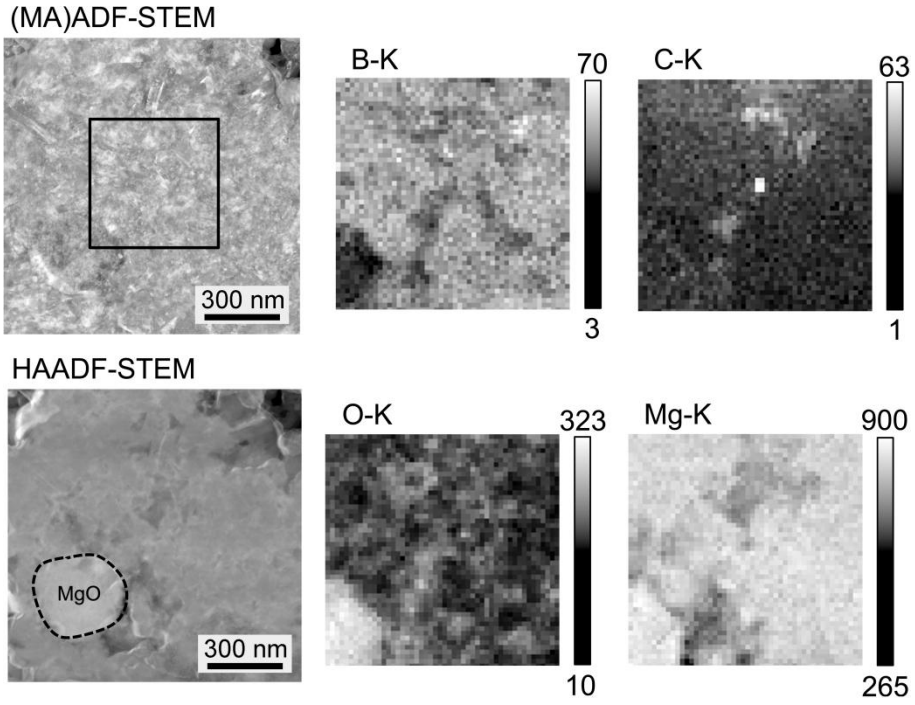

Fig 3.10: STEM image of the MgB_2 and MgO and EDX element maps from the selected area.

Moreover, the low sintering temperature keeps the grain size small, which strongly enhances pinning. To further enhance in-field critical current density, the voids or porosities, which block transport current paths, need to be decreased. Our comprehensive studies provide atomic-level insights that can pave the way for enhancing transport critical current to meet the requirements

of practical applications.

3.5: References

[1] P. Mikheenko, E. Martínez, A. Bevan, J. S. Abell, and J. L. MacManus-Driscoll, Supercond. Sci. Technol. 20, S264 (2007).

[2] A. Yamamoto, J. Shimoyama, K. Kishio, and T. Matsushita, Supercond. Sci. Technol. 20, 658 (2007).

[3] R. Flukiger, M. S. A. Hossain, and C. Senatore, Supercond. Sci. Technol. 22, 085002 (2009).

[4] H. Tanaka, A. Yamamoto, J. Shimoyama, H. Ogino, and K. Kishio, Supercond. Sci. Technol. 25, 115022 (2012).

[5] T. Togano, J. M. Hur, A. Matsumoto, and H. Kumakura, Supercond. Sci. Technol. 22, 015003 (2009).

[6] M. Maeda, J. H. Kim, Y. Zhao, Y.-U. Heo, K. Takase, Y. Kubota, C. Moriyoshi, F. Yoshida, Y. Kuroiwa, and S. X. Dou, J. Appl. Phys. 109, 023904 (2011)

[7] G. Z. Li, M. D. Sumption, M. A. Susner, Y. Yang, K. M. Reddy, M. A. Rindfleisch, M. J. Tomsic, C. J. Thong, and E. W. Collings, Supercond. Sci. Technol. 25, 115023 (2012).

[8] H. Kumakura, J. Phys. Soc. Jpn. 81, 011010 (2012).

[9] J. H. Kim, S. Oh, Y.-U. Heo, S. Hata, H. Kumakura, A. Matsumoto, M. Mitsuhara, S. Choi, Y. Shimada, M. Maeda, J. L. MacManus-Driscoll, and S. X. Dou, NPG Asia Mater. 4 E3 (2012).

[10] Y. Zhu, A. Matsumoto, B. J. Senkowicz, H. Kumakura, H. Kitaguchi, M. C. Jewell, E. E. Hellstrom, D. C. Larbalestier, J. Appl. Phys. 102, 013913 (2007).

[11] B. Birajdar and O. Eibl, J. Appl. Phys. 105, 033903 (2009).

[12] W. Häßler, B. Birajdar, W. Gruner, M. Herrmann, O. Perner, C. Rodig, M. Schubert, B. Holzapfei, O. Eibl, and L. Schultz, Supercond. Sci. Technol. 19, 512 (2006).

[13] S. Hata, H. Sosiati, Y. Shimada, A. Matsumoto, K. Ikeda, H. Nakashima, H. Kitaguchi, and H. Kumakura, J. Mater. Sci. 48, 132 (2013).

[14] S. G. Kang, J. K. Chung, S. C. Park, B. H. Jun, C. -J. Kim, C. J. Kim, Physica C 468, 15 (2008).

[15] X. Y. Song, Ceram. Inter. 39, 4299 (2013).

[16] M. A. Susner, M. D. Sumption, M. A. Rindfleisch, and E. W. Collings, Physica C 490, 20 (2013).

[17] M. Herrmann, W. Haessler, C. Rodig, W. Gruner, B. Holzapfel, and L. Schultz, Appl. Phys. Lett. 91, 082507 (2007).

[18] C. D. Wang, D. L. Wang, X. P. Zhang, C. Yao, C. L. Wang, Y. W. Ma, H. Oguro, S. Awaji, K. Watanabe, Supercond. Sci. Technol. 25, 125001 (2012).

[19] E. W. Collings, M. D. Sumption, M. Bhatia, M. A. Susner, S. D. Bohnenstiehl, Supercond. Sci. Technol. 21, 103001 (2008).

[20] J. H. Kim, S. Oh, H. Kumakura, A. Matsumoto, Y.-U. Heo, K.-S. Song, Y.-M. Kang, M. Maeda, M. Rindfleisch, M. Tomsic, S. Choi, and S. X. Dou, Adv. Mater. 23, 4942 (2012).

[21] M. Maeda, J. H. Kim, Y.-U. Heo, S. K. Kwon, H. Kumakura, S. Choi, Y. Nakayama, Y. Takano, and S. X. Dou, Appl. Phys. Express 5, 013101 (2012).

[22] J. H. Kim, S. X. Dou, J. L. Wang, D. Q. Shi, X. Xu, M. S. A. Hossain, W. K. Yeoh, S.Choi, and T. Kiyoshi, Supercond. Sci. Technol. 20, 448 (2007).

[23] F. Izumi and T. Ikeda, Mater. Sci. Forum 321-324, 198 (2000).

[24] J. Nagamatsu, N. Nakagawa, T. Muranaka, Y. Zenitani, and J. Akimitsu, Nature 410, 63 (2001).

[25] R. A. Young, The Rietveld Method. International Union of Crystallography, Oxford Univ. Press, Oxford (1993).

[26] P. Thompson, D. E. Cox, and J. B. Hastings, J. Appl. Crystallogr. 20 79 (1987).

[27] J. H. Kim, S. X. Dou, Sangjun Oh, M. Jerčinović, E. Babić, T. Nakane, and H. Kumakura, J. Appl. Phys. 104, 063911 (2008).

[28] C. H. Jiang, H. Hatakeyama, and H. Kumakura, Physica C 423, 45 (2005).

[29] M. Maeda, J. H. Kim, Y.-U. Heo, S. K. Kwon, H. Kumakura, S. Choi, Y. Nakayama, Y. Takano, and S. X. Dou, Scripta Mater. 64, 1059 (2011).

[30] P. Kovac, I. Hugek, T. Meligek, J. C. Grivel, W. Pachla, V. Stribik, R. Diduszko, J. Homeyer, and N. H. Andersen, Supercond. Sci. Technol. 17, L41 (2004).

[31] A. Serquis, X. Z. Liao, Y. T. Zhu, J. Y. Coulter, J. Y. Huang, J. O. Willis, D. E. Peterson, F. M. Mueller, N. O. Moreno, J. D. Thompson, V. F. Nesterenko, S. S. Indrakanti, J. Appl. Phys. 92, 351 (2002).

[32] J. H. Kim, S. X. Dou, D. Q. Shi, M. Rindfleisch, and M. Tomsic, Supercond. Sci. Technol. 20, 1026 (2007).

[33] J. M. Rowell, Supercond. Sci. Technol. 16, R17 (2003).

[34] R. H. T. Wilke, S. L. Bud'ko, P. C. Canfield, D. K. Finnemore, R. J. Suplinskas, and S. T. Hannahs, Physica C 424, 1 (2005).

[35] X. X. Xi, A. V. Pogrebnyakov, S. Y. Xu, K. Chen, Y. Cui, E. C. Maertz, C. G. Zhuang, Q. Li, D. R. Lamborn, J. M. Redwing, Z. K. Liu, A. Soukiassian, D. G. Schlom, X. J. Weng, E. C. Dickey, Y. B. Chen, W. Tian, X. Q. Pan, S. A. Cybart, and R. C. Dynes, Physica C, 456, 22 (2007).

[36] A. Sidorenko, V. Zdravkov, V. Ryazanov, S. Horn, S. Klimm, R. Tidecks, A. Wixforth, Th. Koch, and Th. Schimmel, Philosophical Magazine 85, 16 (2005).

[37] M. Eisterer, M. Zehetmayer, and H. W. Weber, Phys. Rev. Lett. 90, 247002 (2003).

Chapter 4: A COMPREHENSIVE STUDY OF THE PINNING MECHANISMS OF MgB_2 WIRES TREATED WITH MALIC ACID AND THEIR RELATIONSHIPS WITH LATTICE DEFECTS

The effects of sintering temperature on the lattice parameters, structural strain, critical temperature (T_c), critical current density (J_c), irreversibility field (B_{irr}), upper critical field (B_{c2}), and resistivity (ρ) of MgB_2 wires treated with 10 wt.% malic acid ($C_4H_6O_5$) are investigated in this paper. The a-lattice parameter of the sample treated with malic acid was drastically reduced, to 3.0745 ˚A, as compared to those for the un-doped samples. Reduction in the a-lattice parameter is related to crystalline imperfections arising from carbon substitution—as confirmed by x-ray diffraction and Raman spectra—which play a vital role in enhancing J_c, B_{c2} and B_{irr}. We have also analyzed the pinning mechanisms, and concluded that flux pinning is dominated by point and correlated pinning at lower and higher magnetic fields, respectively, for the carbon-doped samples sintered at both 700 and 900˚C. The degree of flux pinning enhancement and the ratio RHH (B_{c2}/B_{irr}) have been estimated to guide us towards further enhancement of Jc. We argue that δl and δT_c pinning mechanisms, based on variation of the mean free path (£) and the critical temperature, respectively, coexist in the MgB_2 wires treated with malic acid, regardless of the sintering temperature. The δl pinning is predominant at lower operating temperatures, and δT_c pinning starts close to T_c, which means that spatial variation in the charge carrier mean free path is the main mechanism responsible for the flux pinning in the MgB_2 wires treated with malic acid that were sintered at 700 and 900˚C.

4.1: Introduction

The discovery of MgB_2 as the best candidate among the metallic compounds for superconducting purposes, due to its high critical temperature (Tc ≈ 39 K) [1], superior critical current density (J_c) even at the high temperature of 20 K, and simple crystalline structure, has encouraged researchers to pay extraordinary attention to this compound. Its simple preparation and low production costs, as well as the other aforementioned properties, provide a big potential for MgB_2 to be used in direct current (DC) applications such as in magnetic resonance image (MRI) magnets [2]. Nowadays, MgB_2 is considered as one of the most likely MRI candidates, which has the potential to replace Nb–Ti conventional superconductors in this market. Nevertheless, to make MgB_2 wires/tapes suitable for alternating current (AC) applications, such as in current limiters, motors, and transformers, considerable effort is still needed to overcome AC losses. For industrial application, its critical current density has to be enhanced and should not drop sharply with increasing magnetic field. Poor flux pinning is the major source of these problems when the magnetic field increases. Since superconductor material suddenly quenches due to the in-line movement of vortices with current flow at the irreversibility field (B_{irr}), improvement of the pinning mechanism must be the way to restrict the movement of vortices [3–8]. Inter-grain boundary pinning and point defect pinning are known to be the most effective pinning mechanisms for Jc enhancement [3, 5, 7, 8]. The carbon as a dopant also shows the best effects in terms of enhancement of Jc; therefore, many researchers have been investigating the effects of various sources of carbon on the superconductivity of MgB_2, including organic dopants produced via the chemical solution

method [9, 10], which is an economical fabrication process and has the potential to be implemented in industrial application. Recently, adding malic acid as a source of carbon to MgB_2 has resulted in enhancement of its Jc and upper critical field (B_{c2}). A sample constructed from a homogeneous mixture of malic acid and boron powders in MgB_2 mono-filamentary wire with iron as the outer sheath, with sintering at 650°C, showed a high J_c of 10^4 A cm^{-2} at 4.2 K and 10 T [11]. The Jc performance of malic acid treated MgB_2 after cold high pressure densification (CHPD) has been further improved [12]. This high J_c motivated us to investigate the dominant pinning mechanisms for different sintering temperatures of MgB_2 wires with 10 wt% malic acid additive. It has been proven that δT_c pinning is the dominant pinning mechanism for polycrystalline bulk [6], thin film [13], and single-crystal [14–16] pure MgB_2 samples, while δl becomes dominant for all aforementioned carbon-doped samples [3, 8, 17]. Since not much work has been done yet on the pinning mechanisms in MgB_2 wire form, we have investigated the dominant pinning mechanisms of 10 wt% malic acid treated MgB_2 wire, showing the best performance so far, and analyzed the structural disorder arising from carbon substitution into boron sites and micro-strain in the lattice at different sintering temperatures. Moreover, we have investigated the role of core interactions in vortex flux pinning mechanisms in state of the art MgB_2 material. The core pinning in MgB_2 can be attributed to the random distribution of spatial variations in the transition temperature (δT_c pinning) or to the variations of the charge carrier mean free path (δl pinning) due to crystal lattice defects [3].

4.2: Experimental procedure

10 wt% malic acid treated MgB_2 superconducting wire with iron as the outer sheath was fabricated with a cross-sectional area of 2×2 mm^2, via the powder-in-tube method. Two doped samples 4 cm in length were cut from the aforementioned wire and sintered in a tube furnace in flowing Ar gas at temperatures of 700 and 900 °C for 30 min to obtain samples with small and large MgB_2 grains, respectively. Different sintering temperatures were conducted to investigate the role of MgB_2 grain size in the flux pinning mechanism. A physical properties measurement system (PPMS, Quantum Design) was used for measurement of the magnetic critical current density (J_c), resistivity (ρ), and critical temperature (T_c). A parallel magnetic field has been applied to the length of the samples for physical properties measurement. Magnetic hysteresis loops were collected for all samples over the temperature range of 10–31 K.

The Bean approximation model: $J_c = 20\frac{\frac{\Delta M}{V}}{a(1-\frac{a}{3b})}$, was used for calculation of the critical current density, where ΔM is the height of the M-H hysteresis loop and V is the volume of the sample (V = a × b × c and a < b < c). An x-ray diffraction (XRD) study was carried out with a step size of 0.020° on a GBC MMA x-ray diffraction device using Cu Kα radiation to investigate the structural crystalline properties.

Raman spectroscopy was used to investigate the electron–phonon coupling strength of the 10 wt% malic acid treated MgB_2 wire sintered at different temperatures. An Ar+ laser with a wavelength of 514.5 nm (2.41 eV) was used for excitation of the Raman signal, and our measurements were performed with the Raman shifts ranging from 350 to 1000 cm^{-1}. We

measured at several spots on each sample to eliminate the effects of randomly oriented microcrystals. It has to be mentioned that the iron sheath was pulled off all of our as-prepared samples by using a micro-cutter/polishing device before doing any measurements.

4.3: results and discussion:

From Table 4.1, the a-axis lattice parameter decreased compared to untreated one for malic acid treated MgB_2 (MgB_2+10 wt% $C_4H_6O_5$) samples sintered at 700^{o}C and 900^{o}C for 30 min, suggesting that either an active substitution of carbon into the boron sites occurs and/or strain is introduced into the lattice. The refined data through X-ray analysis and resistivity measurement show that strain and resistivity decrease from 0.396% to 0.264% and from 70 μΩcm to 54 μΩcm, respectively, with increasing sintering temperature, as shown in Table 4.1. Interestingly, estimated a lattice parameters between malic acid treated MgB_2 wires sintered at different sintering temperatures do not show any significant difference, but both samples show smaller a lattice parameter compared to un-doped one [11]. Lattice disorder is an important factor that determines the transition temperature of the malic acid treated samples, as evidenced by the correlations among the lattice strain, the resistivity, and the transition temperature [11]. Both carbon and carbon compound additives in MgB_2 have been shown to cause reductions in the a-axis lattice parameter in a similar manner [18]. Wang et al. reported that the strain effect is the major factor accounting for the lattice parameter reduction for non-carbon additives [19]. Studies of ball milling of doped and un-doped samples [20], or excess Mg with SiC doping [21], or even pure MgB_2 with Mg deficiency [22] revealed that

higher strain imposes larger lattice shrinkage, although at various rates. All these reports are in agreement with our study that the strain effect has a major impact on T_c and lattice distortion, where the cooperative effects of strain and carbon substitution should also be accounted for in carbon-doped samples. The sample sintered at 700°C shows higher micro-strain, 0.396% (Table 4.1), than the sample sintered at 900°C. The higher strain effect due to the crystalline imperfections arising from carbon substitution might be an alternative interpretation for lattice shrinkage in this work. However, the results of Raman spectroscopy still remain unclear, as shown in Figure 4.1 and Table 4.1. It has been reported that the peak at 600 cm^{-1}, the only Raman active mode for MgB_2, is related to the E_{2g} in-plane vibration mode of boron atom [23, 24]. The E_{2g} vibration mode can be obviously affected by atomic substitution or lattice distortion. As shown in Figure 4.1, the Raman spectra for both samples can be fitted by four peaks, which labeled as ω_1, ω_2, ω_3, and ω_4, respectively. Interestingly, the strain analyzed by the X-ray diffraction is higher for the sample sintered at 700°C, whereas the ω_2 peak shift is more pronounced for the sample sintered at 900°C. However, what is important is that, the full-width half maximum (FWHM) of the ω_2 is presenting factor for supporting an electron-phonon coupling in the Raman spectroscopy analysis. From Table 4.1, it is to be noted that the FWHM of the ω_2 for wire sintered at 700°C is obviously higher than that at 900°C. Table 4.1 also presents the measured resistivity (ρ) values, the residual resistivity ratio, (RRR, $\rho_{300\ K}/\rho_{40K}$), and the active cross-sectional area fraction (A_f) for the 10wt. % malic treated MgB_2 samples produced at different sintering temperatures. It was observed that ρ at 40 K and 300 K decreases with increasing sintering

temperature, respectively from 128 to 121 μΩ-cm and from 198 to 175 μΩ-cm. The relatively lower ρ near 300 K may be related to higher sample density and better inter-granular connectivity. On the other hand, the ρ values near the T_c are due to the intra-granular defects, since the phonon contribution to the electron scattering decreases when the temperature decreases [25]. These observations can be further supported by the Δρ and RRR behavior. It is well known that relatively high values of the RRR indicate good quality of the samples. The connectivity factor, A_f, has also been evaluated using the Rowell analysis [25]. As shown in Table 4.1, the value of A_f increases from 0.107 to 0.131 as the sintering temperature increases from 700°C to 900°C. Unfortunately, connectivity is still poor in both samples, but the 900 °C sample is slightly better compared to the 700 °C one.

The magnetic J_c (B, T) results for the samples sintered at 700°C and 900°C are shown in a double-logarithmic plot in Figure 4.2. Figure 4.2(a) shows that, at 8 T and 5 K, the Jc values for both samples are over 10^4 Acm^{-2}, more than four times higher than the values for the un-doped MgB_2 wire. Grain boundary pinning may also play a role, because it is usually important in the low field region, as seen in un-doped MgB_2. From Figure 4.2 (b), the J_c initially shows a plateau at low field and then begins to decrease quickly as the field reaches a crossover field, which is decreased with increasing temperature. For all fields and temperatures higher than 29 K, the J_c of the sample sintered at 900 °C is slightly higher than that of the sample sintered at 700 °C. This is mainly due to lower Tc, which is close to the operating temperature. At low magnetic fields and temperatures, samples sintered at 700°C have higher Jc values than the ones sintered at 900°C.

Table 4.1. Structural and physical properties of 10% malic acid treated MgB_2 samples sintered at different temperatures.

Samples	Lattice parameters		T_c (K)	ρ_{40} (μΩcm)	ρ_{300} (μΩcm)	Δρ	RRR/A_f	Lattice strain %	ω_2		
	a (Å)	c (Å)							Raman shift (cm^{-1})	FWHM(°)	Goodness of fitness
Malic 700	3.0767	3.5274	32.60	128	198	70	1.54/ 0.104	0.396	608.77	0.354	1.194
Malic 900	3.0770	3.5290	33.78	121	175	54	1.44/ 0.135	0.264	614.63	0.236	1.015

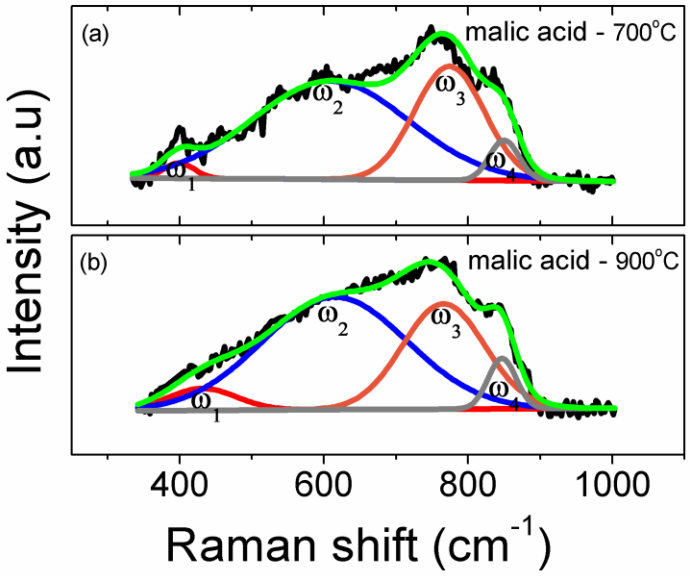

Fig 4.1: Raman spectra with peak fitting of the malic acid treated MgB_2 sintered at 700°C (a) and 900°C (b). The E2g Raman peak shifts to higher frequency with increasing sintering temperature, which is in agreement with the fact that higher temperature processing promotes more carbon substitution.

This result is consistent with our previously published report [26]. In the inset of Figure 4.2(b), it is also shown that the transport Jc values of 10 wt. % malic acid treated wire sintered at 700°C at 4.2 K, 10 K, and 20 K are significantly enhanced compared to the un-doped wire. This is mainly due to fresh carbon originating from the chemical solution route [9, 10], which occur as partial substitution inside the MgB_2 grains.

The temperature dependence of the upper critical field, B_{c2}, obtained from the 90% value of the corresponding resistivity transition (B_{irr} was obtained from 10% value of the resistivity transition), is shown in Figure 4.3. As typically reported, the B_{c2} curve shows a slight upward curvature close to T_c for both sintering temperatures, and it increases with increasing temperature. This fact further indicates the effective role of malic acid additive in forming fresh carbon at its decomposition temperature, which results in excellent field dependence of J_c at the same level as state-of-the-art nano-SiC-doped MgB_2 [18].

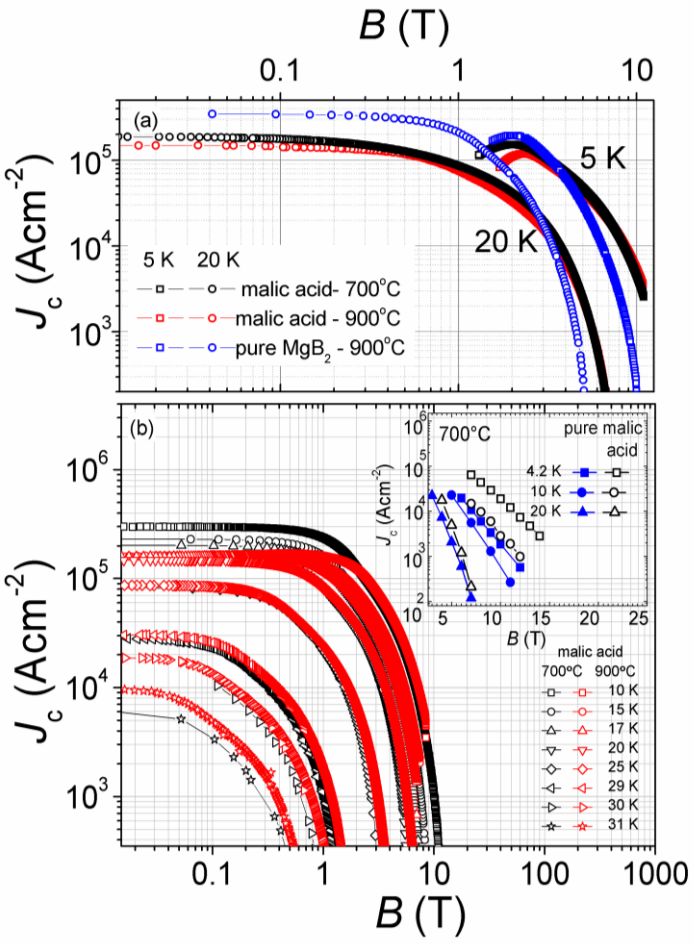

Fig 4.2: Field dependence of magnetic Jc for the malic acid treated MgB_2 wires sintered at 700°C and 900°C has been plotted at 5 K and 20 K for comparison with pure sample (a) and at other various operating temperatures (b). The inset of figure 4.2(b) shows the transport Jc versus magnetic field at 4.2 K, 10 K, and 20 K for the un-doped and malic acid treated MgB_2 sintered at 700°C.

The RRR, i.e., the ratio of the residual resistivity at 300 K to that at T_c has been widely used as a parameter to reflect the degree of electron scattering. It is well known that the RRR is decreased in the dirty-band case. In particular, quantitative value of the RRR only gives an indication of the electron scattering and may have no correlation with the degree of pinning. For better understanding, Wang et al. [19] suggested a new approach, RHH, the ratio of B_{c2} (T) to the irreversibility field, B_{irr} (T). It is obvious that if the RHH value is close to 1, the flux pinning, and thus Birr, has reached its limit. In other words, if effective pinning centers are present in an MgB_2 sample, the RHH should be as close to 1 as possible. If RHH is greater than 2, it means that Birr is only half as great as B_{c2}. In this case, flux pinning is not enhanced, even though the absolute value of B_{irr} may be higher than in MgB_2 with lower B_{c2}.

Now, we consider malic acid treated samples obtained by various heat-treatment conditions from the viewpoint of flux pinning. We need to know if the enhanced in-field J_c or B_{irr} is caused by the enhancement of B_{c2} or the introduction of more effective pinning centers compared to the pristine MgB_2 samples. For this, we calculated the RHH (B_{c2}/B_{irr}) ratios from Figure 4.3 for the malic acid treated MgB_2 samples.

The results are shown in Figure 4.4. As was discussed earlier, if the RHH value is close to 1, it means that flux pinning is very strong. As can be seen from Figure 4.4, the RHH value for the malic acid treated sample sintered at 900°C is closer to those for un-doped MgB_2 than those for the sample sintered at 700°C, indicating that the effective pinning becomes weaker for sintering at lower temperatures. The RHH values or RHH lines give us some guidance on how to further enhance the J_c of MgB_2. For carbon doping, it is clear that we

still have plenty of room to enhance the in-field J_c, if we can reduce the RHH value further or keep it constant at low temperatures by optimizing the fabrication conditions.

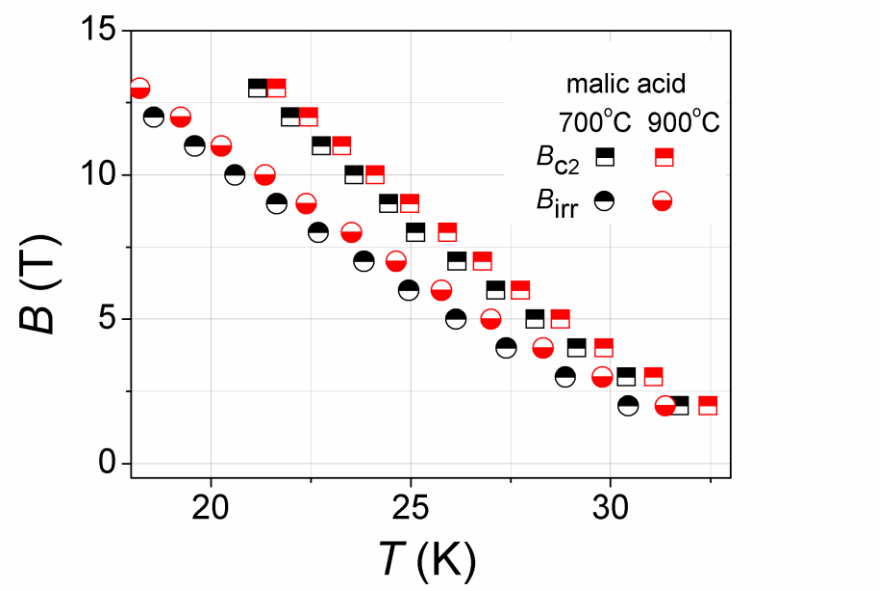

Fig 4.3: Bc2 and Birr versus operating temperature for the malic acid treated MgB_2 wires sintered at 700°C and 900°C.

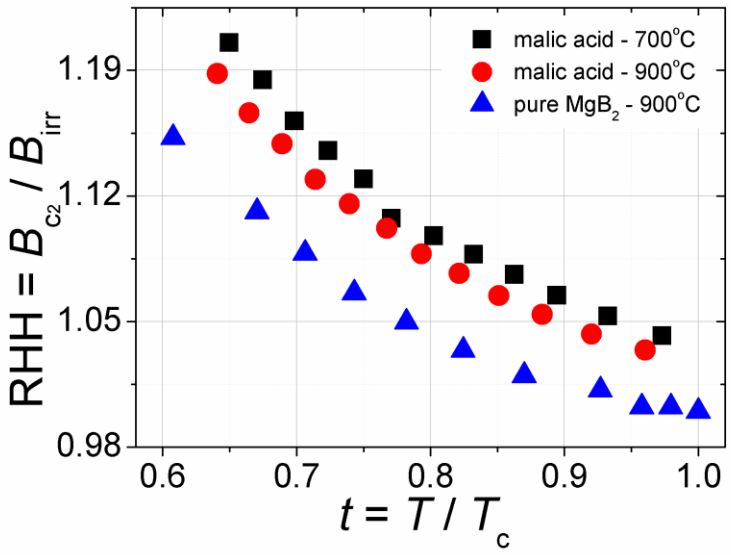

Fig 4.4: RHH ratio as a function of reduced operating temperature for the un-doped and malic acid treated MgB_2 wires sintered at 700°C and 900°C.

According to the two predominant mechanisms of core pinning in type-II

superconductors, δT_c and δl pinning, the crossover field from the single vortex to the small vortex bundle regime (B_{sb}) as a function of temperature as well as B_{th} which is attributed to sample's thermal fluctuations are shown in Figure 4.5 for the samples sintered at 700°C and 900°C. Here, both B_{sb} and B_{th} were extracted from double logarithmic plot of $-\mathrm{Log}[J_c/J_c\,(B=0)]$ versus B at different temperature while the departure point of straight line via positive curvature stands for B_{th} and with negative curvature stands for B_{sb} [8]. As can be seen in Figure 4.5(a), the crossover field B_{sb} is almost the same even under different reaction temperatures. We conclude that B_{sb} is not sensitive to the reaction temperature. In contrast, the $B_{th}(T)$ crossover field, reflecting the thermal regime, is obviously dependent on the sintering temperature. Griessen et al. [27] pointed out that the δT_c and δl pinning mechanisms result in different temperature dependencies of the critical current density j_{sv} in the single-vortex pinning regime. They found that $j_{sv} \propto (1-t^2)^{7/6}(1+t^2)^{5/6}$, with $t = T/T_c$, for the case of δT_c pinning, while for δl pinning, $j_{sv} \propto (1-t^2)^{5/2}(1+t^2)^{-1/2}$. Taking into account collective pinning theory [28], J_c is field independent when the applied field is lower than a crossover field B_{sb} at which the dominant pinning mechanism changes from single vortex to small bundle pinning. In the regime below B_{sb}, a single vortex pinning mechanism governs the vortex lattice and Bsb is proportional to the product of J_{sv} and Bc2. The following B_{sb} temperature dependence can be obtained [6]:

$$B_{sb}(T) = B_{sb}(0)[(1 - t^2)/(1 + t^2)]^{\upsilon} \qquad (4.1)$$

where $\upsilon = 2/3$ and 2 for δT_c and δl pinning, respectively. In Figure 4.5, the red and black curves indicate the δl and δT_c pinning mechanisms, respectively. The curve has a positive curvature in the δT_c pinning case, while the

curvature associated with the δl pinning is negative. As is clear from Figure 4.5(a), the B_{sb}(T) behavior shows a negative curvature. There is also a good agreement between our experimental points and the aforementioned equation with v = 2, which strongly suggests that the δl pinning mechanism is dominant for both sintering temperatures. We have also analyzed the B_{sb} by $B_{sb} = P_1 B_{sb}^{Tc} + P_2 B_{sb}^{l}$ to make a clear understanding of δT_c and δl contribution percentage in our samples, where B_{sb}^{Tc} and B_{sb}^{l}result to δT_c and δl pinning respectively and the sum of fitting parameters (P_1 and P_2) must be one ($P_1 + P_2=1$). Figure 4.5(b) shows the results of pinning mechanisms contribution based on calculated P parameters as $P = P_1 B_{sb}^{Tc}/B_{sb}$ for δTc and $P = P_2 B_{sb}^{l}/B_{sb}$ for δl pinning effects. We figured out that in our malic acid treated MgB_2 wire at both sintering temperatures, the pinning mechanisms depend on operating temperature that means that δl and δT_c pinning mechanisms are dominant mechanisms at low and high temperatures, respectively which is in good agreement with the carbon doped MgB_2 bulk samples reported in Ref. [3].

For obtaining a deeper insight into the pinning mechanism, the extended normalized pinning force density, $f = F/F_{max}$, plotted against $h = B/B_{peak}$ instead of $h = B/B_{irr}$, was examined, where B_{peak} is the magnetic field at the maximum of F. The scaling of f–h is often analyzed in terms of normal point pinning, $f(h) = (9/4)h(1-h/3)^2$, and correlated pinning, $f(h) = (25/16)h^{0.5}(1-h/5)^2$, which has been inferred by Higuchi et al. [29]. The fitting results are shown by the solid curves in Figure 4.6(a) and (b).

In low magnetic fields ($< h_{max}$) the experimental data are in good agreement with the point pinning mechanism for both the 700° C and the 900°C samples,

while correlated pinning seems to become more dominant at higher magnetic fields. As a result, the grain boundary density and its contribution to flux pinning are dominant in both samples, regardless of sintering temperature. Since these results are in good agreement with the fact that homogeneous

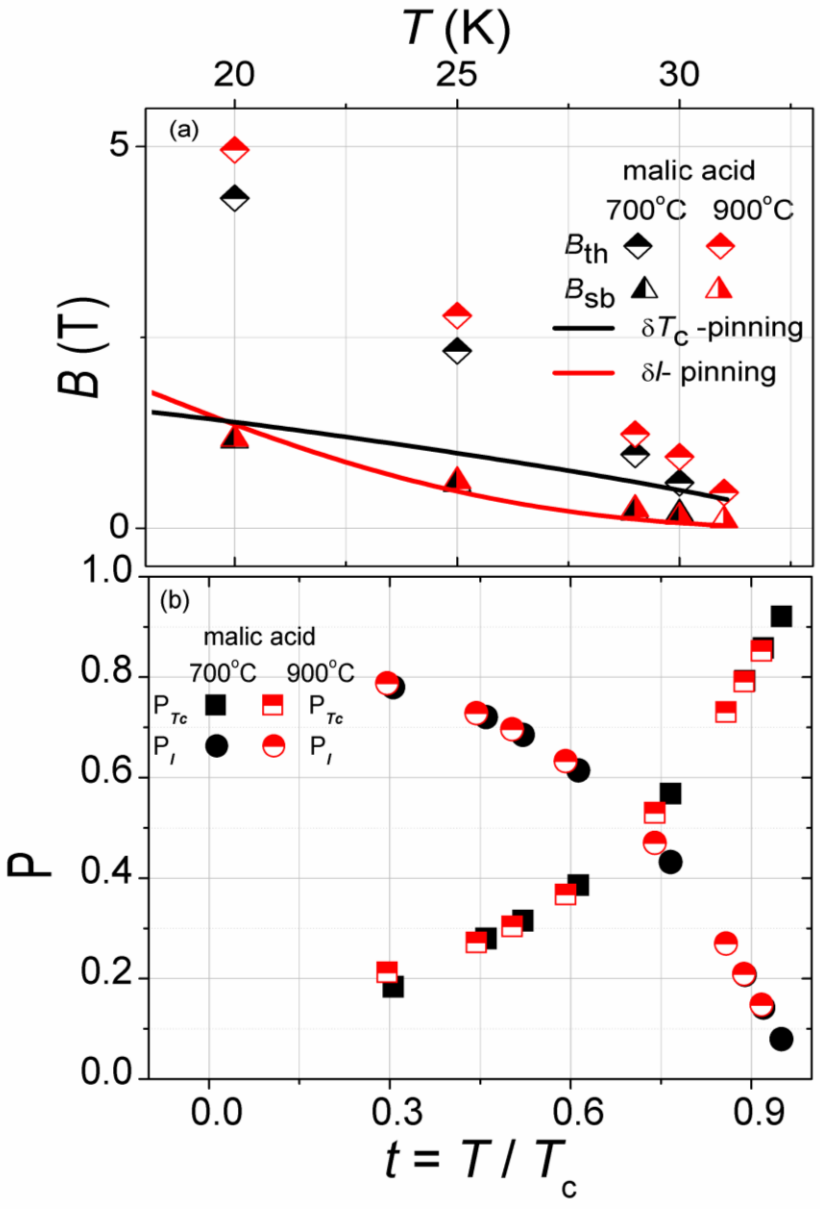

Fig 4.5: B_{sb} and B_{th} crossover field temperature dependence for the malic acid treated samples sintered at 700°C and 900°C, with the black and red fitted lines standing for the δT_c and δl pinning mechanisms, respectively.

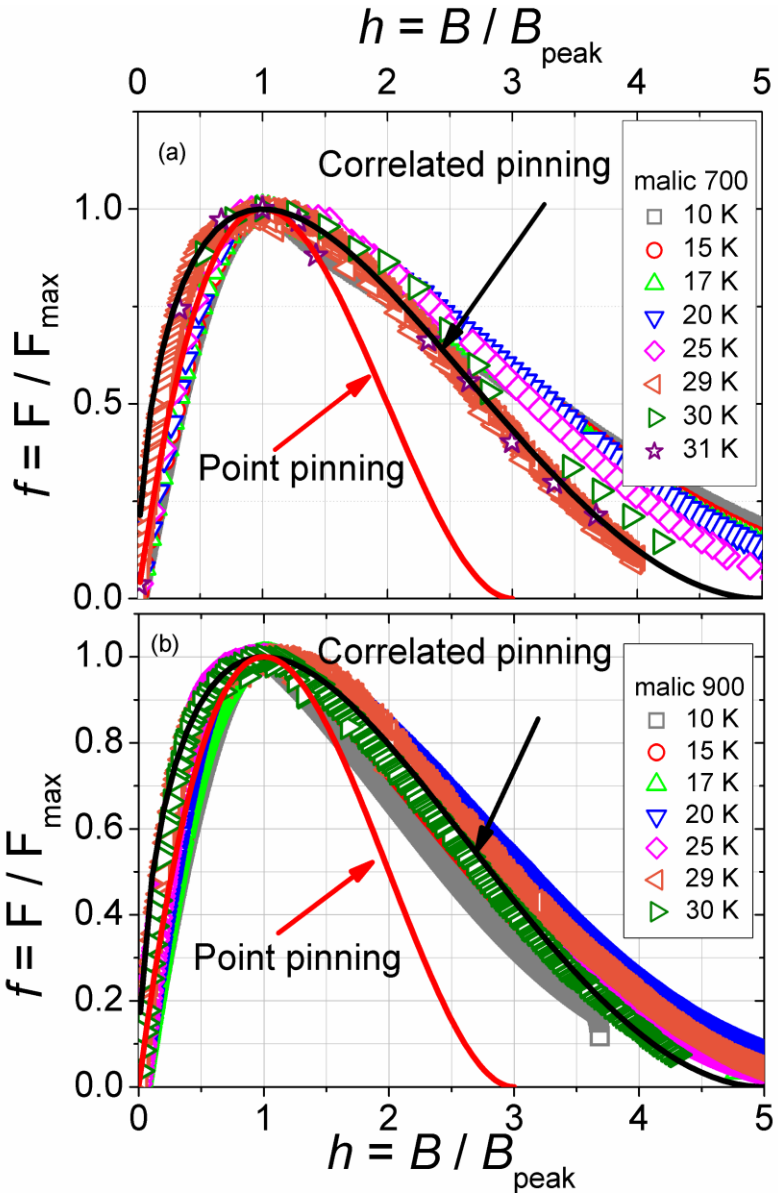

Fig 4.6: Magnetic field dependence in the temperature range of 10 to 30 K of the reduced pinning force f(h) for the malic acid treated MgB_2 wire sintered at 700°C and 900°C.

grains of the malic acid treated MgB_2 were obtained by the chemical solution route followed by sintering at 700°C and 900°C.

4.4: Conclusions

In summary, we have fabricated malic acid treated MgB_2 wires sintered at low and high sintering temperature to study the superconductivity properties

and their relationship with flux pinning mechanism. Both samples show higher J_c due to defects arising from both non-uniform strain and carbon substitution, as evidenced by the reduction of the a-axis lattice parameter and the broadening of the E_{2g} peak, as confirmed by X-ray refinement and Raman spectra analysis. We have also analyzed the pinning mechanism and shown that the degree of flux pinning enhancement can be estimated by RHH (B_{c2}/B_{irr}), which could act as a guide towards further enhancement of J_c. From our results, δl and δT_c pinning mechanisms coexist in the malic acid treated MgB_2 wires, regardless of the sintering temperature. Particularly, the δl pinning is dominant at lower operating temperatures, and δT_c pinning starts to be dominant close to T_c, This means that spatial variation in the charge carrier mean free path is mainly responsible for the flux pinning mechanism in the malic doped MgB_2 wires sintered at 700 and 900°C. Finally, we have analyzed the scaling behavior in terms of the point and correlated pinning mechanisms. The fitting results have shown that the point pinning is dominant at lower magnetic field, and correlated pinning is observed at both higher and lower fields, regardless of the sintering temperatures.

4.5: References

[1] Nagamatsu G J, Nakagawa N, Muranaka T, Zenitali Y and Akimitsu J 2001 Nature 410 63

[2] Tomsic M, Rindfleisch M, Yue J, McFadden K, Doll D, Phillips J, Sumption M D, Bhatia M, Bohnenstiehl S and Collings E.W, Physica C 456 (2007) 203–208

[3] Ghorbani S R, Wang X L, Dou S X, Lee S I and Hossain M S A 2008 Phys. Rev. B 78 184502

[4] Kim M S, Jung C U, Park M S, Lee S Y, Kim K H P, Kang W N and Lee S I 2001 Phys. Rev. B 64, 012511

[5] Dou S X, Pan A V, Zhou S, Ionescu M, Wang X L, Horvat J, Liu H K and Munroe P R 2003 J. Appl. Phys. 94 1850

[6] Qin M J, Wang X L, Liu H K and Dou S X 2002 Phys. Rev. B 65 132508

[7] Wang J, Shi Z X, Lv H and Tamegai T 2006 Physica C 445 462–465

[8] Wang J L, Zeng R, Kim J H and Dou S X 2008 Phys. Rev. B 77 174501

[9] Kim J H, Dou S X, Hossain M S A, Xu X, Wang J L, Shi D Q, Nakane T and Kumakura H 2007 Supercond. Sci. Technol. 20 715

[10] Hossain M S A et al. 2013 Mat. Lett. 91 356

[11] Kim J H, Dou S X, Oh S, Jercinovic M, Babic E, Nakane T and Kumakura H 2008 J. Appl. Phys. 104 063911

[12] Hossain M S A, Senatore C, Flukiger R, Rindfleisch M, Tomsic M, Kim J H and Dou S X 2009 Supercond. Sci. Technol. 22 095004

[13] Prischepa S L, DellaRocca M L, Maritato L, Salvato M, Capua R D, Maglione M G, Vaglio R 2003 Phys. Rev. B 67 024512

[14] Shi Z X, Pradhan A K, Tokunaga M, Yamazaki K, Tamegai T, Takano Y,

Togano K, Kito H and Ihara H 2003 Phys. Rev. B 68 104514

[15] Lee S, Matsui T, Yamamoto A, Uchiyama H and Tajima S 2003 Physica C 397 7

[16] Ohmichi E, Komatsu E, Masui T, Lee S, Tajima S and Osada T 2004 Phys. Rev. B 70 174513

[17] Ghorbani S. R, Wang X. L, Hossain M.S.A, Yao Q.W, Dou S.X, Lee S, Chung K. C and Kim Y, 2010 J.Appl. Phys.107 113921

[18] Dou S X, Shcherbakova O, Yeoh W K, Kim J H, Soltanian S, Wang X L, Senatore C, Flukiger R, Dhalle M, Husnjak O and Babic E 2007 Phys. Rev. Lett. 98 097002

[19] Wang X L, Dou S X, Hossain M S A, Cheng Z X, Liao X Z, Ghorbani S R, Yao Q W, Kim J H and Silver T 2010 Phys. Rev. B 81 224514

[20] Wang C, Ma Y, Zhang X, Wang D L, Gao Z S, Yao C, Wang C, Oguro H, Awaji S and Watanabe K 2012 Supercond. Sci. Technol. 25 035018

[21] Susner M A, Sumption M D, Bhatia M, Peng X, Tomsic M J, Rindfleisch M A and Collings E W 2007 Physica C 456 180

[22] Jiang C H, Nakane T and Kumakura H 2005 Appl. Phys. Lett 25 252505

[23] Li W X, Chen R H, Li Y, Zhu M Y, Jin H M, Zeng R, Dou S X and Lu B 2008 J. Appl. Phys. 103 013511

[24] Li W X, Li Y, Chen R H, Zeng R, Dou S X, Zhu M Y and Jin H M 2008 Phys. Rev. B 77 094517

[25] Rowell J M 2003 Supercond. Sci. Technol. 16 R17

[26] Hossain M S A, Kim J H, Xu X, Wang X L, Rindfleisch M, Tomsic M, Sumption M D, Collings, E W and Dou S X 2007 Supercond. Sci. Technol. 20 L51

[27] Griessen R, Hai-hu W, Van Dalen A J J, Dam B, Rector J, Schnack H G, Libbrecht S, Osquiguil E and Bruynseraede Y 1994 Phys. Rev. Lett. 72 1910

[28] Blatter G, Feigel'man M V, Geshkenbein V B, Larkin A I and Vinokur V M 1994 Rev. Mod. Phys. 66 1125

[29] Higuchi T, Yoo S I and Murakami M 1999 Phys. Rev. B 59 1514

Chapter 5: PERCOLATIVE NATURE OF CURRENT TRANSPORT IN POLYCRYSTALLINE MgB_2 WIRE

The percolation model, taking into account the percolative nature of current transport due to anisotropy, is a powerful tool for predicting the field and temperature dependences of critical current in MgB_2 superconducting wires. The critical current behavior measured from MgB_2 wires can be obviously explained by only four fitting parameters, the anisotropy parameter, the pinning force maximum, the upper critical field along the ab-plane, and the percolation threshold. Moreover, the temperature dependence of the upper critical field is further explained by the dirty-limit two-gap theory.

5.1: Introduction

The first commercial superconducting wire was developed about 50 years ago, in 1962. Even now, the majority of superconducting magnets are made of niobium titanium, NbTi, or niobium tin, Nb_3Sn, wires. From soon after the discovery of its superconductivity in 2001[1], magnesium diboride, MgB_2, has been regarded as a very promising candidate for another type of commercial superconducting wire. Together with its simple crystalline structure and low material cost, its transition temperature around 40 K, enabling cryogen-free operation, is definitely attractive for engineering applications. An MgB_2 conductor, however, still needs to meet the special requirements of practical applications. In particular, the upper critical field and critical current should exceed, or at least be comparable to, those of Nb–Ti. It is well-known that MgB_2 conductor is commonly made with a round wire cross-section [2,3] because it does not need good grain adhesion between grains [4]. It is hard to estimate the anisotropy factor at different operating temperatures. In addition,

the upper critical field is too high to measure directly, especially at 4.2 K [5]. Therefore, we need a modelling tool to predict physical properties depending on the field and temperature dependence of MgB_2 conductors.

Prediction of the critical current in polycrystalline MgB_2, taking into account the percolative nature of current transport due to anisotropy, has been reported by Eisterer and Kim [6–8]. Anisotropic Ginzburg–Landau theory is firstly assumed for the angular dependence of the upper critical field. In addition, the Kramer grain boundary pinning model and percolation theory are adopted. Very interestingly, the critical current of either MgB_2 bulks or wires can be explained by only four fitting parameters: the anisotropy parameter (γ), the pinning force maximum (Fm), the upper critical field along the ab-plane (B_{c2}^{ab}), and the percolation threshold (pc) [8].

For polycrystalline wire samples, the percolation threshold (pc), i.e. the minimum superconducting fraction for a continuous current path, is usually 0.26. In this study, as an extension of our previous work [8,9], the wide field (0–15 T) and temperature (4.2–30 K) dependences of un-doped and doped MgB_2 wire are comprehensively discussed through the percolation model.

5.2: Experimental

Among the various carbon doping approaches [9–13], the chemical solution process via a carbohydrate has become popular and advantageous in terms of both cost and performance [9]. For example, malic acid ($C_4H_6O_5$) is well-known to be easily decomposed below the melting temperature of magnesium, which enables low sintering temperature fabrication to suppress grain growth, as well as the carbon doping. According to the grain boundary pinning model, smaller grains cause a larger pinning force and a higher critical current [14–16].

Subsequently, it was found that more homogeneous mixing would be possible with a liquid agent, compared to any other solid-type dopant [9].

Taking those criteria into account, herein, MgB_2 was fabricated by the in-situ powder-in-tube process. After dissolving 10 wt% malic acid (99.0%) in toluene (C_7H_8, 99.5%), the solution was mixed with an appropriate amount of boron (B, 99.9%) powder in a SPEX mill for 10 min (100 rpm). The slurry was dried at 150°C in a dry oven to form a coating around boron powder particles. This uniform composite was then mixed with a magnesium (Mg, 99%) powder and mixed in a Fritsch planetary mill (500 rpm) for 10 min. The mixed powder was packed into a 140 mm long iron (Fe) tube. The outer and inner diameters of the Fe tube were 10 mm and 8 mm, respectively. The packed tube was drawn till the final outer diameter became 0.83 mm. The fabricated wires were sintered at 650 $^{\circ}$C for 30 min under high purity argon gas with a ramp rate of 5°C min^{-1}.

5.3: results and discussion

The field and temperature dependences of the critical current density for the doped sample compared with the un-doped sample are shown in Figure 5.1. Transport current up to 400 A was measured by the standard four-probe method with a criterion of 1 mVcm^{-1}. The temperature dependence was also studied by a variable temperature insert (VTI) system. At 4.2 K, it was observed that the critical current for the doped sample at high field is much higher than that for the un-doped sample. With increasing operating temperature, the critical current densities of both samples become comparable with each other, for example, at 20 K. Near the transition temperature, at 30 K, the critical current density, Jc, for the doped sample is lower than that for

the un- doped sample at all fields. The measured critical temperatures for the doped and un-doped samples are estimated to be 34 K and 35.4 K, respectively. It should be noted that the critical currents of both samples can be described by the percolation model, whether the sample is doped or not. All the fitting lines in Figure 5.1 were calculated from the percolation theory and are in good agreement with the measured data. The field dependence of the critical current density can be numerically fitted by the following integral equation:

$$J_c = \int_0^{\infty} \left(\frac{P(J)-P(c)}{1-P(c)}\right)^{1.79} dJ \qquad (5.1)$$

where p(J) is the fraction of grains with critical current density above J and Pc is the percolation threshold, the minimum fraction required for a superconducting current flow. The critical current of each grain is calculated with a grain boundary pinning model: $J_c = F_m . \frac{\left(1-\frac{B}{B_{c2}}\right)^2}{\sqrt{B_{c2}B}}$, where Fm is the pinning force maximum. The upper critical field,Bc2, has an angular dependence, which can be described by: $B_{c2}(\theta) = \frac{B_{c2}^{ab}}{\sqrt{\gamma^2 Cos^2(\theta)+Sin^2(\theta)}}$, from the anisotropic Ginzburg-Landau theory.

Here, only four fitting parameters, the uppercritical field (Bc2), the anisotropy parameter (γ), the pinning force maximum (Fm), and the percolation threshold (Pc) are needed to describe the field dependence of the critical current for each temperature. We previously reported that for polycrystalline wire samples, the percolation threshold, Pc, is usually 0.26 [8]. It is noted that the low-field critical current density for doped wire is comparable to that for the un-doped wire, at least up to 20K. We will explain and discuss this point later.

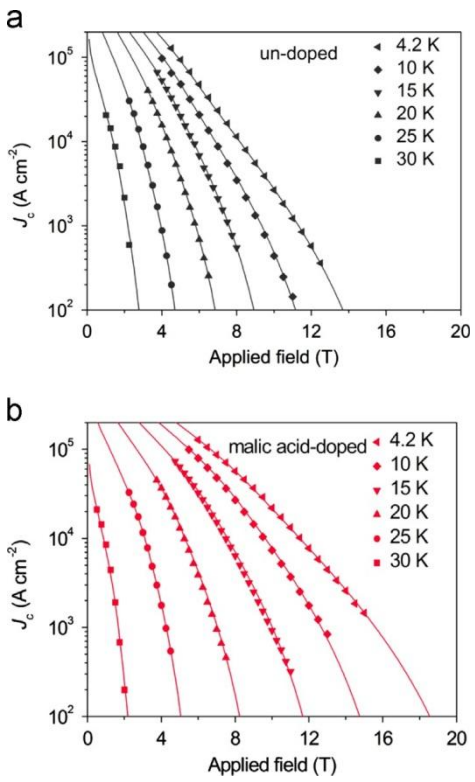

Fig. 5.1. Field and temperature dependences of critical current density for un-doped and malic-acid doped MgB_2 wires. The lines are calculated by the percolation model.

The fitting parameters used for the anisotropy parameter (γ) and the pinning force maximum (F_m) are also shown in detail in Figures 5.2 and 5.3. While MgB_2 is less anisotropic compared with the high-temperature superconductors, it is well known that the anisotropy is in the range of 2–5 [6,17]. It was argued in our previous work that there was a clear decrease in the anisotropy parameter with SiC doping, an example of carbon doping, resulting in a dramatically increased high-field critical current [9]. This phenomenon can be attributed to the increased impurity scattering rate. When carbon is substituted into boron sites in the MgB_2 structure, it stiffens the optical E_{2g} phonon mode, which is strongly linked with anisotropic s bands, and hence, lowers the transition temperature and increases the upper critical field [7,18]. Increased inter-band scattering between the π and the σ bands also can be a cause for the reduced transition temperature [19]. Even without any variation in the inter-band scattering, the intra-band scattering by itself can increase the upper critical

field far beyond that of Nb_3Sn, according to the two-band dirty-limit theory [20].

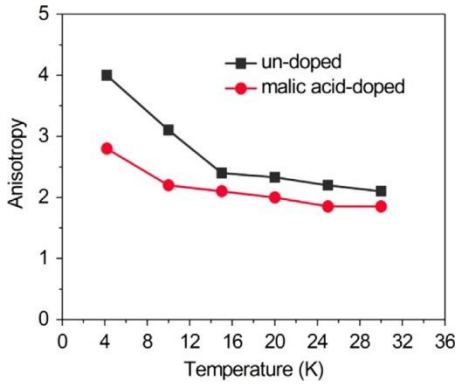

Fig. 5.2. Temperature dependence of the anisotropy for un-doped and malic-acid doped MgB_2 wires.

It has been reported that the anisotropy parameter is decreased by SiC doping. Consequently the pinning force maximum is significantly lowered at all operating temperatures compared to the un-doped wire 9. For example, the pinning force maximum of SiC doped MgB_2 wire were estimated to be 1.84 x 10^6, 1.40 x 10^6, 0.93 x 10^6, 0.48 x 10^6, 0.13 x 10^6, and 0.003 x 10^6 ATcm- 2 respectively, at 4.2, 10, 15, 20, 25 and 30 K.

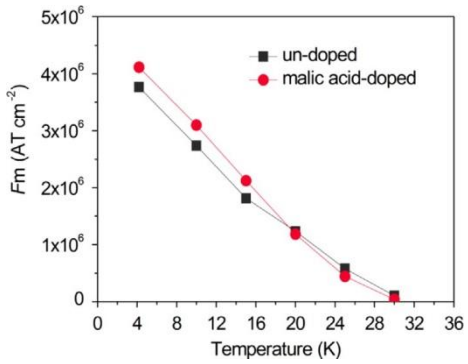

Fig. 5.3. Temperature dependence of the flux pinning maximum for un-doped and malic-acid doped MgB_2 wires.

This is known to be main reason why the low-field critical current is degraded, as has been mentioned. Another reason might be the residual SiC within the MgB_2 phase, because it could act as a barrier to current transport. An interesting feature observed in this study is that the pinning force maximum of the MgB_2 wire made from malic acid treated boron, i.e., carbon coated boron

particles was slightly increased below20K, unlike SiC doped wire. This is mainly related to homogeneous mixing. That is, the inclusion of malic acid leads to boron encapsulation by carbon, which, in turn, prevents agglomeration during sintering process, resulting in fine grains and hence strong pinning. In Figure 5.4, there is a clear up ward curvature in the temperature dependence of the upper critical field parallel to the ab-plane, B_{c2}^{ab}, whether the sample is doped or not. The positive curvature is usually related to the two-band nature of MgB_2, for example, as was reported by Gurevich [20]. All the lines in Figure 5.4 are calculated by Eq. (5.2), based on the dirty-limit two-gap theory.

$$2w\left[\ln t + u\left(\frac{b}{t}\right)\right]\left[\ln t + u\left(\frac{\eta b}{t}\right)\right] + \lambda_2\left[\ln t + u\left(\frac{\eta b}{t}\right)\right] + \lambda_1\left[\ln t + u\left(\frac{b}{t}\right)\right] = 0 \quad (5.2)$$

where t is the reduced temperature T/Tc and b is defined as $\hbar Hc2D\sigma/2\Phi 0kBTc$, where D_σ is the σ band diffusivity and Φ_0 is the flux quantum. The function u(x) is defined as $u(x)=\psi(1/2+x)-\psi(1/2)$, where ψ(x) is the digamma function. η is the ratio of the π band to the σ band diffusivity, D_π/D_σ. w and $\lambda_{1,2}$ can be obtained from the electron–phonon coupling constant λ_{mn} and the Coulomb pseudo- potential matrix μ_{mn} [20]. The electron–phonon coupling constant and the Coulomb pseudo-potential can vary with doping. According to a model calculation based on the two-band Eliashberg theory for MgB_2 [21], the Coulomb pseudo-potential is a slowly decreasing, almost linear function as the carbon content increases. Even within the dirty-limit two-gap theory, inter-band scattering can affect the transition temperature and the upper critical field [7,20]. The variation in the transition temperature due to doping is relatively small, however, (about 1.4 K) for the sample studied in this work. In this case, the variation of λ_{mn} or μ_{mn} due to doping and the effect of inter-band scattering can be neglected [20,22–25] and are not considered here for simplicity.

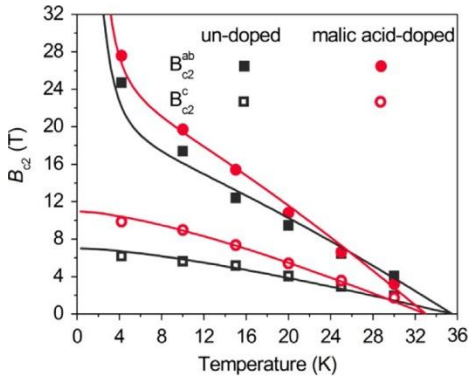

Fig. 5.4. Temperature dependence of the upper critical field along the c-axis and the ab-plane for un-doped and malic-acid doped MgB_2 wires.

The best fits are obtained with the diffusivities listed in Table 5.1. It should be noted that the σ band appears highly anisotropic. In particular, D_σ^c is reduced more than D_σ^{ab} s by the carbon doping .As a result, the impurity scattering is obviously increased by the doping. Consistent with all the results, the low-field increase in the critical current density is most affected by increasing the pinning force maximum (F_m), while the high field performance can be attributed to the impurity scattering and anisotropy. So far, the high field improvement has been confirmed by electrical transport measurements, but only at 4.2K in almost all cases. In other words, despite numerous studies, little is known about the in-field transport critical current performance at various temperatures, especially at helium-cryogen-free temperatures, which is the most important criterion for determining the realistic range of the operation temperature for industrial applications. This is the motivation behind the present fabrication of un-doped and doped MgB_2 wires, the measurement of the field and temperature dependences of the transport critical current, and the detailed analysis using a percolation model.

Table 5.1: Diffusivities used for the calculation of the extracted upper critical field in Fig. 5.4.

	D_{σ}^{ab} ($m^2 s^{-1}$)	D_{π}^{ab} ($m^2 s^{-1}$)	D_{σ}^{c} ($m^2 s^{-1}$)	D_{π}^{c} ($m^2 s^{-1}$)
Un-doped	1.6×10^{-4}	4.2×10^{-6}	4.2×10^{-4}	1.1×10^{-4}
Malic acid-doped	1.2×10^{-4}	2.7×10^{-6}	2.5×10^{-4}	0.65×10^{-4}

5.4: Conclusion

Our comprehensive percolation analysis can be summarized by the following consistent picture of the low- and high-field critical current densities: the field and temperature dependences of the critical current density for un-doped and malic acid-doped MgB_2 wires have been calculated by the percolation model, in which only four fitting parameters are considered. It should be noted that the critical current densities of both the un-doped and the doped wires can be exactly fitted and explained. With the carbon dopant, there was a clear decrease in the anisotropy parameter, resulting in an increased high-field critical current density. In contrast, the pinning force maximum is found to be main factor affecting the low-field critical current density.

5.5: References

[1] J. Nagamatsu, N. Nakagawa, T. Muranaka, Y. Zenitani, J. Akimitsu, Nature 410 (2001) 63.

[2] B.A. Glowacki, M. Majoros, M. Vickers, J.E. Evetts, Y. Shi, I. McDougall, Super- cond. Sci. Technol. 14 (2001) 193.

[3] J.H. Kim, S. Oh, H. Kumakura, A. Matsumoto, Y.-U. Heo, K.-S. Song, Y.-M. Kang,

M. Maeda, M. Rindfleisch, M. Tomsic, S. Choi, S.X. Dou, Adv. Mater. 23 (2011) 4942.

[4] D.C. Larbalestier, L.D. Cooley, M.O. Rikel, A.A. Polyanskii, J. Jiang, S. Patnaik, X. Y. Cai, D.M. Feldmann, A. Gurevich, A.A. Squitieri, M.T. Naus, C.B. Eom, E.E. Hellstrom, R.J. Cava, K.A. Regan, N. Rogado, M.A. Hayward, T. He, J.S. Slusky, P. Khalifah, K. Inumaru, M. Haas, Nature 410 (2001) 186.

[5] M.D. Sumption, M. Bhatia, M. Rindfleisch, M. Tomsic, S. Soltanian, S.X. Dou, E. W. Collings, Appl. Phys. Lett. 86 (2005) 092507.

[6] M. Eisterer, M. Zehetmayer, H.W. Weber, Phys. Rev. Lett. 90 (2003) 247002.

[7] M. Eisterer, Supercond. Sci. Technol. 20 (2007) R47.

[8] J.H. Kim, S.X. Dou, S. Oh, M. Jercinovic, E. Babic, T. Nakane, H. Kumakura, J. Appl. Phys. 104 (2008) 063911.

[9] J.H. Kim, S. Oh, Y.-U. Heo, S. Hata, H. Kumakura, A. Matsumoto, M. Mitsuhara, S. Choi, Y. Shimada, M. Maeda, J.L. MacManus-Driscoll, S.X. Dou, NPG Asia Mater. 4 (2012) E3.

[10] S.X. Dou, S. Soltanian, J. Horvat, X.L. Wang, S.H. Zhou, M.

Ionescu, H.K. Liu, P. Munroe, M. Tomsic, Appl. Phys. Lett. 81 (2002) 3419.

[11] A. Yamamoto, J. Shimoyama, S. Ueda, I. Iwayama, S. Horii, K. Kishio, Supercond. Sci. Technol. 18 (2005) 1323.

[12] H. Yamada, M. Hirakawa, H. Kumakura, H. Kitaguchi, Supercond. Sci. Technol. 19 (2006) 175.

[13] M. Maeda, J.H. Kim, Y.-U. Heo, S.K. Kwon, H. Kumakura, S. Choi, Y. Nakayama, Y. Takano, S.X. Dou, Appl. Phys. Express 5 (2012) 013101.

[14] A. Matsumoto, H. Kumakura, H. Kitaguchi, B.J. Senkowicz, M.C. Jewell, E. E. Hellstrom, Y. Zhu, P.M. Voyles, D.C. Larbalestier, Appl. Phys. Lett. 89 (2006) 132508.

[15] E. Martínez, P. Mikheenko, M. Martínez-López, A. Millán, A. Bevan, J.S. Abell, Phys. Rev. B 75 (2007) 134515.

[16] T. Matsushita, M. Kiuchi, A. Yamamoto, J. Shimoyama, K. Kishio, Physica C 468 (2008) 1833.

[17] O.F. de Lima, R.A. Ribeiro, M.A. Avila, C.A. Cardoso, A.A. Coelho, Phys. Rev. Lett. 86 (2001) 5974.

[18] X.X. Xi, Rep. Prog. Phys. 71 (2008) 116501.

[19] H.J. Choi, D. Roundy, H. Sun, M.L. Cohen, S.G. Louie, Nature 418 (2002) 758. [20] A. Gurevich, Phys. Rev. B 67 (2003) 184515.

[21] G.A. Ummarino, D. Daghero, R.S. Gonnelli, A.H. Moudden, Phys. Rev. B 71 (2005) 134511.

[22] S.C. Erwin, I.I. Mazin, Phys. Rev. B 68 (2003) 132505.

[23] R.S. Gonnelli, D. Daghero, A. Calzolari, G.A. Ummarino, V. Dellarocca, V. A. Stepanov, S.M. Kazakov, N. Zhigadlo, J. Karpinski,

Phys. Rev. B 71 (2005) 060503.

[24] S. Tsuda, T. Yokoya, T. Kiss, T. Shimojima, S. Shin, T. Togashi, S. Watanabe, C. Zhang, C.T. Chen, S. Lee, H. Uchiyama, S. Tajima, N. Nakai, K. Machida, Phys. Rev. B 72 (2005) 064527.

[25] P. Szabó, P. Samuely, Z. Pribulová, M. Angst, S. Bud'ko, P.C. Canfield, J. Marcus, Phys. Rev. B 75 (2007) 144507.

Chapter 6: POWER –LAW RELATIONSHIP BETWEEN CRITICAL CURRENT DENSITY, MICRO STRUCTURE AND THE n-VALUE in MgB_2 SUPERCONDUCTING WIRE

Dissipation-free MgB_2 superconducting wires are valuable in terms of practical applications. Herein, we have found a strong correlation between critical current density (J_c) and the n-value extracted from the electric field versus current density characteristic. The power-law relationship (m) between the J_c and the n-value, $n \propto J_c^m$, represents a critical index, which is strongly dependent on operating temperatures.

6.1: Introduction

Very recently, further enhancement of the critical current density, J_c, and the irreversibility field, Birr, has been reported for carbon doped MgB_2 wires with malic acid additive, produced by the chemical solution method [1-11]. In terms of monofilament conductor, a high J_c of 23,000 Acm^{-2} at 4.2 K and 10 T were achieved in our previous study [12]. However, an inherent problem for MgB_2 wire is still the low mass and low volume densities, which are due to its porous nature. In addition, commonly used carbon dopant, which is known to be effective for achieving a larger upper critical field, tends to aggregate at grain boundaries as a residue, due to the limit of carbon solubility in the MgB_2 structure. Thus, both porosities and residual carbon could act as major current-limiting factors, which are directly reflected in the electric field (E) − current density (J) characteristic.

The E-J characteristic is commonly known to be a crucial index for optimization of the design of superconducting applications. For example, typical values of n for “persistent magnet-grade” conductors are required to be

50-100. However, the index resistance due to low n-value, 10-20, of MgB_2 at higher operating temperature close to 25 K and 3-4 T applied magnetic field is expected to make it impossible to operate an MgB_2-based magnet in persistent mode, i.e., <0.01 ppm/hr, even if all joints are superconducting [13]. From the viewpoint of materials, a high quality sample usually shows a larger n-value, defined by the close approximation of the E-J characteristic by a curve $E \propto Jn$. This means more homogeneous microstructure causes larger n-value. Compared with high temperature superconductors [14], MgB_2 shows a sharper transition from the superconducting state to the normal state with increasing transport current. However, its voltage rise due to its low n–value cannot be negligible, even below the critical current, because it can lead to electrical and thermal dissipation. Thus, dissipation-free superconductor wires have been the primary issue for practical application. In our previous report [15], we undertook malic acid doping of MgB_2 and shown the best J_c performance reported so far. Interestingly enough, we found that boron vacancies and associated stacking faults due to carbon are the main reason for the enhancement of high-field properties. In particular, the carbon from the malic acid uniformly encapsulates the boron, preventing boron agglomeration and reducing porosity. However, the majority of the carbon is still observed at the grain boundaries as a residue. That is to say, it would be hard to obtain ‘clean’ grain boundaries in terms of connectivity. In addition, we expect intrinsic defects within MgB_2 grains due to carbon doping. For these reasons, it is necessary to investigate the effects of carbon dopant on the n-value and microstructure. In this study, we have evaluated in detail the relationship between J_c, microstructure, and the n-value in the best performance carbon doped wire obtained through malic acid doping.

6.2: Experimental procedure

MgB_2/Nb/Monel monofilament wire with 10wt% malic acid additive and un-doped MgB_2 wire as a reference for comparison, both fabricated by Hyper Tech Research Inc., were studied in this work. Details of the experiments have been described elsewhere [1, 12]. Wire samples were sealed in Zr foil and then sintered under flows of high purity Ar gas. Transport critical current up to 400 A was measured by using the standard four-probe method with a criterion of 1 μVcm^{-1}. The magnetic field was increased up to 18 T, while the temperature was varied within the range of 4.2 K to 30 K. The n-values were determined from the slope in the plot of log E versus log J in the electric field (E) range from 0.1 to 10 μVcm^{-1}, based on the power law, $E_c = E(V/V_c)^n$, Where the Ec represents the critical potential Vc in unit length. The critical temperature (T_c) was determined by AC susceptibility measurements at f = 76.97 Hz with $\mu_0 Hc$ = 50 μT, where H_c is the upper critical field. Microscopic studies were carried out using a JEOL JEM-2500SES, a Cs-corrected STEM equipped with a Gantan 776 EELS (Enfina 1000).

6.3: Results and discussion

In order to determine the optimal sintering temperature, transport J_c values for malic acid doped wires sintered at different temperatures were collected and are shown in Figure 6.1.

Quite interestingly, even when sintering at a temperature as low as 550°C, the J_c is still as high as ~18,000 Acm^{-2} at 4.2 K and 10 T. Further enhancement of the J_c is achievable by slightly increasing the sintering temperature and decreasing the sintering time, for example, J_c was 25,000 Acm^{-2} when the

sample was sintered at 600°C for 4 hours. At an external magnetic field of 11.7 T, the J_c is still around 10,000 Acm^{-2}.

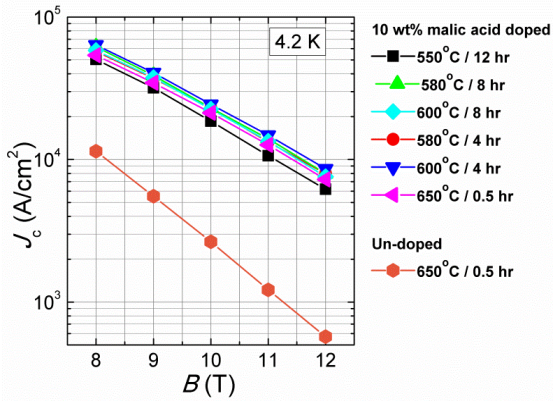

Fig. 6.1. Magnetic field dependence of the transport J_c for malic acid-doped MgB_2 wires with different sintering temperatures.

On the other hand, the J_c of the reference un-doped wire sintered at 650°C for 30 min was about an order of magnitude lower, about 2,800 Acm^{-2} at 4.2 K and 10 T. Interestingly, transport J_c values were found to be strongly dependent on the sintering temperature, which can lead to differences in the T_c. The T_c of the un-doped wire is 36 K, but T_c of all the carbon-doped wires is approximately 34 K. Corresponding to this reduction in T_c, the a-lattice parameter of the malic-acid doped wires was decreased from 3.0832(2) to 3.0758(2) Å. This can be attributed to volume shrinkage due to carbon substitution.

Among them, we choose the best performance wire sintered at 600oC for 4 hours and temperature dependence of J_c(B) is shown in Figure 6.2(a). We observed that the J_c normally decreased with increasing magnetic field. In addition, the slope of J_c(B) became steeper with increasing operating temperature. It is noteworthy that critical current density values at 4.2 K and 20 K are still above 10^4 Acm^{-2}, even in fields up to 10 T and 5 T, respectively. The corresponding n-values are shown in Figure 6.2(b).

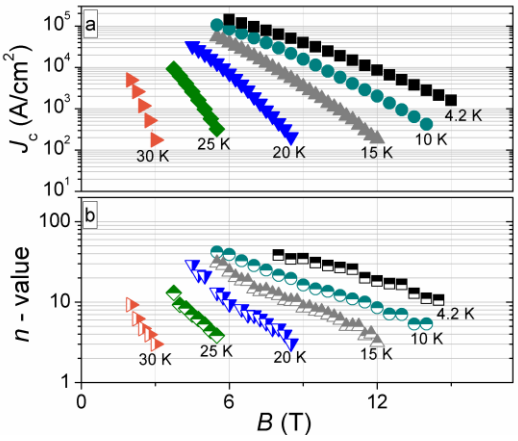

Fig. 6.2. (a) Magnetic field dependence of the transport J_c, and (b) magnetic field dependence of the n-value at 4.2, 10, 14, 20, 25, and 30 K for malic acid-doped MgB_2 wires.

This behavior is similar to that of J_c(B) under different operating temperatures. Here, our natural question is then why the n-value is crucial. It is well known that electrical and thermal properties are significantly degraded at inhomogeneous parts of a sample, thereby reducing the stability of the whole system [13, 16, 17]. In particular, the non-uniformity in the conductor can result in "hot spot formation" that leads to localized thermal quenching [18]. For Nb_3Sn, the n-value sharply decreases as the field approaches the upper critical field and the critical current also decreases sharply [14, 19].

On the other hand, for YBa2Cu$_3$O$_7$ (YBCO) coated conductor, the decrease in the critical current density is rather gradual, and the n-value also changes gradually at the same time [20]. This proves that different kinds of superconducting wires show unexpected n-value behavior under magnetic fields.

In particular, effect of various dimensional defects in MgB_2 necessary to study on the current-carrying performances, i.e., carbon doping. When carbon is doped into the MgB_2, it is believed that it substitutes for boron, stiffens the optical E_{2g} phonon mode, which is strongly linked with anisotropic σ bands,

hence, lowers the transition temperature [21]. Even if carbon doped wire still shows better J_c, inhomogeneous microstructure remains rooms for degradation of n-value. Figure 6.3 shows a lattice distortion inside MgB_2 grain.

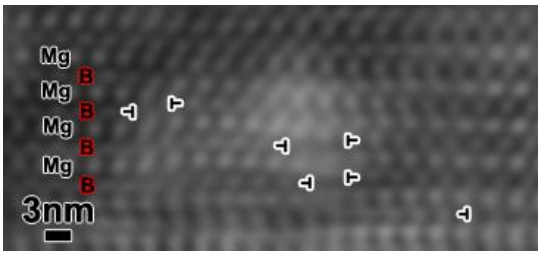

Fig. 6.3. Lattice distortion inside carbon doped MgB_2

Many dislocations can be occurred, resulting in severe crystallographic imperfections. These structural defects produce an increase in the impurity scattering rate, which thereby enhance the upper critical field and the high-field J_c.

In order to examine in detail the correlation between J_c values and n-values, we plotted the power-law relationship between the J_c and the n-value, $n \propto Jc^m$, at different operating temperatures, as shown in Figure 6.4.

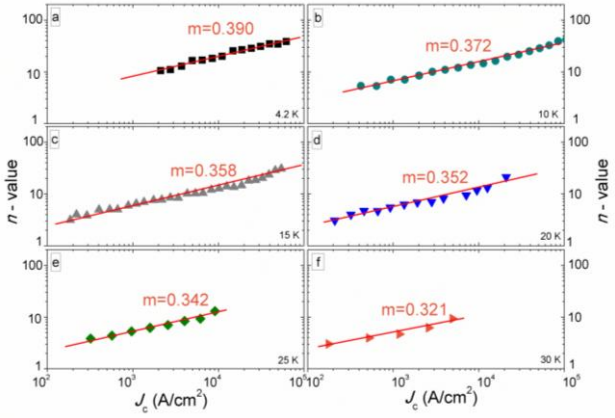

Fig. 6.4. Correlation between the J_c and the n-value for malic acid-doped MgB_2 wire at different temperatures: (a) 4.2 K, (b) 10 K, (c) 15 K, (d) 20 K, (e) 25 K, and (f) 30 K.

We found that there was a close relationship between the n-value and the J_c. Here, the corresponding index m values were estimated to be 0.390, 0.372, 0.358, 0.352, 0.342, and 0.321, respectively, at 4.2, 10, 15, 20, 25, and 30 K.

As was expected, m values become smaller with increasing operating temperatures, and the quantitative n-values show noticeable differences. Interestingly, the J_c values are proportional to the n-values. The power-law relationship between the J_cs and the n-values of wire evaluated over all temperature ranges is shown in Figure 6.5. The index m value was estimated to be 0.399, which is comparable to our previous result [21]. In the literatures, Martinez et al [22], Kitaguchi et al [23], and Li et al [16] reported that m-indexs were estimated to be 0.72, 0.69, and 0.5, respectively. Among these, HIPed bulk samples show larger m-value [23]. This means it depend on microstructure even if m-index does not vary much.

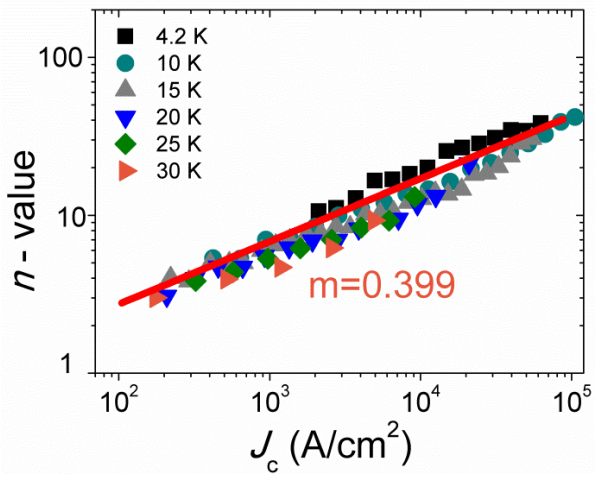

Fig. 6.5. Correlation between the J_c and the n-value for malic acid-doped MgB_2 wire in the operating temperature range of 4.2 to 30 K.

It is noteworthy that higher J_c values can be attributed to larger n-values. Kiss et al, reported the similar power law relationship analytically within the frame work of percolation network model by taking into account statistical J_c distribution [24]. From our results, the quantitative n-value of current MgB_2 wire is demonstrated to need further improvement, especially for persistent magnet-mode.

6.4: Conclusion

MgB_2 conductors still can have an impact in Magnetic Resonance Imaging (MRI) applications for the following reasons: (1) respectable properties for low to mid-field magnets operating at temperatures as high as 20 K; (2) wire manufacturing no more difficult than Nb-Ti wire manufacturing; (3) Mg and B are lower cost raw materials than Nb and Ti; (4) MgB_2 is 1/3 the density of Nb-Ti, so that the same kg of raw material will yield three times the piece length; (4) faster charging rate compared to Nb-Ti based magnet; and (5) the high critical temperature offers a larger thermal margin than the 9 K of Nb-Ti. This gives proof that the performance of MgB_2 conductors can rival and exceed those of conventional low temperature superconductors such as Nb-Ti.

In summary, the correlation between Jc and the n-value in MgB_2 superconducting wires was evaluated under different operating temperatures. From the E-J characteristics, we found that Jc is proportional to the n-value, which is strongly dependent on the operating temperature. Large n-values > 30 are expected to make it possible to operate an MgB_2-based magnet in persistent mode at 20 K.

6.5: References

[1] J. H. Kim, S. Zhou, M. S. A. Hossain, A. V. Pan, S. X. Dou, Appl. Phys. Lett. 89, 142505 (2006)

[2] Z. S. Gao, Y. W. Ma, X. P Zhang, D. L. Wang, H. Yang, H. H. Wen, K. Watanabe, Supercond. Sci. Technol. 21, 015016 (2008).

[3] X. P. Zhang, Y. W. Ma, D. L. Wang, Z. S. Gao, L. Wang, Y. P. Qi, S. S. Awaji, K. Z. Watanabe, E. Mossang, Supercond. Sci. Technol. 22, 045019 (2009)

[4] Y. Ma, Z. Gao, X. Zhang, D. Wang, Z. Yu, K. Watanabe, H. Wen, E. Mossang, J. Mater. Res. 22, 2987 (2007)

[5] Z. S. Gao, Y. W. Ma, X. P. Zhang, D. L. Wang, H. Yang, H. H. Wen, K. Watanabe, Appl. Phys. Lett. 91, 162504 (2007)

[6] Z. S. Gao, Y. M. Ma, X. P. Zhang, D. L. Wang, Z. G. Yu, H. Yang, H. H. Wen, E. Mossang, J. Appl. Phys. 102, 013914 (2007)

[7] B. H. Jun, Y. J. Kim, K. S. Tan, C. J. Kim, Supercond. Sci. Technol. 21, 105006 (2008)

[8] Y. J. Kim, B. H. Jun, K. S. Tan, B. G. Kim, J. M. Sohn, C. J. Kim, Physica C 468, 1372 (2008)

[9] B. H. Jun, C. J. Kim, Supercond. Sci. Technol. 20, 980 (2007)

[10] A. Vajpayee, V. P. S. Awana, S. Balamurugan, E. Takayama-Muromachi, H. Kishan, G. L. Bhalla, Physica C 466, 46 (2007)

[11] A. Vajpayee, V. P. S. Awana, G. L. Bhalla, P. A. Bhobe, A. K. Nigam, H. Kishan, Supercond. Sci. Technol. 22, 015016 (2009)

[12] J. H. Kim, S. X. Dou, S. Oh, M. Jercinović, E. Babić, T. Nakane, H. Kumakura, J. Appl. Phys. 104, 063911 (2008)

[13] J. H. Kim, S. X. Dou, A. Matsumoto, S. Choi, T. Kiyoshi, H. Kumakura, Physica C 470, 1207–1210 (2010)

[14] A. Rimikis, R. Kimmich, Th. Schneider, IEEE Trans Appl Supercond. 10, 1239–1242 (2000)

[15] J. H. Kim, S. Oh, Y. U. Heo, S. Hata, H. Kumakura, A. Matsumoto, M. Mitsuhara, S. Choi, Y. Shimada, M. Maeda, J. L. MacManus-Driscoll, S.X. Dou, NPG Asia Materials 4, e3 (2012)

[16] G. Z. Li, Y. Yang, M. A. Susner, M. D. Sumption, E. W. Collings, Supercond. Sci. Technol. 25, 025001 (2012)

[17] A. Stenvall, A. Korpela, R. Mikkonen, G. Grasso, Supercond. Sci. Technol. 19, 184–9 (2006)

[18] P. Kovac, B. Birajdar, I. Husek, T. Holubek, O. Eibl, Supercond. Sci. Technol. 21, 045011 (2008)

[19] H. Murakami, A. Ishiyama, H. Ueda, N. Koizumi, K. Okuno, IEEE Transactions on Applied Superconductivity 17, 2 (2007)

[20] N. Amemiya, S. Kasai, K. Yoda, Z. Jiang, G. A. Levin, P. N. Barnes, C. E. Oberly, Supercond. Sci. Technol. 17, 1464–1471 (2004)

[21] J.H. Kim, S.X. Dou, A. Matsumoto, S. Choi, T. Kiyoshi, H. Kumakura, Physica C 470, 1207–1210 (2010)

[22] E. Martinez, A. Angural , S.I. Schlachter, P. Kovač, Supercond. Sci. Technol.22, 015014 (2009)

[23] H. Kitaguchi, A. Matsumoto, H. Hatakeyama, H. Kumakura, Physica C 401, 246 (2004)

[24] T. Kiss, H. Okamoto, IEEE Trans. Applied. Supercond. 11, 3900-3913 (2001)